Title
Regeneration of Functional Intestinal Smooth Muscle

Author
Wang, Qianqian

Publication Date
2018

UNIVERSITY OF CALIFORNIA

Los Angeles

Regeneration of Functional Intestinal Smooth Muscle

A dissertation submitted in partial satisfaction of the

requirements for the degree Doctor of Philosophy

in Bioengineering

by

Qianqian Wang

2018

ABSTRACT OF THE DISSERTATION

Regeneration of Functional Intestinal Smooth Muscle

by

Qianqian Wang

Doctor of Philosophy in Bioengineering

University of California, Los Angeles, 2018

Professor James C.Y. Dunn, Chair

Although important for studies of gut motility and essential for intestinal regeneration, the *in vitro* culture of smooth muscle with peristaltic function remains a significant challenge. Many different culture systems have been established to restore the correct morphology or cellular components of intestinal muscle layers, but few have been developed to allow the appropriate function. Intestinal peristalsis is effected by smooth muscle cells (SMC), coordinated by the enteric neurons, and paced by interstitial cells of Cajal (ICC). Previously, different media have been developed to specifically culture primary muscle, ICC, neurons—or two of the three in combination—but no media could preserve all the three in one system. Here we report the first serum-free culture methodology that

consistently maintains spontaneous and periodic contractions of murine and human intestinal smooth muscle for months. In this system, SMC expressed the mature marker myosin heavy chain while ICC, neurons and glial cells not only preserved a substantial morphological diversity but also formed self-organized networks. To further investigate whether those different cells were functionally involved in the observed contractions, we used a collection of drugs targeting each type of cells and monitored the subsequent alternations of the contractile activity. To better characterize the transcriptional profile of cells in the new serum-free culture, we employed the RNA-sequencing methodology and explored the mechanism behind this functional regeneration. Moving forward, we incorporated the electrospun poly-caprolactone and gelatin scaffolds into the culture to provide topological guidance and morphological control for the regenerated intestinal muscle. Finally, with the addition of intestinal epithelial cells, this platform enabled up to 11 types of cells from mucosa, muscularis and serosa to coexist and epithelial cells were stretched by the contracting muscle cells. The methods here provide a powerful tool for mechanistic studies of gut motility disorders and the functional regeneration of the engineered intestine.

Supplementary Materials:

S2.1 Video Contractions of murine muscle strips (real time).

S2.2 Video Representative murine IMC contractions (real time).

S2.3 Video IMC contractions d7-d56 (real time).

S2.4 Video Contractions of passaged IMC (real time).

S2.5 Video Contractions of filtered IMC (real time).

S2.6 Video No contractions in traditional serum medium (real time).

S2.7 Video Carbachol effect, short and full versions (real time).

S2.8 Video Carbachol effect, muscle strips (real time).

S2.9 Video SNP effect (real time).

S2.10 Video Niflumic acid effect (real time).

S2.11 Video Niflumic acid effect, muscle strips (real time).

S2.12 Video Calcium oscillations (real time).

S2.13 Video Calcium propagation (real time).

S2.14 Video TTX effect (speed 2x).

S2.15 Video TTX effect, muscle strips (speed 2x).

S2.16 Video Effects of DMPP, DMPP with Hexamethonium and DMPP with L-NAME (speed 2x).

S2.17 Video Contractions of human IMC (speed 20x).

S2.18 Video Human muscle strips (speed 20x).

S4.1 Video IMC on PCL scaffold (real time).

S4.2 Video IMC on gelatin scaffold (real time).

S5.1 Video Epithelium moving with IMC in co-culture (real time).

S5.2 Video Human epithelium moving with IMC (speed 20x).

The dissertation of Qianqian Wang is approved.

Martín G. Martín

Benjamin M. Wu

Min Lee

James C.Y. Dunn, Committee Chair

University of California, Los Angeles

2018

DEDICATION

This thesis is dedicated to my dad, Yusheng Wang and my mum, Aiqin Liu. Everything will be OK as long as they are here with me.

I would also like to thank my husband. I am so lucky to find my soulmate.

TABLE OF CONTENTS

Title	Page
ABSTRACT OF DISSERTATION	ii
COMMITTEE MEMBERS	v
DEDICATION	vi
TABLE OF CONTENTS	vii
LIST OF FIGURES	ix
LIST OF TABLES	xii
LIST OF MATLAB CODES	xiii
LIST OF SUMPPLEMENTARY NOTES	xiii
LIST OF ABBREVIATIONS	xiv
LIST OF SUPPLEMENTARY MATERIALS	xvi
ACKNOWLEDGEMENTS	xxiv
VITA/BIOGRAPHICAL SKETCH	xxvi
CHAPTER 1: INTRODUCTION	1
CHAPTER 2: BIOENGINEERED INTESTINAL MUSCULARIS COMPLEXES WITH LONG-TERM SPONTANEOUS AND PERIODIC CONTRACTIONS	5
CHAPTER 3: RNA SEQUENCING REVEALS THE COMPLEX MECHANISM FOR MAINTENANCE OF CONTRACTILE INTESTINAL MUSCLE	34
CHAPTER 4: PERIODICALLY CONTRACTING MUSCLE SHEETS	53
CHAPTER 5: INTESTINAL MUSCLE-EPITHELIUM INTERACTION	65
CHAPTER 6: CONCLUSIONS AND FUTURE DIRECTIONS	73
APPENDICES	75

REFERENCES 110

LIST OF FIGURES

Figure	Page
Figure 2.1 IMC in the muscularis medium exhibited long-term periodic and spontaneous contractions (no stimulation)	17
Figure 2.2 The muscularis medium maintained mature smooth muscle cells, ICC, neurons and glial cells	19
Figure 2.3 The muscularis medium maintained various cell types at the gene level	21
Figure 2.4 Role of smooth muscle cells and ICC in the observed contractions in the muscularis medium	23
Figure 2.5 Role of the neural signals in the observed contractile activities in the muscularis medium	25
Figure 2.6 Reversible switch between contractile and non-contractile states of IMC	27
Figure 2.7 Contractility and cellular maturation of human fetal IMC	29
Figure 3.1 Contractile IMC substantially differed from the proliferative IMC	38
Figure 3.2 Transcriptionally, contractile IMC were more differentiated than proliferative IMC	40
Figure 3.3 Proliferative IMC expressed more growth factor genes	43
Figure 3.4 The synthesis of elastin, collagen and laminin were significantly enhanced in contractile IMC	45
Figure 3.5 The maintenance of IMC maturation and contractility was regulated by a collection of pathways	48

Figure 3.6 IMC's ability to support intestinal mucosa varied at different states 50

Figure 4.1 Controlling the alignment of the electrospun fibers 57

Figure 4.2 Spontaneous periodic contractions of IMC sheets on aligned electrospun PCL scaffolds in the muscularis medium 60

Figure 4.3 IMC on double-layered PCL scaffolds 61

Figure 4.4 IMC on gelatin scaffolds in the muscularis medium 63

Figure 5.1 Intestinal epithelium and functional IMC both survive in the muscularis medium 69

Figure 5.2 Serosal mesothelial cells also existed in epithelium-muscularis co-culture 70

Figure 5.3 Human IMC and epithelium co-culture in the human muscularis medium 70

Figure 5.4 Physical separation abolished the beneficial effects of IMC on intestinal epithelium 70

Figure S2.1 Contractions of cell clusters were represented by the intensity change 75

Figure S2.2 Drug vehicles (distilled water and DMSO) had little effect on the contraction frequency of IMC in the muscularis medium 76

Figure S2.3 IMC in the EC medium displayed neurites-like structure 77

Figure S2.4 Contractions of IMC at early time points in the muscularis medium 78

Figure S2.5 Effects of TTX on fresh muscle strips and IMC in the muscularis medium 79

Figure S2.6 The presence of Nac substantially limited the survival of mature human smooth muscle cells 80

Figure S2.7 Periodic contractions of human postnatal IMC in the human muscularis medium 81

Figure S2.8 Supplemental information of DMPP, TTX and L-NAME effects 82

LIST OF TABLES

Table	Page
Table S2.1 Table Antibodies, primers and probes used in the study (Chapter 2)	83
Table S2.2 Components in the EC medium and their possible functions in IMC culture	85
Table S2.3 Selected results of medium component assessment for IMC culture	86
Table S3.1 Gene enrichment analysis of PC1 highest loading genes (Top 10 GO terms)	105
Table S5.1 Antibodies, primers and probes used in the study (Chapter 5)	107

LIST OF MATLAB CODES

MATLAB CODES	Page
S2.1 Code Contraction frequency test for GFP cells	89
S2.2 Code Contraction frequency test for GFP cells (strong background noise)	94
S2.3 Code Contraction frequency test for non-GFP cells	99

LIST OF SUPPLEMENTARY NOTES

SUPPLEMENTARY NOTES	Page
S2.1 Note The development of the muscularis medium for IMC culture	87

LIST OF ABBREVIATIONS

ABAM	Antibiotic-antimycotic
BSA	Bovine serum albumin, Fraction V
CCh	Carbachol
Chga	Chromogranin A
DAPI	4',6-Diamidine-2'-phenylindole dihydrochloride
DMPP	1,1-Dimethyl-4-phenyl-piperazinium iodide
DMSO	Dimethyl sulphoxide
EGF	Epidermal growth factor
ENS	The enteric nervous system
ESC	Embryonic stem cells
FBS	Fetal bovine serum
FFT	Fast Fourier Transform
GFAP	Glial fibrillary acidic protein
GFP	Green fluorescent protein
HFIP	1,1,1,3,3,3-Hexafluoro-2-propanol
ICC	Interstitial cells of Cajal
IMC	Cells isolated from intestinal muscle layers, containing SMC, ENS and ICC
Lyz	Lysozyme
L-NAME	Nω-nitro-l-arginine methylester HCl
MC	Maximum contraction state
MHC	Myosin heavy chain
Muc 2	Mucin 2

MR	Maximum relaxation state
MS	Muscle strips
Nac	N-acetyl-L-cysteine
NO	Nitric oxide
Nuc	Nuclei
PBS	Phosphate buffered saline
PCL	poly-caprolactone
PSC	Pluripotent stem cells
ROI	Region of interest
RT-PCR	Reverse transcription polymerase chain reaction
SMC	Smooth muscle cells
SNP	Sodium nitroprusside
TTX	Tetrodotoxin
β-Tub III	β-tubulin III
Vil	Villin

LIST OF SUPPLEMENTARY MATERIALS

S2.1 Video Contractions of murine muscle strips (real time). Spontaneous periodic contractions of the non-GFP muscle strip (from a 5-day-old mouse) after 6-hour incubation in DMEM with ABAM at 37℃, corresponding to **Fig 2.1C**. Real time. Arrow indicates the spot tested to show the recording of intensity change in **Fig 2.1C**. N = 62 spots from n = 21 animals, and here only one representative sample is shown. Magnification, 40x. Contractile assessments were conducted at room temperature (22 to 25 ℃).

S2.2 Video Representative murine IMC contractions (real time). Two samples of spontaneously and periodically contracting murine IMC in the muscularis medium. They are biologically independent. Sample 1 is GFP IMC in the muscularis medium at day 19 (00:00 to 00:30, 30 seconds); Sample 2 is non-GFP IMC in the muscularis medium at day 28 (00:30 to 01:33, ~1 minute). Both real time. n = 80 biologically independent samples, and here only two representative ones are shown. Magnification, 40x. Contractile assessments were conducted at room temperature (22 to 25 ℃).

S2.3 Video IMC contractions d7-d56 (real time). Spontaneous and periodic contractions of GFP murine IMC in the muscularis medium at day 7, 14, 21, 28, 35, 42, 49 and 56, corresponding to **Fig 2.1B**-**C** and **S2.4 Fig**. Each about 30 seconds. All real time. All videos at different time points were taken from the same sample. n = 4 biologically independent samples, and here only one representative sample is shown. Magnification, 40x. Contractile assessments were conducted at room temperature (22 to 25 ℃).

S2.4 Video Contractions of passaged IMC (real time). Contractions of murine IMC initially cultured in the serum medium for 4 days then passaged and cultured for 14 days. Passaged cells were cultured in the muscularis medium. Real time. n = 3 biologically independent samples, and here only one representative sample is shown. Magnification, 40x. Contractile assessments were conducted at room temperature (22 to 25 ℃).

S2.5 Video Contractions of filtered IMC (real time). Spontaneous and periodic contractions of filtered murine IMC in the muscularis medium for 21 days. Real time. n = 3 biologically independent samples, and here only one representative sample is shown. Magnification, 40x. Contractile assessments were conducted at room temperature (22 to 25 ℃).

S2.6 Video No contractions in traditional serum medium (real time). Murine GFP IMC in the serum medium at day 7, 14, 21, 28, 35, 42, 49 and 56. No contractions were generated. Each about 30 seconds. All real time. All videos at different time points were taken from the same sample and this sample was from the same animals as the sample in **S2.3 Video**. n = 3 biologically independent samples, and here only one representative sample is shown. Magnification, 40x. Contractile assessments were conducted at room temperature (22 to 25 ℃).

S2.7 Video Carbachol effect, short and full versions (real time). Effects of carbachol on non-GFP murine IMC in the muscularis medium at day 28 (first a short version for a quick view of the effect, 00:00-00:47, then the full version, 00:47-04:05). **Short version:** First half (magnification, 40x): before adding carbachol (00:04-00:13), adding carbachol (00:13-00:16) and after adding 50 μM carbachol (00:16-00:24); second half (magnification, 100x): before adding carbachol (00:26-00:36), adding carbachol (00:36-00:40) and after adding 10 μM carbachol (00:40-00:47). **Full version:** First half (magnification, 40x): before adding carbachol (00:50-01:29), adding carbachol (01:29-01:32) and after adding 50 μM carbachol (01:32-02:33); second half (magnification, 100x): before adding carbachol (02:35-03:07), adding carbachol (03:07-03:10) and after adding 10 μM carbachol (03:10-04:05). Real time. n = 3 biologically independent samples for each concentration, and here only one representative sample for each concentration is shown. CCh, carbachol. Contractile assessments were conducted at room temperature (22 to 25 ℃).

S2.8 Video Carbachol effect, muscle strips (real time). Effects of carbachol on murine muscle strips (after 6-hour incubation in DMEM with ABAM at 37℃). **First half:** before adding carbachol (00:02-00:39), adding carbachol (00:39-00:50) and after adding 50 μM carbachol (00:50-01:45); **second half:** before adding carbachol (01:47-02:15), adding carbachol (02:15-02:25) and after adding 10 μM carbachol (02:25-03:19). Real time. n = 3 animals for each concentration, and here only one representative sample for each concentration is shown. Magnification, 40x. Contractile assessments were conducted at room temperature (22 to 25 ℃).

S2.9 Video SNP effect (real time). Effects of 100 μM SNP on non-GFP murine IMC in the muscularis medium at day 28. The video captures the same spot before (00:00-01:00) and after (01:00-02:00) adding 100 μM SNP in culture. Arrow indicates the cell cluster tested to show the recording of intensity change in **Fig 2.4A**. Both real time. n = 3 biologically independent samples, and here only one representative sample is shown. Magnification, 40x. Contractile assessments were conducted at room temperature (22 to 25 ℃).

S2.10 Video Niflumic acid effect (real time). Effects of 300 μM niflumic acid on non-GFP murine IMC in the muscularis medium at day 35. The video captures the same spot before (00:00-00:44) and after (00:44-01:29) adding 300 μM niflumic acid in culture. Arrow indicates the cell cluster tested to show the recording of intensity change in **Fig 2.4C**. Both real time. n = 3 biologically independent samples, and here only one representative sample is shown. Magnification, 40x. Contractile assessments were conducted at room temperature (22 to 25 ℃).

S2.11 Video Niflumic acid effect, muscle strips (real time). Effects of 300 μM niflumic acid on non-GFP murine muscle strips (after 6-hour incubation in DMEM with ABAM at 37℃). The video captures the same muscle strip before (00:00-00:45) and after (00:45-01:30) adding 300 μM niflumic acid. Both real time. n = 6 animals, and here only one representative sample is shown. Magnification, 40x. Contractile assessments were conducted at room temperature (22 to 25 ℃).

S2.12 Video Calcium oscillations (real time). Spontaneous periodic Ca^{2+} oscillations of murine IMC in the muscularis medium for 28 days. Arrow indicates the cell cluster tested to show the recording of intensity change in **Fig 2.4D**. Real time. n = 3 biologically independent samples, and here only one representative sample is shown. Magnification, 100x. Contractile assessments were conducted at room temperature (22 to 25 ℃).

S2.13 Video Calcium propagation (real time). Ca^{2+} flux propagation in murine IMC cultured in the muscularis medium for 28 days, corresponding to **Fig 2.4E**. Real time. n = 3 biologically independent samples, and here only one representative sample is shown. Magnification, 100x. Contractile assessments were conducted at room temperature (22 to 25 ℃).

S2.14 Video TTX effect (speed 2x). Effects of TTX on non-GFP murine IMC in the muscularis medium at day 28. **First half:** before (00:00-00:23) and after (00:23-00:45) adding 10 μM TTX in culture. **Second half:** before (00:46-01:09) and after (01:09-01:31) adding 400 μM TTX in culture. Arrows indicate the cell clusters tested to show the recording of intensity change in **Fig 2.5A** and **S2.5 Fig**. n = 6 biologically independent samples for each concentration, and here only one representative sample for each concentration is shown. Magnification, 40x. This video is at 2x speed. Contractile assessments were conducted at room temperature (22 to 25 ℃).

S2.15 Video TTX effect, muscle strips (speed 2x). Effects of TTX on non-GFP murine muscle strips (after 6-hour incubation in DMEM with ABAM at 37℃). **First 1/3:** before (00:01-00:23) and after (00:23-00:45) adding 10 μM TTX. **1/3 to 2/3:** before (00:46-01:09) and after (01:09-01:31) adding 400 μM TTX. **2/3 to end:** before (01:33-01:55) and after (01:55-02:17) adding 1 mM TTX. Arrows indicate spots tested to show the recording of intensity change in **S2.5 Fig**. n = 6 animals for each concentration, and here only one representative sample for each concentration is shown. Magnification, 40x. This video is at 2x speed. Contractile assessments were conducted at room temperature (22 to 25 ℃).

S2.16 Video Effects of DMPP, DMPP with Hexamethonium and DMPP with L-NAME (speed 2x). Effects of 10 μM DMPP, 10 μM DMPP with 300 μM hexamethonium or 10 μM DMPP with 100 μM L-NAME on non-GFP murine IMC in the muscularis medium at day 28. **DMPP, 00:00-00:34:** Before (00:00-00:17) and after (00:17-00:35) adding 10 μM DMPP in culture. Arrow indicates the cell cluster tested to show the recording of intensity change in **Fig 2.5B**. n = 6 biologically independent samples, and here only one representative sample is shown. **DMPP with Hexamethonium, 00:35-01:09:** Before

(00:35-00:52) and after (00:52-01:09) adding 10 μM DMPP simultaneously with 300 μM hexamethonium in culture. Arrow indicates the cell cluster tested to show the recording of intensity change in **Fig 2.5C**. n = 3 biologically independent samples, and here only one representative sample is shown. **DMPP with L-NAME, 01:09-01:44:** Before (01:09-01:27) and after (01:27-01:44) adding 10 μM DMPP with a 3-min pre-treatment of 100 μM L-NAME in culture. Arrow indicates the cell cluster tested to show the recording of intensity change in **Fig 2.5D**. n = 3 biologically independent samples, and here only one representative sample is shown. Magnification, 40x. This video is at 2x speed. Contractile assessments were conducted at room temperature (22 to 25 ℃).

S2.17 Video Contractions of human IMC (speed 20x). Spontaneous (no stimulation) and periodic contractions of human IMC in the human muscularis medium. **First half:** 16-week-old human fetal IMC in the human muscularis medium. (Sample 1 at day 14: 00:03-00:17; Sample 1 at day 28: 00:17-00:32; Sample 2 at day 14: 00:32-00:47). Sample 1 is the same muscularis complex shown in **Fig 2.7B**. n = 6 biologically independent samples. **Second half:** human IMC from a 12-year-old patient in the human muscularis medium at day 14 (00:50-01:04); human infant IMC in the human muscularis medium at day 22 (01:05-01:18) and day 28 (01:19-01:34), matching **S2.7A**-**B Fig**. Magnification, 200x. This video is at 20x speed. Contractile assessments were conducted at room temperature (22 to 25 ℃).

S2.18 Video Human muscle strips (speed 20x). Spontaneous and periodic contractions of the human fetal muscle strip (16-week-old) after 2-day incubation in DMEM with ABAM at 37℃. n = 3 biologically independent samples, and here only one representative spot is shown. Magnification, 40x. This video is at 20x speed. Contractile assessments were conducted at room temperature (22 to 25 ℃).

S4.1 Video IMC on PCL scaffold (real time). Spontaneously and periodically contracting murine IMC sheets on PCL scaffolds in the muscularis medium at day 21(00:00-00:30) and day 28 (00:30-01:00), matching the recording of intensity change in **Fig 4.2**. Both real time. n = 3 biologically independent samples, and here only one representative sample is shown. Magnification, 40x. Contractile assessments were conducted at room temperature (22 to 25 ℃).

S4.2 Video IMC on gelatin scaffold (real time). Spontaneously and periodically contracting murine IMC sheets on gelatin scaffolds in the muscularis medium at day 21, matching the images shown in **Fig 4.4**. Real time. n = 6 biologically independent samples, and here only one representative sample is shown. This video is at 4x speed. Contractile assessments were conducted at room temperature (22 to 25 ℃).

S5.1 Video Epithelium moving with IMC in co-culture (real time). The movement of murine intestinal epithelium and IMC in the muscularis medium after co-cultured for 4 days. The arrow and asterisk indicate two epithelial clusters. The arrow points to the epithelial cell cluster tested to show the deformation in **Fig 5.1G**-**H**. Real time. n = 6 biologically independent samples, and here only one representative sample is shown. Magnification, 100x. Contractile assessments were conducted at room temperature (22 to 25 ℃).

S5.2 Video Human epithelium moving with IMC (speed 20x). The movement of human intestinal epithelium and IMC in the human muscularis medium after co-cultured for 4 days. The arrow points to one epithelial cell cluster sitting on top of the contracting IMC. n = 3 biologically independent samples. Magnification, 100x. This video is at 20x speed. Contractile assessments were conducted at room temperature (22 to 25 ℃).

ACKNOWLEDGEMENTS

Dr. Dunn for his support and guidance. It would be impossible to count all the ways that he has helped me in my Ph.D. Thank him for always being so kind to me, for always tolerating my crazy ideas, and for always pointing me in the right direction.

Dr. Martin for opening my eyes to new directions and research.

Dr. Wu and Dr. Lee for their mentorship and support, and for guiding me through the right path in material science.

Vaidehi Joshi, my first mentor in bioengineering. Steve Po-Yu Lin, for the endless happy time we have shared together in lab. Christopher M. Walthers and Francisco Lei for guiding me to become a better researcher.

Jenny Jiafang Wang and R. Sergio Solorzano-Vargas for their generous help with my experiments and research, and also for supporting me as friends.

All lab members in Dunn Lab who have always supported me.

My parents, Yusheng Wang and Aiqin Liu, my husband Xuanrong Guo, and all my family members for always loving me.

All my friends, especially, Ao Liu, Ke Wang, Ke Ding, Di Liang, Junfei Lu, Jin Zhang and Soyon Kim. Without them, I cannot survive through my Ph.D.

Thanks for the copyright permission of KEGG for the pathway map image, ECM-receptor interaction (map04512) used in the dissertation.

Chapters Two, Four and Five are included with copyright permission from Wang, Q., Wang, K., Solorzano-Vargas, R.S., Lin, P.Y., Walthers, C.M., Thomas, A.L., Martín, M.G.,

and Dunn, J.C.Y. (2018). Bioengineered intestinal muscularis complexes with long-term spontaneous and periodic contractions. PLoS One 13 (5), e0195315. doi:10.1371/journal.pone.0195315

This research was supported by US National Institutes of Health (NIH) grant R01 DK083119 to 640 J.C.Y.D. and Q.W. was supported by a scholarship from China Scholarship Council (CSC).

VITA/BIOGRAPHICAL SKETCH

EDUCATION

Zhejiang University

Chu KoChen Honors College

Bachelors of Engineering with honors, Polymer Materials & Engineering

Bachelors of Arts, English Language & Literature

PUBLICATIONS

Wang, Q. *et al.* Bioengineered intestinal muscularis complexes with long-term spontaneous and periodic contractions. *PLoS One* **13,** 1–29 (2018).

Kobayashi, M., Lei, N. Y., **Wang, Q.**, Wu, B. M. & Dunn, J. C. Y. Orthogonally oriented scaffolds with aligned fibers for engineering intestinal smooth muscle. *Biomaterials* **61,** 75–84 (2015).

Guo, G., **Wang, Q**. Review of *the Quickening Maze*. *Word Literature Recent Developments (Chinese Journal)* **1** (147), 28-30 (2011).

PATENTS

Ma L., Wang M., Dong J., **Wang, Q.**, Gao C. “Artificial bile duct bionic stent with double-layered compound structure and preparation method of artificial bile duct bionic stent.” China Patent No. CN102641160A; Priority Date: 2012-04-24.

PRESENTATIONS

2016 TERMIS (Tissue Engineering & Regenerative Medicine International Society) – Americas Conference and Exhibition, San Diego, December, 2016. Long-term maintenance of periodically contracting intestinal smooth muscle organoids.

CHAPTER ONE

INTRODUCTION

1.1 Background

Short bowel syndrome (SBS) is a complex disease which occurs when over 70% bowel segment was lost[1–3]. It is the most common cause of intestinal failure in children[4], with an overall mortality rate of 20-40%[5,6]. Individuals with SBS often suffer from a wide range of severe functional deficiencies, including the malabsorption of various nutrients and the gut motility disorder. The first-line treatment of SBS is long-term parenteral nutrition (PN). The PN treatment can cause multiple complications, such as diarrhea, cholestatic liver injury, bone disorders, catheter thrombosis and multiple systemic infections, however, today more than 40,000 US patients still count on it for survival[7,8]. When the PN fails, intestinal transplantation is considered as the only available life-saving option.

The treatment of SBS is far from ideal. It also brings an extremely high financial burden on the patients' family. Many attempts have been made, and various new therapeutic strategies have been discovered to improve the treatment of SBS. Clinically, drugs such as Teduglutide[9] was developed to promote the absorptive function and reduce the PN dependence of patients. Apart from the traditional intestinal lengthening procedures[10], spring devices were developed to produce mechanical-force-induced tissue growth[1,5,11–15]. This method successfully promoted a 1.5-fold to 3-fold intestinal lengthening in various animal models[1,5,11–15]. In addition, enormous progress has been achieved in intestinal tissue engineering. New ideas, methods and knowledge keep emerging and bring in the constant renewal of our understanding of intestinal tissue regeneration. Different *in vitro* culture systems have been established for intestinal organoids, epithelium or intestinal muscle[16–24]. Cultures based on induced pluripotent stem cells or embryonic stem cells provide additional platforms for mechanism study and personalized regenerative medicine[25–30]. Evolutionary development in biomaterials has advanced the fabrication of better biomimetic intestinal tissue[31–36]. Studies[34,37–39] that focus on refining implantation techniques further enrich our knowledge and experiences in the interaction between the implants, such as biomaterials and cell-based products, and the surrounding host environment.

This work was inspired by those recent advances, motivated by the final goal of building functional tissue-engineered intestine at clinically relevant scales for treatment of SBS, and concentrated on the regeneration of functional intestinal muscle layers. The intestinal muscle comprises two perpendicular layers, one outer longitudinal layer and one inner circular layer. A third layer of smooth muscle may be found in some species such as human, which locates right underneath the mucosal epithelium. Within the muscle layers, there are smooth muscle cells, the enteric nervous system and the pacemaker interstitial cells of Cajal (ICC). Those cells work together to control gut motility[40,41]. The contraction in a single smooth muscle cell is regulated by Ca^{2+} concentration[42]. Depolarization of smooth muscle cells opens the voltage-dependent Ca^{2+} channel to allow Ca^{2+} to flood into the cells. Accumulated Ca^{2+} then binds to calmodulin, activates the myosin light chain kinase, and starts the force generation cycle[42]. ICC initiate the basic slow wave to control muscle contraction rhythm, while the myenteric plexus provides additional instruction[41] for the muscle to generate complex motility patterns.

Many different culture systems have been established to restore the correct morphology or cellular components of intestinal muscularis in vitro, but few have been developed to allow the appropriate function. In previously reported *in vitro* culture systems[20,22,26,27,29,43–45], cultured cells can display spontaneous but transient contractions, or spontaneous but irregular contractions, or electrical/chemical induced contractions. With *in vivo* incubation, the contractility is enhanced but still differs from that of native tissue[26]. Freshly isolated intestinal muscle strips can display continuous, spontaneous and periodic contractions with distinct physical movements[46,47]. In this study, we sought to reproduce this type of contractions *in vitro* by developing a serum-free culture methodology for cells isolated from intestinal muscle strips.

1.2 Novel findings

- Here we developed a novel serum-free culture condition in which, for the first time, long-term spontaneous and periodic contractions of murine and human intestinal muscularis cells were generated *in vitro*, with distinct physical movements and a frequency matching the tissue of origin.
- Previously, different media have been developed to specifically culture primary smooth muscle cells[48], ICC[20,43], or ENS[21]--or two of the three[49] in combination—but here we provide the first culture medium that preserves all three in one system for an extended period.
- Using RNA-seq methodology, we discovered that the maintenance of contractile intestinal muscle was correlated with (1) the continuous activation of specific master regulator genes such as *Myocd*; (2) ECM remodeling; (3) suppression of growth factor genes; (4) coordinated interplay of MAPK, Wnt, BMP pathways; (5) Eph-Ephrin

signaling for synapse organization; and (6) the preservation of ICC and enteric neurons.

- We generated a periodically contracting intestinal muscle sheet utilizing the electrospun poly-caprolactone and gelatin scaffolds.
- We established the first primary-cell based epithelium-muscularis co-culture that has spontaneous, periodic contractions.

CHAPTER TWO

BIOENGINEERED INTESTINAL MUSCULARIS COMPLEXES WITH LONG-TERM SPONTANEOUS AND PERIODIC CONTRACTIONS

2.1 Introduction

In the small intestine, the mucosa processes partially digested food and absorbs nutrients while the muscularis actuates the peristaltic flow to transport luminal content aborally. Gut motility is central to its digestive and absorptive function. The intestinal muscularis contains various types of cells. Of these, smooth muscle cells, the enteric nervous system (ENS)[50,51], and the pacemaker interstitial cells of Cajal (ICC)[52] are three important players involved in the development of gut motility. Recent studies of intestinal tissue engineering have highlighted the importance of regenerating the functional intestinal muscularis[26–29,45,53,54]. A variety of systems derived from different cell sources, including pluripotent stem cells (PSC)[26,27,29], embryonic stem cells[28] and primary cells[45,53], have been established to accomplish this goal and different contractile activities were developed in these systems. Notably, spontaneous contractions have been generated in culture systems that contained both ICC and smooth muscle cells[20,22,26,29,43,44]. In addition, electrical-induced neurogenic contractions were also successfully produced[26,27,45] when

ENS was introduced into culture. In one of the most recent studies, after *in vivo* incubation, both spontaneous contractions and electrical-induced neurogenic contractions were developed in a PSC-based culture system[26].

All of these approaches have substantially advanced the study of intestinal diseases and intestinal regeneration, yet contractions similar to those observed in native tissue have not been generated in previous *in vitro* culture systems. Freshly isolated intestinal muscle strips can display continuous, spontaneous and periodic contractions with distinct physical movements[46,47] (n = 21 animals, **S2.1 Video**). In this study, we sought to reproduce this type of contractions in cell culture by developing a serum-free culture methodology for intestinal muscularis cells (IMC).

IMC are cells isolated from the intestinal smooth muscle layers. For disease modeling and therapeutic testing of gut motility disorders, IMC are the most accessible cell source and the best representative of the various cellular components of the whole tissue. However, the applications of IMC are significantly limited by the technical difficulties in their long-term *in vitro* preservation. In the traditional serum-containing medium[44,45,55] (hereafter "**serum medium**") for IMC culture, smooth muscle cells rapidly de-differentiate and lose their contractility[23,56,57] while ICC[20] and ENS[44] do not survive in long term. The most common and already commercialized methods to re-differentiate smooth muscle cells are to reduce the amount of serum and to add heparin in culture[58,59]. However, media developed through those methods are designed only for smooth muscle cell monoculture and lack essential nutrients for other cells including neurons and ICC in IMC. Various protocols have been developed to specifically culture primary smooth muscle cells[48], ICC[20,43], or enteric neural elements[21]--or two of the three[49] in combination--but here, for the first time, we developed a single culture medium (termed "**muscularis medium**") that preserves all three in one system for an extended period and restored the spontaneous, rhythmic contractile function of IMC.

In this study, we demonstrated from multiple aspects the significant enhancements of murine IMC culture in the new muscularis medium. Using video microscopy and contraction frequency analysis, we showed that in the muscularis medium, primary murine IMC, for the first time *in vitro*, exhibited continuous self-paced periodic contractions for over two months. Using immunofluorescence and RT-PCR analysis, we demonstrated that smooth muscle cells, ICC, neurons and glia, all thrived in the muscularis medium. In addition, smooth muscle cells expressed the mature marker myosin heavy chain while ICC, neurons and glial cells not only preserved a substantial morphological diversity but also formed self-organized networks. To further investigate whether different cells all functionally participated in the observed contractions, we used a collection of drugs targeting different cells and monitored the subsequent alternations of the contractile activity. As a result, we showed that functional smooth muscle cells in the muscularis medium responded to carbachol stimulation for contraction as well as to nitric oxide for relaxation. ICC preserved the pacemaker activity, which was indicated by the presence of the spontaneous calcium oscillations in the muscularis medium. Blocking the pacemaker activity of ICC by niflumic acid abolished the contractions of smooth muscle cells. Moreover, neuromuscular communication, especially the nitrergic neuromuscular inhibitory mechanism, was explored by TTX, DMPP, hexamethonium and L-NAME. Finally, a new medium for human IMC was formulated on the basis of the muscularis medium for murine IMC, which successfully maintained the contractility and the protein and gene expressions of human fetal IMC.

2.2 Materials and methods

Mice and human specimens

Wild-type mice (C57BL/6, Charles River Laboratories, Wilmington, MA) or mice expressing green fluorescent protein (GFP, C57BL/6-Tg(Actb-EGFP)1Osb/J, Jackson Laboratory, Bar Harbor, ME) were used in the study. If not specifically mentioned in the context, intestinal muscularis was isolated from 3 to 7-day-old mice. Intestinal crypts were isolated from 6-week-old mice. All animal studies were approved by Animal Research Committee and Office of Animal Research Oversight at University of California Los Angeles (UCLA) as protocol number 2005-169 or by Stanford University Institutional Animal Care and Use Committee A3213-01. All efforts were made to minimize animal pain and suffering. For human studies, de-identified healthy small intestine tissues from discarded surgical samples of infant, teenager or adult patients were obtained through the Department of Pathology Translational Pathology Core Laboratory at UCLA. Fourteen to 18-week-old fetal bowels were obtained upon the written informed consent from each patient. All human studies were approved by UCLA Institutional Review Board.

IMC isolation

IMC isolation was performed using previously published protocols[44]. Intestines were removed and placed on ice in Hank's Buffered Saline Solution lacking magnesium and calcium (HBSS, Life Technologies, Carlsbad, CA) with 1x antibiotic-antimycotic (ABAM, Invitrogen, Carlsbad, CA). Intestinal muscles containing both longitudinal and circular muscle layers were carefully stripped off from the intestine using forceps, collected in HBSS buffer with 1x ABAM in 15 ml conical tubes on ice, and centrifuged at 1,000 rpm for 5 minutes. Next, muscles were re-suspended into the freshly-made digestion buffer: 1 mg/ml collagenase from Clostridium histolyticum, Type XI (Sigma, St. Louis, MO) in HBSS. The content was gently mixed by taping the bottom of the tubes for 10 times, then incubated at 37°C for 30 minutes. During digestion, at each 10-min interval, the content was re-mixed by tapping the bottom of the conical tube for 3-5 times. 10 ml DMEM, low glucose, GlutaMAX™ Supplement, pyruvate (Life Technologies, Carlsbad, CA) with 10% fetal bovine serum (FBS, Invitrogen) and 1x ABAM was added to terminate the process. The cells were pelleted by centrifugation at 1,000 rpm for 5 minutes and re-suspended in the serum medium prior to culture. IMC isolation from the human tissue followed the same methods used for mice.

Cell culture

Three different culture media were used in this study: 1. Serum medium: DMEM with 10% FBS and 1x ABAM; 2. The muscularis medium: Advanced DMEM/Ham's F-12 (Invitrogen) with 1x N2 (Invitrogen), 1x B27 (Invitrogen), 1 mM N-acetylcysteine (Nac, Sigma), 10 mM HEPES (Invitrogen), 2 mM GlutaMAX (Invitrogen), 100 ng/mL recombinant murine Noggin (Stemgent, Cambridge, MA), 1 μg/mL recombinant human R-spondin1 (R&D Systems, Inc., Minneapolis, MN), 10 μM Y27632 (Peprotech, Rocky Hill, NJ) and ABAM; and 3. The human muscularis medium: subtracting Nac from the muscularis medium. For murine IMC, IMC in the serum medium were plated onto the 24-well culture plates (Corning, Corning, NY) with a density of 320,000 cells/well (or 48-well plates at 160,000 cells/well). IMC in all the conditions were cultured in a 37˚C incubator with 10% carbon dioxide. Media were changed every other day. For culture using (human) muscularis media, IMC were first pre-cultured in the serum medium for 2 days to allow cells to attach and grow, then transferred to (human) muscularis media. For the (human) muscularis media, all the components can be pre-mixed and stored for two weeks at 4˚C, except noggin, R-spondin1 and Y27632, which need to be added right before changing media. IMC were passaged by TrypLE™ Select Enzyme (Life technologies). A 28 gauge syringe (Fisher) was used to break up the cell clusters. The passaged cells were plated with the serum medium. For cells cultured in totally serum-free conditions, 10% FBS in the serum medium in the pre-incubation was replaced by 10% (10 g/100 ml) bovine serum albumin, Fraction V (BSA, Fisher Scientific, Pittsburgh, PA) and cells were pre-incubated for 4 days instead of 2 days. In most cases, IMC were unfiltered. For the experiment testing whether or not the muscularis medium was effective on filtered IMC, IMC were filtered by a 70 micron nylon filter (Corning, Corning, NY)[44].

Contractile assessment

Contractions of IMC were analyzed using video microscopy. IMC formed contracting cell clusters when cultured in the (human) muscularis media. Fluorescence (for GFP^+ IMC) and phase contrast (for non-GFP IMC) videos of the cultured cell clusters or fresh muscle strips were recorded by a camera connected to the Olympus IX71 or IX73 microscope with CellSens software (Olympus, Center Valley, PA) at room temperature (22℃ to 25℃). Each video was acquired at 40x magnification which captured an area of about 3.7 mm^2 for >30 seconds. Every periodically contracting cell cluster captured in videos was analyzed. Based on our previous work[44], custom MATLAB programs (**S2.1-2.3 Codes**) were written to estimate the frequency of contractions. We first manually selected the regions of interest (ROIs) on the contracting cell clusters. The contraction-relaxation cycles of the cells caused a periodical change of intensity in the selected ROIs (**S2.1 Fig.**). For GFP^+ cells**,** in the contracted state, the size of the cluster became smaller while the number of cells in each cluster remained the same, leading to an increase of the cell density, and subsequently fluorescently brighter cell clusters, i.e. an increase of the fluorescence intensity in ROIs (**S2.1A Fig.**). When cells were relaxed, the size of cell clusters extended, the density of the cells decreased, and the clusters became dim, i.e. a decrease of the fluorescence intensity in ROIs (**S2.1A Fig.**). If cells were not contracting, no obvious intensity change could be detected. For non-GFP cells, contractions were recorded under phase contrast mode (black and white). In contrast to GFP^+ cells, non-GFP cell clusters in contraction state demonstrated a more compact and darker formulation than that in relaxation state, leading to a decrease in intensity (darker image, **S2.1B Fig.**). In some rare cases, ROIs were selected at the periphery of contracting clusters and intensity in these ROIs changed when the cell clusters contracted to reveal the background underneath (**S2.1C Fig.**). We hypothesized that the frequency of the intensity change can represent the frequency of the contractions. Using custom MATLAB programs, we measured the frequency of the intensity change. The averaged intensity value within ROIs for each frame was calculated and compared to that from the first frame in each stack to generate a normalized intensity profile. A Fast Fourier Transform (FFT) was performed on the average intensities for each ROI in the temporal domain. Contraction frequency was then identified as the frequency response with the second largest magnitude, the period of contractions as the reciprocal of the identified frequency. To acquire the sufficient sensitivity and a good signal/noise ratio for detecting the differences of the intensity among each frame, histogram equalization was used to suppress image noises and eliminate environmental illuminations prior to the FFT. For epithelium-IMC co-culture and human IMC culture, frames that captured the maximum contraction state and maximum relaxation state of the cell clusters were manually selected and extracted from the videos. Then, an optical-flow analysis was conducted based on previous work[60] to estimate and visualize the displacement of each pixel on the cell clusters between these two states.

Intracellular Ca^{2+} imaging

IMC were cultured in the muscularis medium for 28 days. Then calcium flux was visualized using the Fluo-4 Direct™ Calcium Assay Kit[44,61] (Thermo Fisher Scientific) following the product protocol. Fluorescence intensity change caused by intracellular Ca^{2+} flux was recorded using video microscopy at room temperature (22˚C to 25 ˚C) and ROIs were selected. The frequency of fluorescence intensity change within the ROIs was quantified using a custom MATLAB script (**S2.2 Code**).

Immunofluorescence

Immunostaining was performed following the typical protocol. Samples were fixed by formalin (Fisher Scientific) for 25 min at room temperature, permeabilized with 0.5% Triton X-100 and incubated in a blocking solution of 4% goat serum (Vector Laboratories, Burlingame, CA) with 2% BSA in phosphate buffered saline (PBS, Life Technologies) for 1 hour at room temperature. The primary antibodies were incubated overnight at 4˚C, rinsed, and incubated with fluorescently-conjugated secondary antibodies for 2 hours at room temperature. All the antibodies were diluted into the blocking solution. The antibodies used were listed in **S2.1 Table**. For staining of c-Kit, IMC were cultured on the glass chamber slides (Fisher Scientific, seeding density: 250,000 cells/chamber), fixed by acetone (Fisher Scientific) for 30 min at 4˚C and permeabilized with 0.1% Triton X-100 in blocking solution. Images were taken by the Olympus IX71 or IX73 microscope with CellSens software.

Quantitative real-time RT-PCR

RNA was isolated from cultured IMC, freshly isolated muscle strips or crypts (as the control) with a Qiashredder (Qiagen, Germantown, MD) and RNeasy kit (Qiagen). Quantitative real-time RT-PCR was carried out with QuantiTect Probe RT-PCR kit (Qiagen) on the 7500 Real Time PCR System (Applied Biosystems, Invitrogen). Relative expression was calculated based on the ΔΔCt method with *Gapdh* as reference. For human markers, *MYH11, C-KIT, TUBB3, GFAP* and *GAPDH*, real-time RT-PCR was performed with qScript™ One-Step SYBR® Green qRT-PCR Kit (Quanta Biosciences, Beverly, MA). Validated primers and probes used here were listed in **S2.1 Table**.

Pharmacological responses

Prior to the tests, IMC were cultured in muscularis medium for 28-35 days. Carbachol (Thermo Fisher Scientific), sodium nitroprusside (SNP, Sigma), tetrodotoxin citrate (Tocris, Bristol, United Kingdom), 1,1-dimethyl-4-phenyl-piperazinium iodide (DMPP, Sigma), hexamethonium chloride (Sigma) and Nω-nitro-l-arginine methylester HCl (L-NAME, Sigma) were dissolved in distilled water as stock solution. Niflumic acid (Sigma) were dissolved in dimethyl sulphoxide (DMSO, ATCC, Manassas, VA). All stock solutions were prepared on the day of experimentation. Dilutions, pre-incubated to 37℃, were directly administrated into the bath medium. Each concentration for all drugs was non-cumulatively applied to individual samples. The doses and incubation times of each drug were chosen based on previous work in literature[26,44,69–71,47,62–68]. Carbachol and DMPP were applied while recording videos since the effects of carbachol and DMPP were immediate[44,64]. IMC with SNP, TTX and niflumic acid were incubated for 3 mins[62], 5 mins[26] and 15 mins[63] (respectively) at 37℃ to obtain stable responses and videos were taken immediately after the incubation to record any change of cell contractility. For the study of neuronal nicotinic acetylcholine receptors, DMPP, or DMPP simultaneously with hexamethonium[71] was applied to the culture. For the examination of the nitrergic pathway in the neuromuscular coupling, samples were pretreated with L-NAME for 3 min at 37℃ before the DMPP stimulation. Prior to the experiments, distilled water or DMSO alone was administrated into the culture in exactly the same way that we used to administrate the drugs (using the same volumes (≤1% of the bath medium), same incubation times, same mixing methods, etc.) and resulted in no obvious effects on the contraction frequency of IMC (**S2.2 Fig.**, n = 3 bio-independent samples for each condition). For calculating the IC50 value of SNP, an area that contained about 10 cell clusters for each sample was recorded before and after the 3-min application of SNP. For each cell cluster present in each video, we counted the number of contractions of the same clusters within one minute (COM) before (set as control) and after the administration of SNP. The inhibition effect on the contraction frequency was expressed as percent decrease of COM from control. All the contractile assessments were conducted at room temperature (22 to 25 ℃).

Statistics

All the results were present as mean values ± standard deviations with n indicating the number of biologically independent samples. Differences between groups were evaluated using one-way analysis of variance (ANOVA) and Tukey's post hoc method of multiple comparisons. For two-group comparison, tests for data variance were first performed. The two-tailed unpaired Student's t-test was used for two groups with equal variances; the unpaired Student's t-test with Welch's correction was used for groups with unequal variances; and the paired Student's t-test was used for paired data (data normality was first determined by Shapiro-Wilk test). Frequency counts were conducted in Origin Pro 2015 (Student Version, OriginLab Corp, Northampton, MA) for histograms showing the distribution of contraction periods at each time point. Differences between distributions were determined by the two-sided Kolmogorov–Smirnov test. A p-value <0.05 was treated as statistically significant. Based on the concentration-inhibition curve, the IC_{50} value of SNP was obtained by fitting the data to the sigmoidal dose–response model. All the statistical studies were carried out using OriginPro 2015 or 2016. Graphs were drawn using GraphPad Prism 6 (GraphPad Software Inc., San Diego CA).

2.3 Results

The development of the muscularis medium

We tested several medium formulations used to culture other muscle cells and also examined the medium used for intestinal epithelial cell culture[18,72–74] (EC medium) for the development of co-culture platforms. Interestingly, we found that EC medium supported the culture of IMC, with the appearance of the neural network but without spontaneous contractions (**S2.3 Fig.**). We hypothesized that the EC medium could be modified into a new formulation suitable for IMC culture. We systematically removed one or more components of the EC medium, assessed the resultant effects on cultured IMC contractility and discovered that epidermal growth factor (EGF, a well-known stimulator of cell growth) in the EC medium prevented the IMC regular contractions (**S2.2-2.3 Tables**, **S2.1 Note**). Upon removal of EGF, cultured IMC displayed striking spontaneous contractility (**S2.2-2.3 Tables**, **S2.1 Note**, **S2.2 Video**). In contrast to the **serum medium**[44,45,55] for IMC culture, this new **muscularis medium** does not contain serum and has defined molecules added, including B27, N2, N-acetylcysteine, Noggin, R-spondin1, and Y27632.

Long-term spontaneous and periodic contractions of murine IMC

The muscularis medium potently supported the spontaneous periodic contractions of IMC (n = 80 bio-independent samples). Murine IMC formed interconnected cell clusters in the muscularis medium, a morphology different from that observed in the traditional serum medium (**Fig 2.1A**). Without any externally applied stimuli, most clusters initiated visible spontaneous contractions within 7 days, as indicated by the distinct change of the clusters' physical sizes under microscope (**S2.3 Video**). The contraction was a coordinated activity of a group of cells, indicating the possible involvement of gap junction coupling (**S2.2-2.3 Videos**). By day 21, contractions were faster and more regular than contractions at day 7 (**Fig 2.1B**, **S2.4 Fig.**, **S2.2-2.3 Videos**). Specifically, at day 28, the distribution of contraction periods of IMC clusters was not significantly different than that of fresh muscle strips (Kolmogorov–Smirnov test, p>0.05, **Fig. 2.1B-C**, **S2.1-2.3 Videos**). The contractions of IMC clusters resembled those of native tissue and persisted for at least 56 days (n = 4 bio-independent samples), with contraction periods clustering around 2-5 seconds (>50%, **Fig. 2.1B-C**, **S2.1-2.3 Videos**). We further observed that passaged IMC in the muscularis medium also generated similar contractions (**S2.4 Video**, n = 3 bio-independent samples). The muscularis medium was always effective, whether or not IMC

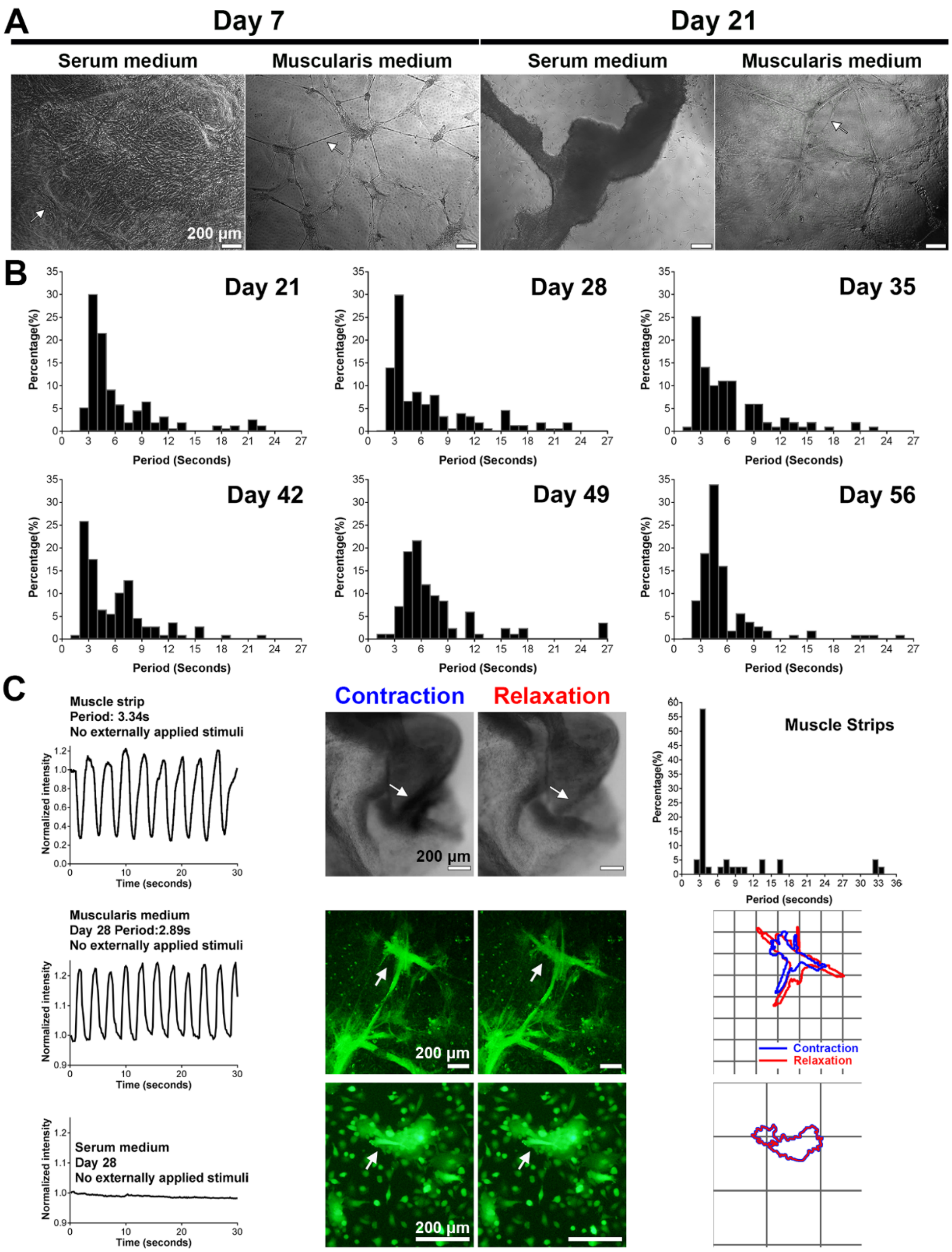

Fig. 2.1 IMC in the muscularis medium exhibited long-term periodic and spontaneous contractions (no stimulation). (**A**) Representative phase contrast images of IMC in serum and muscularis media at day 7 and 21. Arrow in the first image points to the hill-and-valley pattern. Arrow in the second image indicates neurite-like connections between clusters. Arrow in the last image points to partially detached cell clusters. (**B**) Distributions of contraction periods of IMC in the muscularis medium at 21 (*153*, **4**; N = *153* cell clusters from n = **4** biologically independent samples), 28 (*173*, **6**), 35 (*99*, **3**), 42 (*108*, **3**), 49 (*83*, **3**) and 56 (*106*, **3**) days. No externally applied stimuli. See distributions for day 7 and 14 in **S2.4 Fig**. (**C**) Typical recordings of spontaneous periodic contractions (left), shape changes (arrow, middle) and outlines (right; grid, 200 µm) of the IMC clusters in the muscularis medium and the serum medium at day 28 as well as the recording (left) and shape changes (arrow, middle) of the contracting spot on the muscle strip. For the outline image of IMC in the serum medium: the blue line is thicker than the red line. Top right image shows the distribution of contraction periods of muscle strips (N = 38 spots from n = 9 animals). Scale bars in (**A**) and (**C**), 200 µm. All the contractile assessments were conducted at room temperature (22 to 25 °C).

were filtered prior to seeding (**S2.5 Video**, n = 3 bio-independent samples). In contrast, cells in the serum medium remained static (**Fig. 2.1C**, **S2.6 Video**, n = 3 bio-independent samples).

Before transferring cells to muscularis medium, IMC were first plated in the serum medium for 2 days to allow cells to adhere and grow. To render the whole culture system serum-free, we replaced serum with bovine serum albumin. Although fewer cells adhered, periodic contractions could still be observed, indicating that serum was not essential. Effects of the muscularis medium varied across IMC isolated from mice at different ages.

Maintenance of mature smooth muscle cells, ICC, neurons and glia

Mature smooth muscle cells, ICC, neurons and glia all thrived in the muscularis medium as shown by immunofluorescence (n = 3 bio-independent samples). The protein marker myosin heavy chain (MHC) is expressed only when smooth muscle cells are mature[23,57]. Smooth muscle cells in the muscularis medium showed intense expression of MHC and displayed features associated with the mature phenotype, such as the typical fusiform shape and bundled microfilaments, indicating they were maintained at a differentiated, contractile state (**Fig 2.2A-B**).

The muscularis medium also effectively sustained ICC (c-Kit^{+}[52]) which demonstrated different morphologies. Some of the c-Kit^{+} cells were dipolar, a morphology reminiscent of the shape of intramuscular ICC; some of the c-Kit^{+} cells were multipolar, similar to the morphology of myenteric ICC[75] (**Fig 2.2A**, **C**). Multipolar c-Kit^{+} cells connected to each other and formed networks (**Fig 2.2A**, **C**).

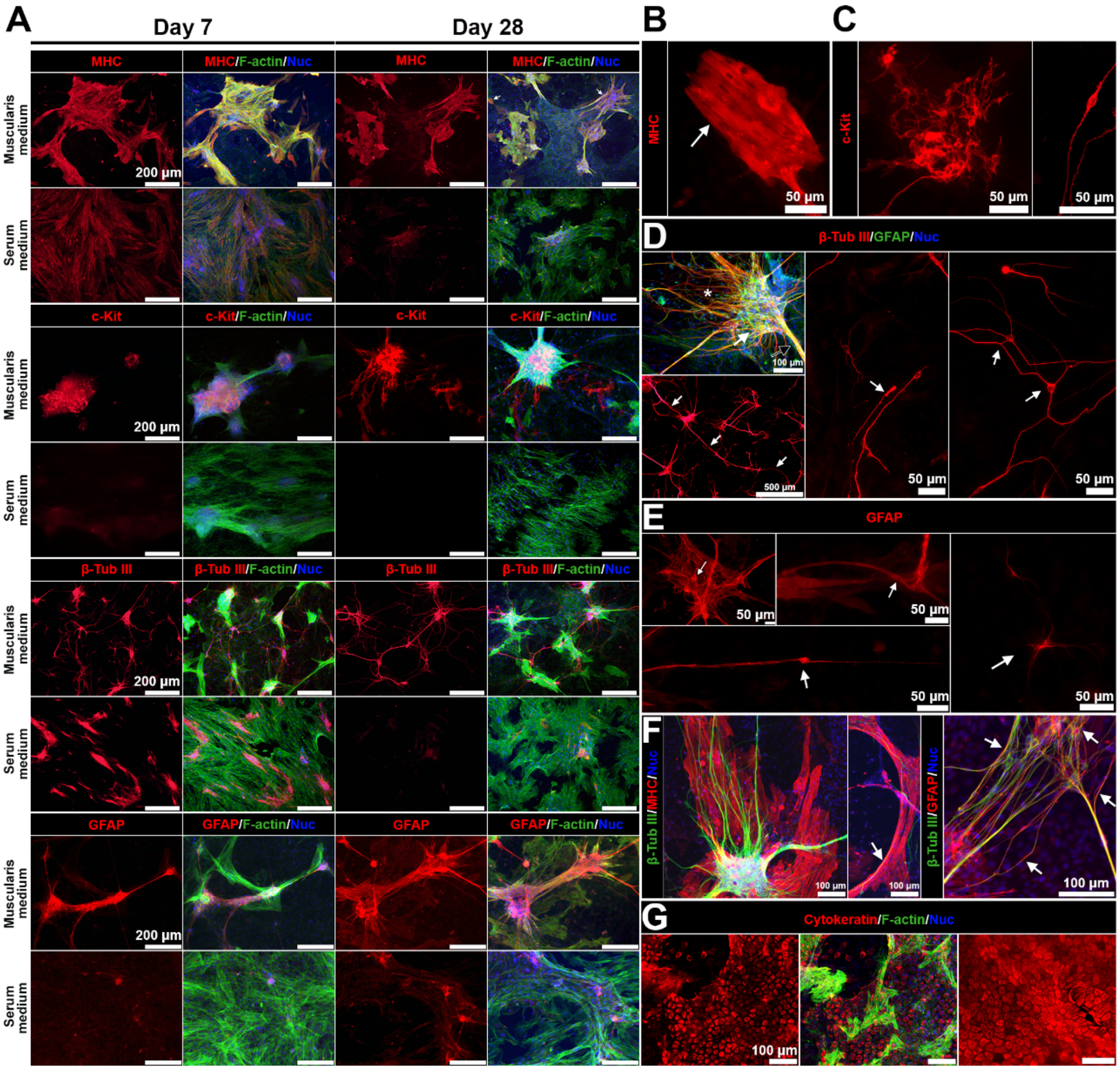

Fig. 2.2 The muscularis medium maintained mature smooth muscle cells, ICC, neurons and glial cells. (**A**) Immunofluorescence of MHC, c-Kit, β-tubulin III, and GFAP in the serum or muscularis media at d7 and d28. Nuclei (DAPI, blue); F-actin (phalloidin, green). Scale bars, 200 µm. (**B-E**) Details of cells in the muscularis medium at day 28. (**B**) Filament bundles in contractile smooth muscle cells (arrow). (**C**) Multipolar ICC network (left) and dipolar ICC (right, day 21). (**D**) Ganglia-like neural aggregates (white arrow), thick neurite bundles (black arrow) and neural fibers (white asterisk) are present in the muscularis medium, top left, scale bar, 100 µm; neurites extend over 2,000 µm (left bottom, arrows, scale bars, 500 µm); and different types of neurons (middle and right). (**E**) Four different types of glial cells (arrows). (**F**) Close associations of smooth muscle cells, neurons and glial cells (arrows). (**G**) Serosal mesothelial cells (cytokeratin, red) in the muscularis medium at day 28 (left, middle) and in muscle strips (right). Scale bars, 100 µm.

The immunofluorescence of β-tubulin III[76]and GFAP[21,77] demonstrated that IMC in the muscularis medium contained numerous neurons and glial cells (respectively). Together these cells reconstituted key morphological features of ENS[50,75], including ganglia-like neural aggregates, thick connective nerve strands out from these neural aggregates, and individual nerve fibers probably innervating smooth muscle cells (**Fig. 2.2A**, **D**-**F**). Again, neurons and glial cells with different morphologies were observed in the muscularis medium. We observed both uniaxonal neurons (similar to Dogiel type I morphology) and multipolar neurons (similar to Dogiel type II morphology) (**Fig. 2.2D**). In addition, we were able to pinpoint four morphologically distinct subsets of glial cells[51] (**Fig. 2.2E**).

Different cell types were closely associated with each other (**Fig. 2.2F**) in the muscularis medium. The neural aggregates, ICC networks, and mature smooth muscle cells together formed periodically contracting intestinal muscularis complexes among the sheet of serosal mesothelial cells (**Fig. 2.2F-G**). Over 2,000-μm-long neurites (**Fig. 2.2D**), along with processes from glial cells, built large networks to connect these contracting intestinal muscularis complexes.

Compared with the muscularis medium, expressions of MHC, c-Kit, and GFAP were either low or totally absent in the traditional serum medium (**Fig. 2.2A**). The expression of β-tubulin III existed at the early time point in the serum medium but dramatically decreased with time (**Fig. 2.2A**).

The gene expression patterns examined by quantitative real-time RT-PCR further supported the presence of these various cell types. During the two-month culture, IMC in the muscularis medium had consistently higher gene expression of mature smooth muscle cells (*Myh11*), ICC (*c-Kit*), neurons (*Tubb3*, *Rbfox3*) and glial cells (*S100β*, *Gfap*) than in traditional serum medium (**Fig. 2.3A**, n = 3 bio-independent samples). In both muscularis and serum media, cultured IMC maintained α-smooth muscle actin (*Acta2*), a marker that appears in both mature and synthetic smooth muscle cell phenotypes[59] (**Fig. 2.3A**, n = 3 bio-independent samples). In addition, the platelet-derived growth factor receptor alpha-positive (PDGFRα$^+$) cell is another important cell type fundamental to the pacemaker activities in the intestine[52]. IMC in the muscularis medium expressed high level of *Pdgfra*, suggesting the successful preservation of PDGFRα$^+$ cells in the muscularis medium (**Fig. 2.3A**, n = 3 bio-independent samples). Furthermore, different enteric neuronal markers (*Vip*, *Th*, *Calb1*, *Chat*, *Nos1*, **Fig. 2.3B**, n = 3 bio-independent samples) were detected in the muscularis medium, indicating notable neuronal diversity in the system. IMC in the muscularis medium also expressed genes related to synaptogenesis, such as *Syp* (synaptophysin, a presynaptic marker[27]) and *Dlg4* (PSD-95, a postsynaptic marker[78]) (**Fig. 2.3C**, n = 4 bio-independent samples).

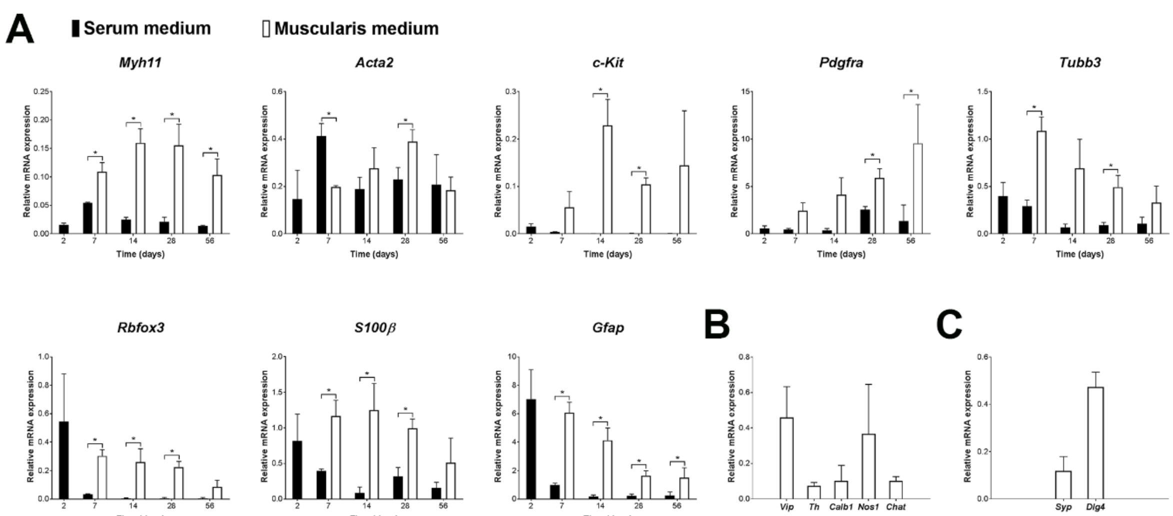

Fig. 2.3 The muscularis medium maintained various cell types at the gene level. (**A**) Relative mRNA expression of indicated markers in serum and muscularis media at day 2 (pre-incubation in the serum medium), 7, 14, 28 and 56, real-time RT-PCR. (**B**) Relative mRNA expression of various enteric neuronal markers in the muscularis medium at day 28, real-time RT-PCR. (**C**) Relative mRNA expression of synaptogenesis-related markers in the muscularis medium at day 28, real-time RT-PCR. Control: muscle strips; housekeeping gene: *Gapdh*. Error bars, S.D. (n = 3 (**A-B**) or 4 (**C**) biologically independent samples). Two-tailed Student's t-test, *p < 0.05.

Role of ICC, neural networks and muscle in contractile activity

To ascertain whether the neural network, ICC and smooth muscle cells contributed to the contractions observed in the muscularis medium, several drugs targeting each were tested in culture. The contractions were altered accordingly when smooth muscle cells were affected by adding carbachol or sodium nitroprusside (SNP), suggesting the involvement of functional smooth muscle cells in the contractile activity. We tested the effects of carbachol, a cholinergic agonist, at concentrations of 10 and 50 μM (usually from 0.1 to 100 μM[65–67] for studies of murine intestinal smooth muscle). Similar to previous observations[44,64,79,80], the addition of carbachol caused a tonic contraction (> 1 minute (50 μM), **S2.7 Video** (first a short version for a quick view of the drug effect, then the full version), for each concentration, n = 3 bio-independent samples). The effects of carbachol on IMC were similar to its action on muscle strips (**S2.8 Video**, for each concentration, n = 3 bio-independent samples). In contrast to carbachol, the smooth muscle relaxant SNP, a nitric oxide (NO) donor[64,81], reduced the frequency of the contractions in a dose-dependent manner with an IC_{50} value of 24 μM (**Fig 2.4A**-**B**, **S2.9 Video**, for each concentration, n = 3 bio-independent samples). Consistent with previous studies[26,47,64], at 100 μM, about 80-100% of the contractions were abolished by SNP (**Fig 2.4A**, **S2.9 Video**, n = 3 bio-independent samples).

The Ca^{2+}-activated Cl^- channel, Anoctamin 1 (ANO 1), is essential to the pacemaker activity of ICC[63]. To determine whether the periodic contractions in the muscularis medium were ICC-dependent, we blocked ANO 1 channel by niflumic acid (300 μM[63], a concentration effective for murine intestine), which resulted in the inhibition of IMC contractions (**Fig 2.4C**, **S2.10** (IMC)-**S2.11** (muscle strips) **Videos**, n = 3 (IMC) or 6 (muscle strips) bio-independent samples).

In addition, smooth muscle contractions result from intracellular Ca^{2+} oscillations[82]. A functional ICC network produces periodic Ca^{2+} pulses to effect the contractile pattern[82]. To further examine the participation of ICC in the observed contractions, we loaded a fluorescent Ca^{2+} indicator into cultured IMC to visualize the intracellular Ca^{2+}. Fluorescence intensity change caused by intracellular Ca^{2+} flux was recorded and quantified using a customized MATLAB script. The highest fluorescence intensity represented the highest Ca^{2+} level. We observed spontaneous and periodic Ca^{2+} oscillations of the contracting cell clusters in the muscularis medium (**Fig 2.4D**, **S2.12-2.13 Videos**, n = 3 bio-independent samples). During contraction, the physical movements of cells followed the influx of Ca^{2+} with a short delay (0.03-0.27 seconds, **S2.12 Video**). The Ca^{2+} flux also propagated from one part of the cultured IMC to another.

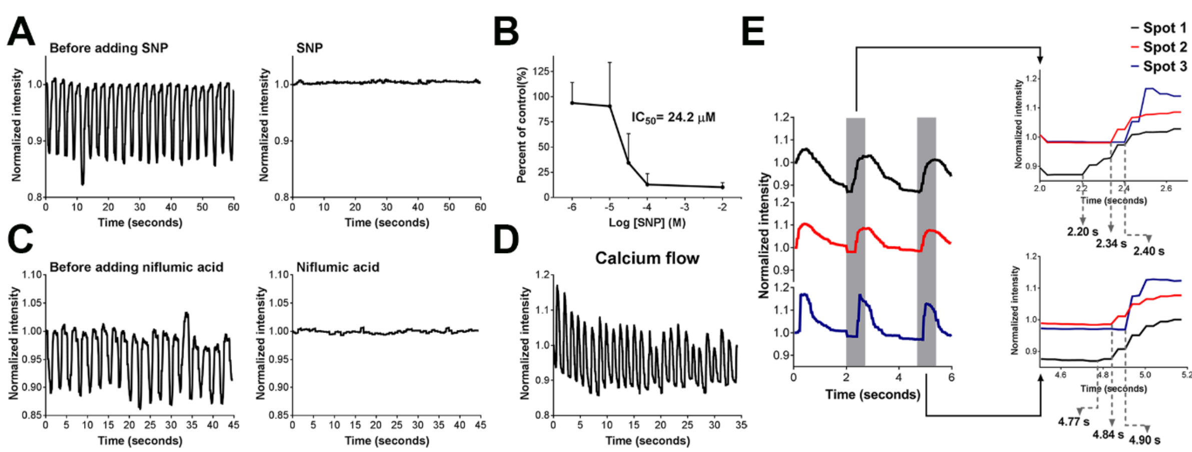

Fig. 2.4 Role of smooth muscle cells and ICC in the observed contractions in the muscularis medium. (**A**) Representative recordings of the effect of 100 µM SNP on IMC cultured in the muscularis medium at d28 (**S2.9 Video**). (**B**) Concentration–response curve for frequency of the contractions in response to SNP. Error bars, S.D. (N = 42, 55, 36, 30, 42 cell clusters for -2, -4, -4.5, -5, -6 log [SNP] (M) respectively, each from n = 3 biologically independent samples). (**C**) Representative recordings of the effect of 300 µM niflumic acid on IMC cultured in the muscularis medium at d35 (**S2.10 Video**, n = 3 biologically independent samples). (**D**) Representative recordings of the spontaneous periodic Ca^{2+} oscillations in the muscularis medium at d28 (**S2.12 Video**, n = 3 biologically independent samples). (**E**) Ca^{2+} influx onset was propagated along correlated contracting spots (the first three contractions shown in **S2.13 Video**, n = 3 biologically independent samples). All the contractile assessments were conducted at room temperature (22 to 25 °C).

Correlated contracting clusters experienced the influx of Ca^{2+} one by one (**Fig 2.4E**, **S2.13 Video**). These results support the role of ICC in the spontaneous contractions of IMC in the muscularis medium.

Next, to investigate the neural signals in IMC culture, we applied the neural blocker tetrodotoxin (TTX) to IMC in the muscularis medium and also explored the nitrergic neuromuscular inhibitory mechanism for muscle relaxation. It has been shown that TTX ≤ 10 μM cannot block the ICC-involved spontaneous contractions[47,68]. Consistent with the literature, we observed that IMC in the muscularis medium and fresh muscle strips continued to contract after the administration of 10 μM TTX, but the frequency of the contractions was slightly altered (**Fig 2.5A**, **S2.5 Fig.**, **S2.14** (IMC)-**S2.15** (muscle strips) **Videos**, each n = 6 bio-independent samples). TTX terminated the contractions of cultured IMC at 400 μM and severely disrupted the contractions of fresh muscle strips at 1 mM (**S2.5 Fig.**, **S2.14-15 Videos**, each n = 6 bio-independent samples).

In native tissue, stimulation of the nicotinic acetylcholine receptors (nAChR) on post-ganglionic nerves can activate inhibitory motor neurons to release NO, which is the major inhibitory neurotransmitter to cause muscularis relaxation[64,70,83]. In this study, we stimulated the neurons by a typical ganglionic nAChR agonist, 1,1-dimethyl-4-phenyl-piperazinium iodide (DMPP, 10 μM[26,64,69]), which elicited an immediate relaxation in the muscularis medium (**Fig 2.5B**, **S2.16 Video**, n = 6 bio-independent samples). Hexamethonium (300 μM[71]), as a ganglionic nAChR antagonist, inhibited the effect of DMPP (**Fig 2.5C**, **S2.16 Video**, n = 3 bio-independent samples). To further confirm the participation of NO in the muscle relaxation, we used Nω-nitro-l-arginine-methylester HCl (L-NAME) to block the NO synthesis[47]. The relaxation evoked by DMPP was significantly

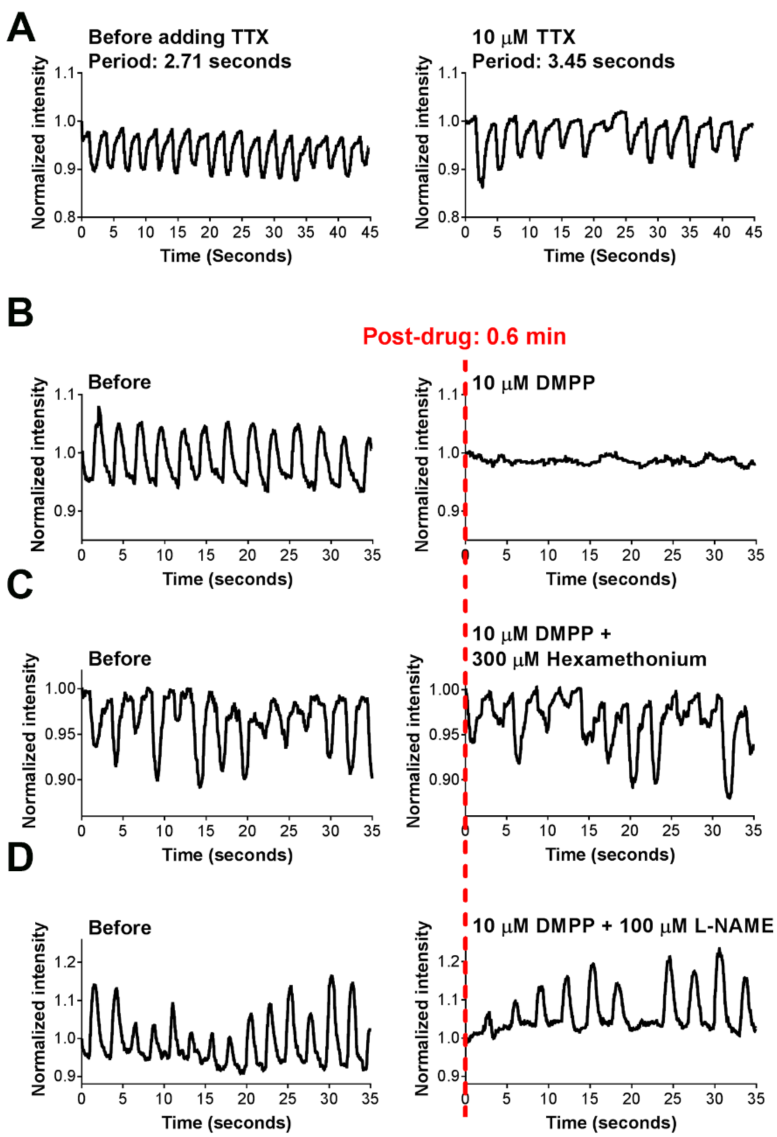

Fig. 2.5 Role of the neural signals in the observed contractile activities in the muscularis medium. (**A**) Representative recordings of the effect of 10 μM TTX on IMC cultured in the muscularis medium at d28 (**S2.14-2.15 Videos**). See **S2.5 Fig** for TTX effects on IMC at 400 μM and its effect on muscle strips at 10 μM, 400 μM and 1 mM. (**B**) Representative recordings of the effects of 10 μM DMPP on IMC cultured in the muscularis medium at d28 (**S2.16 Video**, n = 6 biologically independent samples). (**C**) Representative recordings of the effects of 10 μM DMPP simultaneously with 300 μM hexamethonium on IMC cultured in the muscularis medium at d28 (**S2.16 Video**, n = 3 biologically independent samples). (**D**) Representative recordings of the effects of 10 μM DMPP with 100 μM L-NAME (3 min pretreatment) on IMC cultured in the muscularis medium at d28 (**S2.16 Video**, n = 3 biologically independent samples). All the contractile assessments were conducted at room temperature (22 to 25 °C).

attenuated in the presence of L-NAME (100 μM[47], **Fig 2.5D**, **S2.16 Video**, n = 3 bio-independent samples). These results together indicate the involvement of NO-dependent neurogenic activities in the relaxation of IMC in the muscularis medium.

Reversible switch between contractile and non-contractile states of IMC

IMC underwent reversible changes between contractile and non-contractile states by altering the serum/muscularis media. Mature smooth muscle cells, neurons, glial cells and ICC disappeared over time in the serum medium (**Fig 2.2**, **Fig 2.6A**). Consequently, IMC were rendered into a non-contractile state. Strikingly, for IMC initially cultured in the serum medium for no more than 11 days, by switching the medium to the muscularis medium, this non-contractile state could be switched to the contractile state, and IMC expressed marker genes at higher levels (**Fig 2.6B**). Alternating culture media from muscularis (Stage 1, S1) to serum (Stage 2, S2) and back to muscularis (Stage 3, S3) medium, periodic contractions of IMC were switched from on (S1) to off (S2) and back on (S3). These changes also correlated with alternating expressions of *Myh11*, *c-Kit*, *Tubb3*, and *Gfap* (**Fig 2.6C**). The total cell mass as estimated by *Gapdh* changed in the opposite direction, and the total cell mass at S3 was more than that at S1 (**Fig 2.6C**). Therefore, multiple switches between serum and muscularis media could increase the cell mass in a stepwise fashion while preserving the contractility of IMC. When the medium was alternated in a repeated 2-day serum followed by 8-day muscularis cycle (2-8 Switch), after 28 days, IMC in 2-8 Switch had similar periodic contractions, expression of contraction-related genes, and increased (p<0.05) cell mass as compared to IMC cultured in the muscularis medium for 28 days (**Fig 2.6D**).

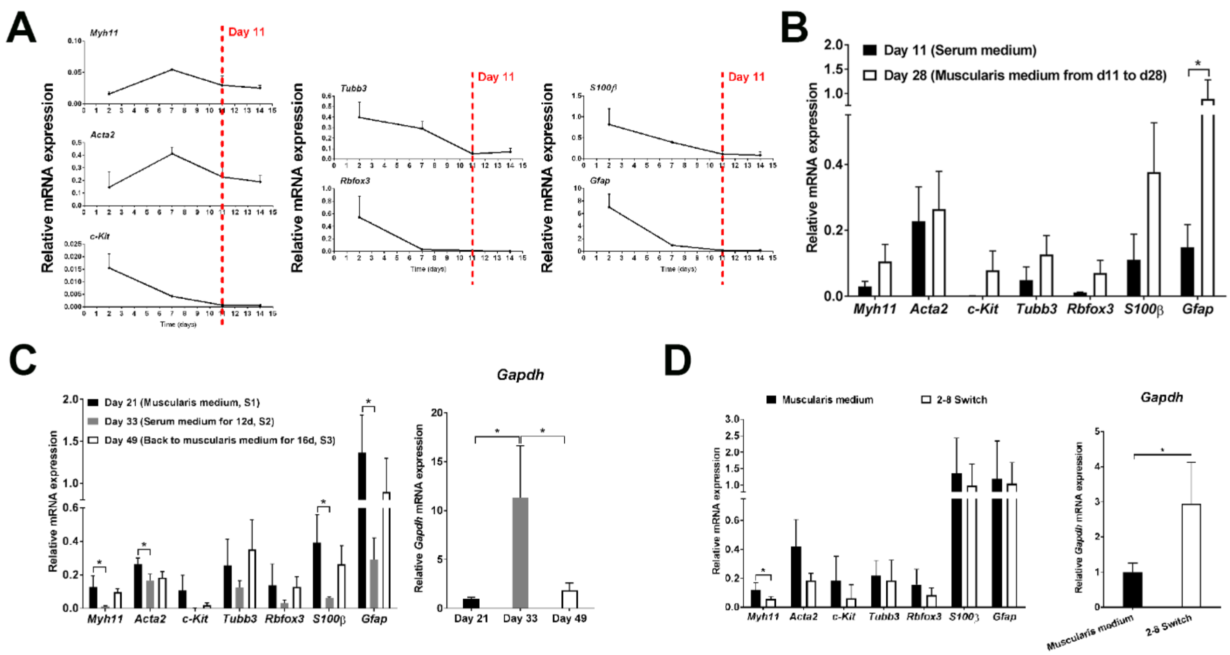

Fig. 2.6 Reversible switch between contractile and non-contractile states of IMC. (**A**) Relative mRNA expression of indicated markers decreased with time when IMC cultured in the serum medium. (**B**) Relative mRNA expression returned to higher levels after replacing the serum medium with the muscularis medium. (**C**) The change in expression of indicated genes along with media switch. (**D**) Relative mRNA expression of indicated markers of IMC in the muscularis medium or in the '2-8 Switch' condition after cultured for 28 days. For (**A-D**), muscle strips served as control, *Gapdh* as the housekeeping gene. For *Gapdh* change, mRNA expression was normalized to *Gapdh* expression in the serum medium at day 21. All error bars, S.D. (n = 3 (**A-C**) or 4 (**D**) biologically independent samples). Experimental groups were compared by Student's t-test (**B**, **D**) or ANOVA and Tukey's post hoc method (**C**). $^{*}p < 0.05$.

Contractions of human IMC in the human muscularis medium

To realize the full potential of our new IMC system, we next investigated the capability of the muscularis medium for human cells. We noted that one component in the muscularis medium, N-acetyl-L-cysteine (Nac), can protect neurons against apoptosis[84] but induces apoptosis of smooth muscle cells[85]. Though Nac in the muscularis medium did not bring substantial damage of murine smooth muscle cells; for human smooth muscle cells, Nac considerably limited their survival and consequently attenuated human IMC contractility (**S2.6 Fig.**). Upon removal of Nac, human fetal and postnatal IMC in this new medium (human muscularis medium) formed similar muscularis complexes with visible, spontaneous and periodic contractions (**Fig 2.7A**-**B**; **S2.7 Fig.**, **S2.17 Video**, n = 3 (postnatal) or 6 (fetal) bio-independent samples). The periods of contractions for human fetal IMC clustered around 10-30 seconds at day 14 and 10-40 seconds at day 28 (**Fig 2.7A**-**B**, n = 3 bio-independent samples), which was similar to those of human fetal muscle strips (**S2.17**-**2.18 Videos**, for muscle strips, n = 3 bio-independent samples). In addition, compared with the previous serum medium, the human muscularis medium also strongly supported the growth of mature smooth muscle cells, ICC, neurons and glial cells (**Fig 2.7C**-**E**, n = 3 bio-independent samples). In this medium, mature smooth muscle cells distributed throughout the whole culture area; neurons and glia again co-localized to form structures reminiscent of the native myenteric plexus; networks formed by multipolar ICC were associated with the neural aggregates; while dipolar ICC resided along with the smooth muscle cells (**Fig 2.7C**-**D**).

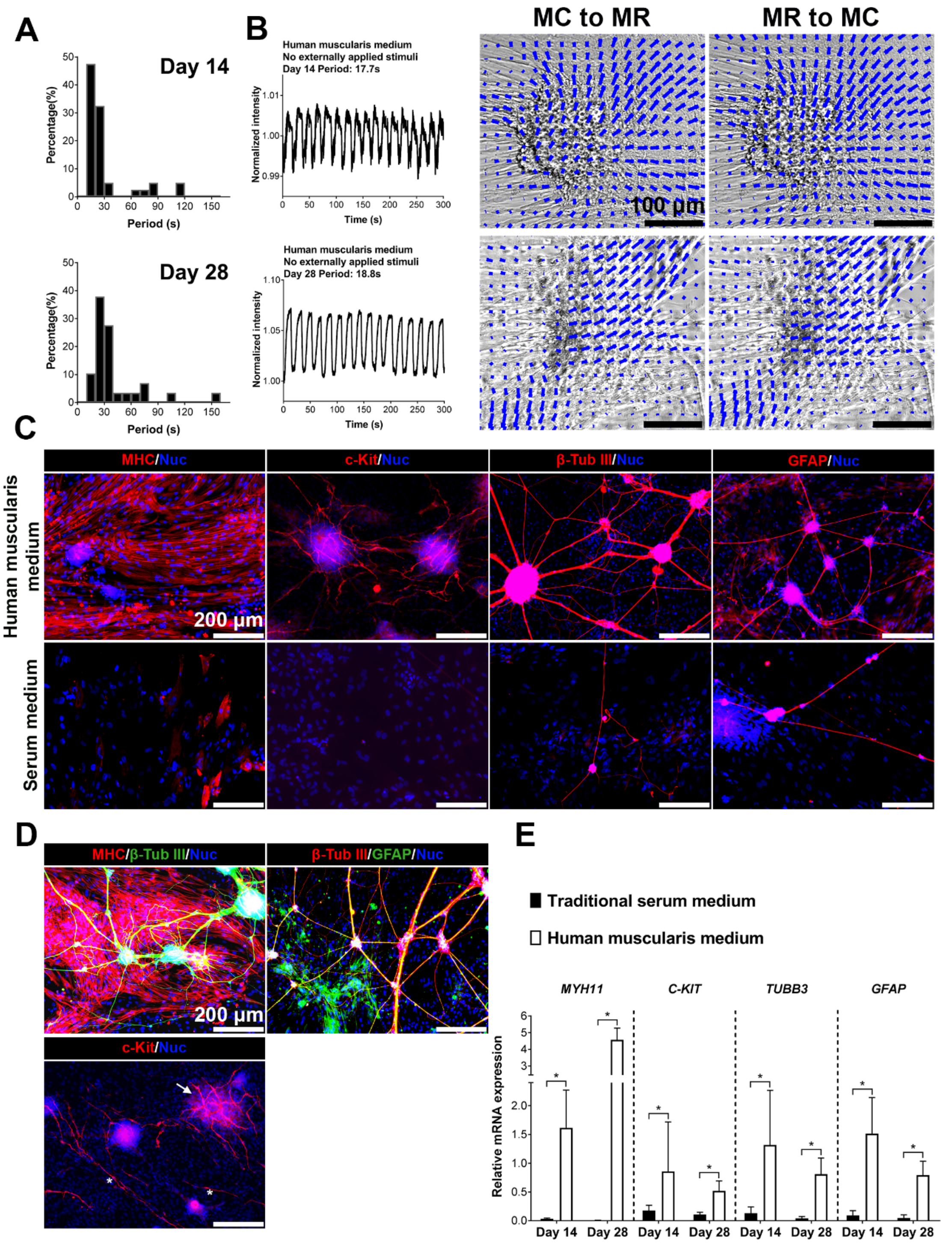

Fig. 2.7 Contractility and cellular maturation of human fetal IMC. (**A**) Distributions of contraction periods of human fetal IMC in the human muscularis medium at day 14 (*40*, **3**; N = 40 cell clusters from n = 3 independent biological samples) and 28 (*29*, **3**). Spontaneous contractions (no stimulation, at room temperature, 22 to 25 °C). (**B**) Recordings of spontaneous periodic contractions of one cell cluster in the human muscularis medium at day 14 and 28 (left). Images (right) of the same cluster from maximum contraction state to maximum relaxation state (MC to MR) and vice versa (MR to MC). See **S2.17 Video**. The direction and magnitude of the displacement at each location are indicated by the direction and length of each blue vector. Scale bars, 100 μm. (**C**) Immunofluorescence of MHC, c-Kit, β-tubulin III, and GFAP in the serum medium and human muscularis medium at d28. (**D**) Mature smooth muscle cells and neurons (left); neurons and glial cells co-localized to form neural networks (middle); multipolar ICC network (right, arrow) and dipolar ICC (right, asterisks). (**E**) Relative mRNA expression of indicated markers of human fetal IMC in the traditional serum and human muscularis media at day 14 and 28. Control: human fetal muscle strips; Housekeeping gene: *GAPDH*. Error bars, S.D. (n = 9 wells from 3 independent samples). Two-tailed Student's t-test, *$p < 0.05$.

2.4 Discussion

Both human and murine IMC cultured in our serum-free media (muscularis medium and human muscularis medium) possess many features that are not achievable under conventional serum-containing conditions. Contractions of IMC in traditional serum cultures are transitory and irregular[27,29,79], in most cases, relying on external stimuli[27,79]. In contrast, contractions of murine and human fetal IMC in our media are 1) spontaneous (no stimulation), 2) periodic, 3) long-term, 4) with distinct physical movements and 5) with a frequency closely resembling that of native smooth muscle (murine at day 28; human fetal from day 14 to day 28; **Figs 2.1B**-**C**, **2.7A**-**B**; **S2.1**-**2.3**, **S2.19**-**2.20 Videos**). For human postnatal IMC, contractions in the human muscularis media are spontaneous, periodic but slower than those associated with fetal IMC. Researchers have shown that the frequency of contractions will increase when temperature is raised[22]. In this report, all the contraction frequency tests, both for IMC and muscle strips, were conducted at room temperature (22℃ to 25℃). Cells and tissues may contract faster at 37℃.

For an extended period, all critical cell populations from intestinal muscularis, including mature smooth muscle cells, neural networks and ICC, not only survived but retained their histotypic morphology. The discovery of neurons, glia and ICC with different morphologies implies that the (human) muscularis media can preserve the microenvironment for regional specialization. Furthermore, the formation of the neural networks that share many common morphological features with the native myenteric plexus suggests that the muscularis media can also maintain the unique cell-cell associations within intestinal muscularis complexes. The inability of reverting intestinal smooth muscle cells into the mature phenotype *in vitro* has been often discussed in the literature[56,57,86]. Here we reverted non-contractile smooth muscle cells to the mature contractile phenotype by culturing them in the (human) muscularis media. Studies have suggested that neuron-smooth muscle cell interactions are essential for developments of both smooth muscle and ENS[27]. The acquisition of maturity for smooth muscle cells, ICC, neurons and glial cells in the (human) muscularis media may be a result of the close connectivity among these cells.

The serum-free muscularis media also offer a defined environment for mechanistic studies. In the muscularis medium, different components in combination displayed a potent synergistic effect on IMC contractility. While simpler formulations of serum-free media can be used, the efficiency of periodic contractions was reduced (**S2.1 Note**). In particular, we observed a marked decline of *c-Kit* expression when noggin, R-spondin1 and Y27632 were omitted, suggesting pathways controlled by these three components may modulate the growth and maturation of ICC.

For deciphering the role of neurons, we used different drugs such as TTX, DMPP, hexamethonium and L-NAME. TTX is a very potent signature drug for manipulating enteric neurons. It has been suggested that 10 μM TTX is more than enough to completely block the nervous Na^+ channels[22]. Here in our experiment, with 10 μM TTX administrated into the culture, the contractions in the muscularis medium persisted but became slightly slower (**Fig 2.5A**). However, this does not mean that the contractions in our system are neural-independent. It has been demonstrated in the literature that in the muscle strips, with functional neurons, ICC-mediated contractions can persist in the presence of 10 μM TTX[47,52]. We showed that the contractions of IMC in our culture were ICC-mediated (**Fig 2.4C-E**). Our result was consistent with the literature. To further validate the results, we also tested the effect of 10 μM TTX on muscle strips, which was very similar to its action on our cultured cells (**S2.5 Fig.**). From the literature and the results of muscle strips, we believe that (1) TTX at the typical concentration (10 μM) does not have a noticeable effect on ICC pacemaker behavior; (2) if the contractions of smooth muscle cells are mediated by both neurons and ICC, the contractions will not be blocked entirely by TTX at the typical concentration (10 μM). 10 μM TTX may have already blocked the neurogenic part of the contractions, but the myogenic part of the contractions persists. As a result, the overall effect is that the smooth muscle is still contracting but in a disturbed way. In addition, 10 μM TTX efficiently blocked the DMPP stimulation of neurons in our system (**S2.8A Fig.**). Using L-NAME to block the inhibitory neural pathway, we successfully speeded up the initial spontaneous contractions in the muscularis medium (**S2.8B Fig.**), which is a direct evidence showing that the spontaneous contractions in the muscularis medium are mediated by neural signals.

In summary, this is the first report of a platform that successfully maintains long-term spontaneous and periodic contractions of primary-cultured IMC in defined, serum-free conditions. The method can be broadly used and may ultimately assist in the full-thickness regeneration of functional intestine when in combination with other various technologies such as bio-scaffold and culture methods for intestinal epithelium. The new media can even be used together with the pluripotent stem cell-based culture method[26] to help identify the pathways that promote the intestinal fate. Contractile motion of smooth muscle is essential for intestinal barrier function[87]. IMC culture in the new media may also be of unique value when introduced into the gut-on-a-chip micro-devices for studies of microbiome-host interactions[87]. The serum-free cultures described here provide a more realistic model for utilization in therapeutic testing and future mechanistic studies of gut motility disorders. The findings from this new culture may also shed light on the regeneration of other organs in the gastrointestinal tract.

2.5 Acknowledgements

The author thanks J.C.Y. Dunn for supervising the whole project; K. Wang and C.M. Walthers for writing the MATLAB code for contraction frequency analysis; K. Wang also for performing the optical flow analysis for videos of co-culture and human samples; R.S. Solorzano-Vargas for assisting the culture of human fetal intestinal muscularis cells, performing the RT-PCR of human fetal samples and providing technical assistance of figure preparation; A. Thomas for helping culture human cells; M.G. Martin and C.M. Walthers for editing the manuscript.

The author also thanks X. Guo, A. Liu and X. Bao for helpful suggestions and critical reading of the manuscript; K. Ding and Z. Wang for scientific discussions; all the staff of the Division of Laboratory Animal Medicine at UCLA; V. Ciobanu and his team at Department of Pathology and Laboratory Medicine, David Geffen School of Medicine at UCLA and staff at Ronald Reagan UCLA Medical Center for providing human tissue.

This research was supported by US National Institutes of Health (NIH) grant R01 DK083119 to J.C.Y.D. and Q.W. was supported by a scholarship from China Scholarship Council (CSC). The funders had no role in study design, data collection and analysis, decision to publish, or preparation of the manuscript.

CHAPTER THREE

RNA SEQUENCING REVEALS THE COMPLEX MECHANISM FOR MAINTENANCE OF CONTRACTILE INTESTINAL MUSCLE

3.1 Introduction

In the intestinal muscle layers, gut motility is a result of the coordinated work of smooth muscle cells (SMC), the pacemaker interstitial cells of Cajal (ICC) and the enteric nervous system (ENS). Primary cells isolated from the intestinal muscle layers (hereafter, "**IMC**"), containing SMC, ENS, and ICC, cannot grow well in the traditional serum-containing culture medium[44,45,55] (hereafter, "**serum medium**"). In such condition, SMC quickly lose their contractility[23,56,57], while ENS and ICC cannot survive in the long term. IMC were confined at a "proliferative but not differentiated" state in the serum medium[23,56,57]. Previously we have developed a serum-free medium[88], the **muscularis medium**, in which IMC preserved their tissue-like contractility, and SMC, ICC, enteric neurons and glia all survived for over two months. In contrast to the proliferative IMC in the serum medium, IMC was highly contractile and preserved at the differentiated state. Here we investigated the transcriptional changes in IMC under those two conditions using RNA sequencing to understand the mechanism behind the maintenance of IMC maturation and function.

From the results, we discovered that the contractile smooth muscle expressed a high level of myocardin-encoded gene *Myocd*. It was also interesting to see that contractile IMC expressed significantly more elastin than proliferative IMC. In addition, intestinal smooth muscle dedifferentiation in the traditional serum medium might be a result of excessive secretion of various growth factors including heparin-binding EGF-like growth factor, epiregulin, interleukin-6, connective tissue growth factor, tumor necrosis factor-α and fibroblast growth factor-2. We also noticed that the maintenance of contractile IMC depended on the active interplay of MAPK, Wnt and BMP. Finally, IMC's ability to support intestinal mucosa varied at different states.

3.2 Materials and Methods

For materials and methods in "**Mice and human specimens**", "**IMC isolation** ", "**Cell culture for IMC**", "**Immunofluorescence**", "**Quantitative real-time RT-PCR**", and "**Statistics**", please check **CHAPTER TWO, 2.2 Materials and Methods**.

RNA sequencing analysis

Total RNA was isolated from IMC in the serum medium at day 28, IMC in the muscularis medium at day 28 and muscle strips using the method described in **CHAPTER TWO 2.2 Materials and Methods**, **"Quantitative real-time RT-PCR"**. For each condition, three parallel bio-independent samples were used for processing. RNA-seq libraries were prepared using the Illumina TruSeq RNA preparation kit (RS-122-2001, Illumina, San Diego, CA) following the manufacturer's instruction. Single-end 50-bp RNA sequencing was performed on the Illumina Hi-Seq 2000 (Illumina) at the High Throughput Sequencing Facility of the Broad Stem Cell Research Center at UCLA.

Data pre-processing was performed using the previously developed pipeline. Samples were aligned against the Mus Musculus GRCm38 genome model using STAR[89] with the default setting. Raw counts were generated using HTSeq[90] for further analysis. RNA-seq analysis was conducted entirely in RStudio software v3.4.4. Data normalization, PCA analysis, and Heatmap generation were performed using DESeq2 package following its own protocol[91]. For PCA analysis, genes with the highest loading for principal component 1 were extracted, and functional enrichment was performed on them using limmaquickpca2go from pcaExplorer v1.0.2 package. Significant genes were identified after the differential expression analysis using the two-sided Wald test with Benjamini–Hochberg false discovery[91] at a threshold of adjusted P value < 0.05 for all the analysis in this work. Functional enrichment analysis was performed using the Database for Annotation, Visualization and Integrated Discovery (DAVID) Bioinformatics Resource[92]. Plots were generated using tidyverse v1.2.1 and GOplot v1.0.2 packages.

EGF test

Epidermal growth factor (EGF, PeproTech, Rocky Hill, NJ) was dissolved in 0.1% BSA in PBS. Dilutions were directly administrated into the bath medium. Each concentration was non-cumulatively applied to individual samples (n = 3 biologically independent samples for each concentration). IMC were cultured in the muscularis medium for 21 days, then EGF was added to culture for two days. Contractions of 10 to 20 clusters for each sample were recorded at day 21 before adding EGF and day 23 after IMC cultured with EGF for two days. For each cell cluster present in each video, we counted the COM (number of contractions in one minute) following 2-day culture with EGF and compared it with same clusters in the same samples before the application of EGF (set as control). The effect on the contraction frequency was expressed as percent change of COM from control.

3.3 Results

Contractile IMC substantially differed from the proliferative IMC

RNA sequencing revealed the differential gene expression in the contractile IMC in the muscularis medium compared to muscle strips and the proliferative IMC in the serum medium (**Fig 3.1**). We conducted the principal component analysis (PCA) to observe the possible correlation and variation between those three groups. Compared with the relation between proliferative IMC and muscle strips, the result suggested a higher degree of similarity between contractile IMC and muscle strips (**Fig 3.1A**). Principle component (PC) 1 separated the three groups by 79% variance (**Fig 3.1A**). Enrichment analysis on the genes with the highest loading in PC1 showed that PC1 discriminated the three groups mainly through pathways involved in the immune process (positive), ion transport (negative), neuron differentiation (negative) and muscle contraction (negative) (**Fig 3.1A**, **S3.1 Table**).

Among annotated 24,526 genes, 6,426 genes were significantly altered (adjusted $p < 0.05$, 3,487 upregulated, 2,939 downregulated) between contractile IMC in the muscularis medium and proliferative IMC in the serum medium. The GO analysis highlighted the change in the developmental process, nervous system development, mesenchymal cell differentiation, muscle contraction, cell differentiation, cell maturation and extracellular matrix organization (**Fig 3.1B**). Upregulated genes in the contractile IMC compared with the proliferative IMC were significantly enriched in pathways concerning tissue development, cell differentiation, cell communication, neuron and glial cells differentiation, synapse assembly and organization, neurotransmitter transport, axon guidance and development, muscle development and contraction, as well as extracellular matrix structure (**Fig 3.1C**). In the meantime, downregulated genes in the contractile IMC compared with the proliferative IMC mainly concentrated in pathways related to growth,

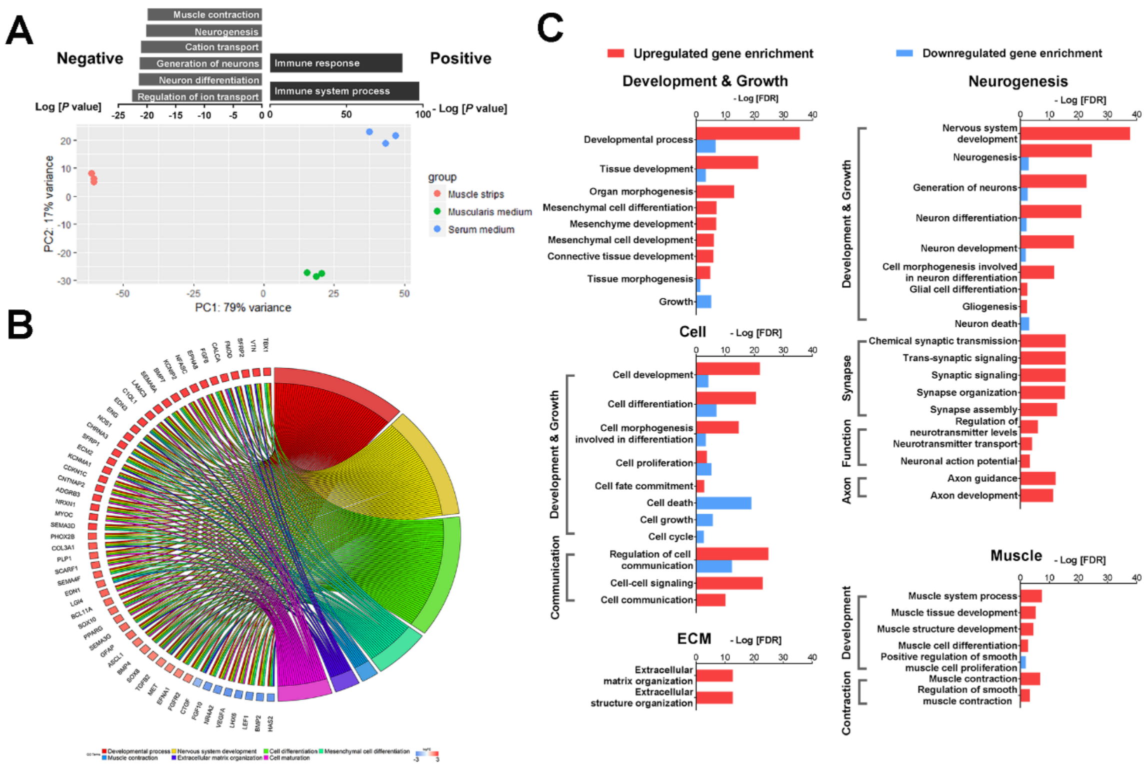

Fig. 3.1 Contractile IMC substantially differed from the proliferative IMC. (**A**) PCA analysis of proliferative IMC in the serum medium at d28, contractile IMC in the muscularis medium at d28 and muscle strips (n = 3 biological independent sample for each condition). GO terms for genes with the highest loading in PC1 are shown on top of the PCA graph. (**B**) Functional enrichment of biological processes in contractile IMC compared with proliferative IMC (n = 3 biological independent sample for each condition). Differentially expressed genes with adjusted *p*-value < 0.05 and Log_2 (fold change) < -1 or >1 were used. (**C**) Functional enrichment analysis of upregulated and downregulated genes in contractile IMC compared with proliferative IMC (n = 3 biological independent sample for each condition). Differentially expressed genes with adjusted *p*-value < 0.05 were used. FDR, FDR adjusted *p*-value.

cell proliferation and cell death (**Fig 3.1C**). Those results showed that the contractile IMC demonstrated a high level of cell maturation, neuron development, and muscle function while the proliferative IMC mainly contained fast proliferating cells with low differentiation level.

The most significant change in the contractile IMC compared with the proliferative IMC was in the enteric neuron growth (**Fig 3.1B-C**, **Fig 3.2A**). We observed a marked increase in the expression of genes for neuronal development[93] (**Fig 3.2A**), including *Ret* (adjusted p = 4.56E-3), *Phox2b* (adjusted p = 2.18E-19), *Ascl1* (adjusted p = 2.02E-05) and *Sox10* (adjusted p = 3.94E-10), indicating normal developmental pathways were utilized for preserving neuron differentiation and maturation in the contractile IMC. Consistent with our previous observation[88], apart from those genes involved in the developmental process, mature neuron markers[93], such as *Tubb3* (adjusted p = 2.02E-05), *Rbfox3* (adjusted p = 8.51E-03), *Elavl3* (adjusted p = 8.26E-08) and *Elavl4* (adjusted p = 2.27E-08), and specific markers for various neuron subtypes[76,93], such as *Vip* (adjusted p = 6.50E-05), *Nos1* (adjusted p = 1.48E-17) and *Calb2* (adjusted p = 3.03E-10), are all significantly upregulated, indicating a genetic heterogeneity of neurons was preserved in the contractile IMC (**Fig 3.2A**). In addition, genes related to glial cell differentiation[93] were also substantially elevated in the contractile IMC as compared to the proliferative IMC (**Fig 3.2A**).

We observed a combined upregulation of ICC-related and SMC-related markers, including the signature markers such as *c-Kit* (adjusted p = 2.12E-07) and *Ano1* (adjusted p = 9.08E-05) for ICC and *Myh11* (adjusted p = 8.38E-04) and *Smtn* (adjusted p = 4.95E-

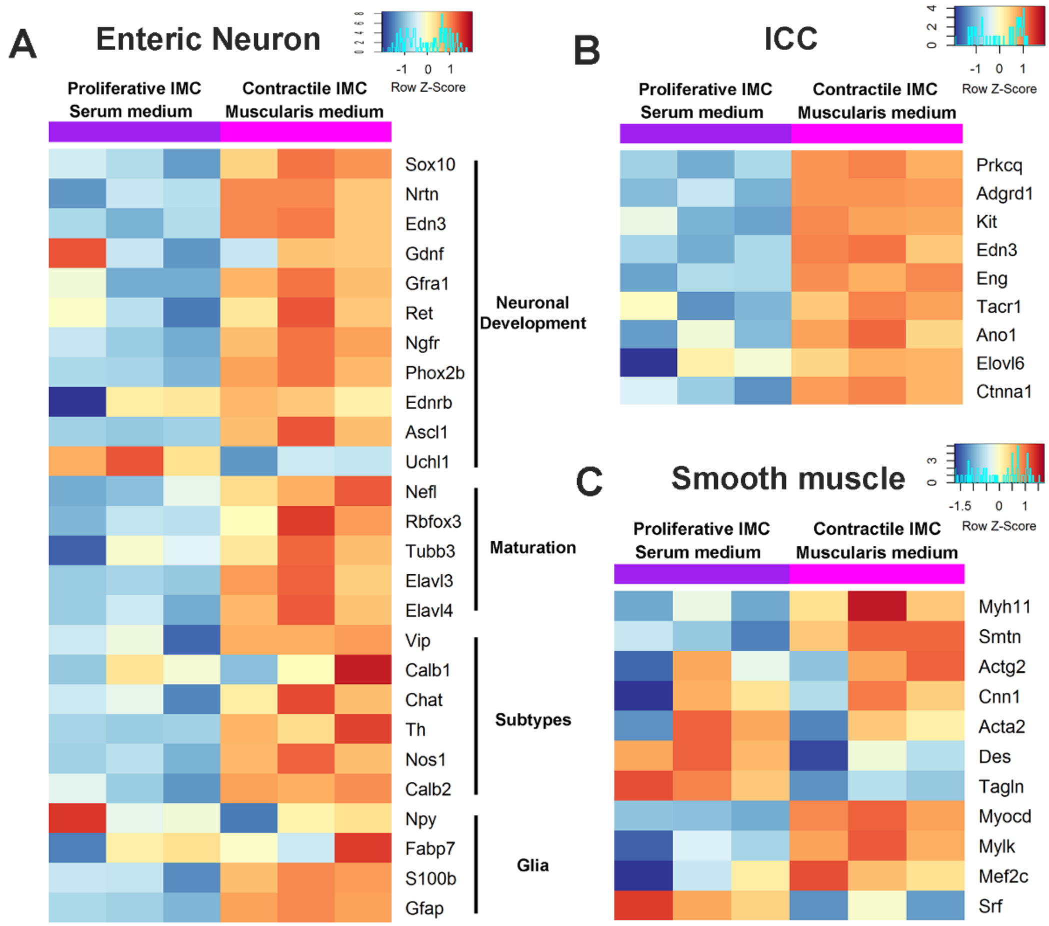

Fig. 3.2 Transcriptionally, contractile IMC were more differentiated than proliferative IMC. Expression levels of marker genes for (**A**) Enteric neurons and glia, (**B**) ICC, and (**C**) smooth muscle cells.

07) for mature smooth muscle (**Fig 3.2B-C**). In addition, active regulators of muscle development, including *Myocd*[94,95] (adjusted p = 4.82E-26) and *Mylk*[96] (adjusted p = 1.60E-07), were markedly increased in the contractile IMC in comparison with the proliferative IMC (**Fig 3.2C**). Myocardin (*Myocd*) has been identified as the master control of smooth muscle differentiation[94]. Myocardin activates the smooth muscle differentiation cascade through the interaction with serum response factor (SRF)[94]. SRF can be found in various cell types while myocardin exclusively exists in cardiac or smooth muscle cells[94]. Our data showed that unlike *Myocd* having a 25-fold increase, the SRF level (*Srf*) did not increase in the contractile IMC. The low level of *Srf* in the contractile IMC was an overall reflection of *Srf* expression in all the cells of IMC. It was hard to assess how much *Srf* was expressed specifically in smooth muscle cells in culture from the current experiment setting. However, the clear message from the results was that the high level of *Myocd* correlated with the high differentiation level of smooth muscle cells.

Growth factor genes: pushing the button to switch muscle phenotype

Proliferative IMC expressed the premature marker smooth muscle actin (*Acta2*) but not the mature marker myosin heavy chain (*Myh11*) (**Fig 3.2C**). The expression of the synthetic phenotype signature gene such as *Tpm4*[97,98] (Tropomyosin 4, adjusted p = 5.45E-04) was also significantly enhanced in the proliferative IMC (**Fig 3.3A**). Dedifferentiated IMC demonstrated a strong ability of proliferation. To understand the mechanism behind this phenomenon, we explored related gene expression and discovered that highly proliferative IMC might be the result of the excessive secretion of various growth factors. Growth factor genes previously shown to promote muscle proliferation, such as *Hbegf* (heparin-binding EGF like growth factor[99], adjusted p =

2.29E-32), *Ereg* (epiregulin[100], adjusted p = 4.68E-25), *Il6* (interleukin-6[101], adjusted p = 1.33E-26), *Ctgf* (connective tissue growth factor[100], adjusted p = 1.04E-20), *Tnf* (tumor necrosis factor-α[102], adjusted p = 3.14E-03), Fgf2 (fibroblast growth factor-2[103], adjusted p = 4.52E-03), were all significantly enhanced in the proliferative IMC when compared to the contractile IMC (**Fig 3.3A**). In parallel with the co-upregulation of growth factor genes in the proliferative IMC was the high expression of the proliferation-associated matrix material, metalloproteinase-9[104] (*Mmp9*, adjusted p = 3.57E-13). Those results indicated that the high rate of turnover observed in the dedifferentiated IMC was caused by the modulation of extracellular matrix components and activation of growth factor genes.

Krüppel-like Factor 4 (*Klf4*) and 5 (*Klf5*)[105–107] are crucial factors in phenotype switching of vascular smooth muscle cells. *Klf4* and *Klf5* also play key roles in the regulation of intestinal stem cells[108,109]. *Klf4* is often identified as a growth arrest-associated gene who behaves as a suppressor of cell proliferation, while Klf5 has the opposing effect and acts as a promoter of cell proliferation[105–107]. *Klf5* also stimulates de-differentiation in vascular smooth muscle cells, however, the role of *Klf4* in vascular smooth muscle cell differentiation is controversial[105,107]. Opposite functions of Klf4 were observed in different studies[105]. Here we found that compared with the proliferative IMC, the expression of *Klf4* in the contractile IMC was highly upregulated (adjusted p = 3.47E-02) while the expression of *Klf5* significantly went down (adjusted p = 3.43E-02) (**Fig 3.3A**). Even more interestingly, there was no statistical difference in the expression of both *Klf4* and *Klf5* between the contractile IMC and muscle strips. It seemed that *Klf4* might also exert the growth inhibiting effect while *Klf5* acted as the growth promoter for intestinal smooth muscle, similar to what was seen in vascular smooth muscle cells. Studies showed that

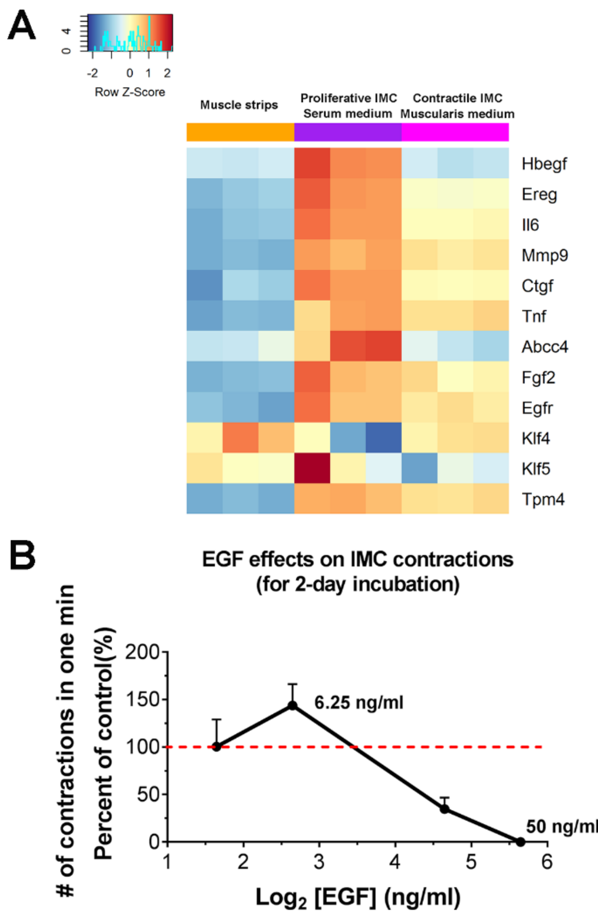

Fig. 3.3 Proliferative IMC expressed more growth factor genes. (**A**) Expression levels of proliferation-related genes across different conditions (n = 3 biologically independent samples for each condition). (**B**) Concentration-response curve for frequency of the contractions in response to EGF. Error bars, S.D. (N = 49, 46, 51, 43 cell clusters for 1.64, 2.64, 4.64, 5.64 log2 [EGF] (ng/ml) respectively, each from n = 3 biologically independent samples).

Klf4 could inhibit the differentiation of vascular smooth muscle cells by repressing the expression of *Myocd*[105]. However, in the contractile IMC, the increase of *Klf4* expression did not bring down the expression of *Myocd* (**Fig 3.2C**, **3.3A**).

The proliferation and differentiation in IMC were not mutually exclusive. Over-powered proliferation did affect IMC function, as what was seen in the proliferative IMC and in various intestinal muscle diseases[110]. However, we found that a slight increase in proliferation could enhance muscle contraction. Previously we showed that the addition of 50 ng/ml Epidermal grow factor (EGF) abolished the periodic contractions of IMC in the muscularis medium[88] and cells proliferated extensively under the effect of 50 ng/ml EGF. Here we found that when EGF was added at a low concentration (6.25 ng/ml), IMC proliferation was increased but the contractility of IMC was also enhanced (**Fig 3.3B**).

The synthesis of elastin, collagen and laminin were significantly enhanced in the contractile IMC

The extracellular matrix (ECM) underwent an extensive change between the proliferative IMC and the contractile IMC (**Fig 3.4**). 135 genes relating to ECM organization and interaction were significantly altered. The expression of collagen-encoded genes, Laminin-encoded genes and the elastin-encoded gene (*Eln*) all substantially elevated in the contractile IMC (**Fig 3.4**). Specifically, the expression of *Eln* was increased 38.6-fold (adjusted *p*-value = 5.38E-127) in the contractile IMC than that in the proliferative IMC, reaching a similar level as that expressed in native muscle strips (adjusted *p*-value = 0.15). Elastin actively participates in smooth muscle contraction[111–114]. In the intestine, elastin closely associates with ICC bundles[111] and myenteric plexus[114]. In vascular smooth muscle, lack of elastin is often accompanied by abnormal organization of the contractile

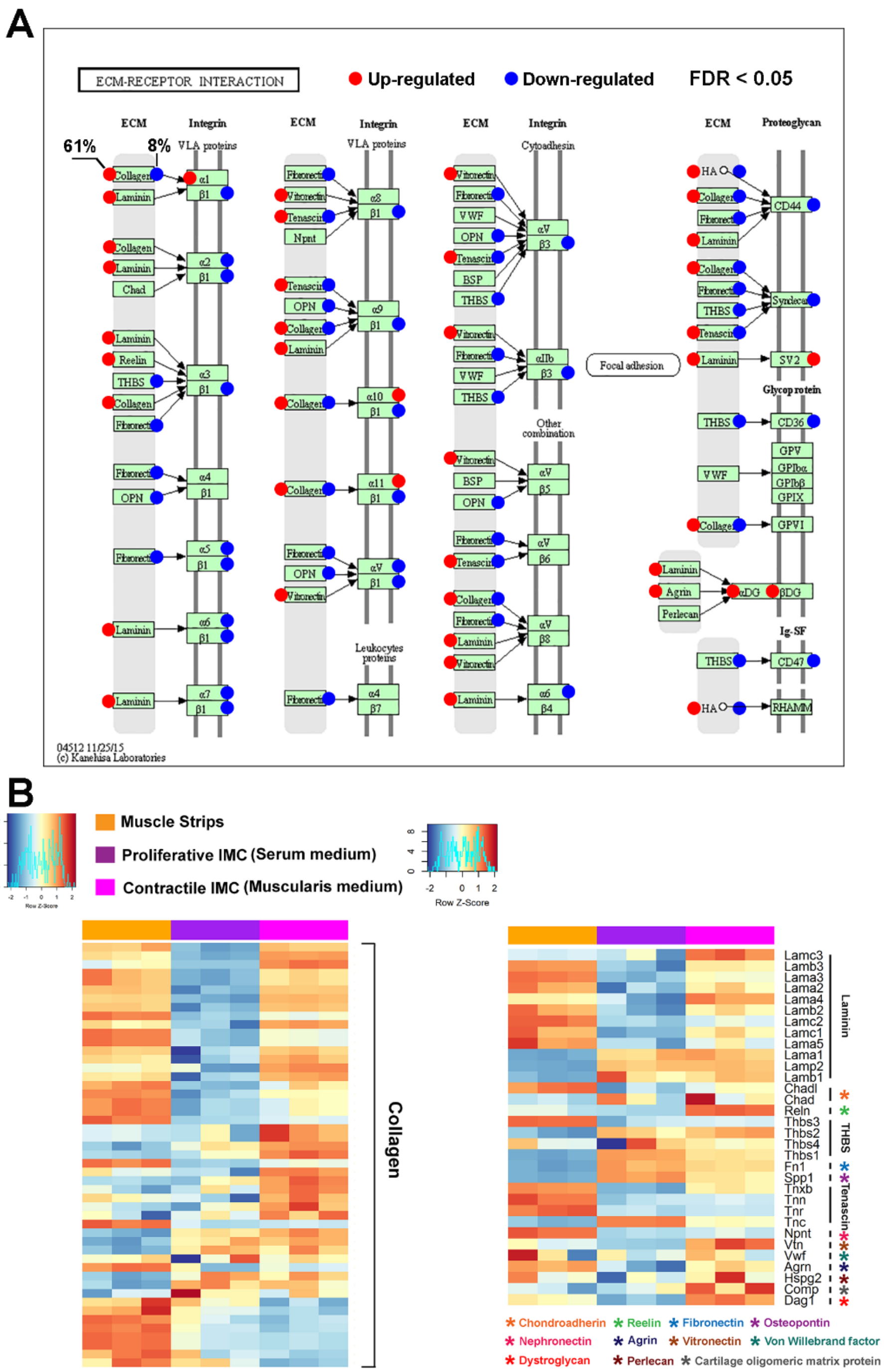

Fig. 3.4 The synthesis of elastin, collagen and laminin were significantly enhanced in contractile IMC. (**A**) Schematic map showing ECM-receptor interaction, based on KEGG map[116]. (**B**) Expression levels of ECM-related gene markers across different conditions (n = 3 biologically independent samples for each condition).

apparatus[113,115]. The high increase of *Eln* expression correlated with the high contractility of the contractile IMC, indicating that IMC actively regulated the surrounding ECM to create a suitable environment for their normal function.

About 61% and 8% of collagen-encoded genes were significantly up- or downregulated, respectively[116] (**Fig 3.4**). Notably, among the upregulated genes, *Col14a1* (collagen type XIV, α1), *Col3a1* (collagen type III, α1) and *Col19a1* (collagen type XIX, α1) are the genes involved in muscle tissue development; *Col25a1* (collagen type XXV, α1) and *Col3a1* (collagen type III, α1) participate in the process of neuron differentiation and development; and *Col4a5* (collagen type IV, α5) helps regulate the synapse organization. Although the overall expression pattern of collagen-encoded genes in the contractile IMC differed from that observed in muscle strips, the expression level of several specific genes in the contractile IMC, such as *Col6a1* (collagen type VI, α1), *Col6a2* (collagen type VI, α2), *Col6a3* (collagen type VI, α3), *Col6a5* (collagen type VI, α5) and *Col11a1* (collagen type VI, α2), were similar to that observed in the muscle strips.

Compared with the proliferative IMC, almost all the Laminin-encoded genes were enhanced in the contractile IMC (**Fig 3.4**). Laminin α5 chain has been identified as a crucial regulator of intestinal smooth muscle differentiation in early gut development[117]. Lack of Laminin α5 chain is paralleled by the delayed differentiation of intestinal SMC[117]. In the contractile IMC, we observed a 1.7-fold increase in the expression of *Lama5* (Laminin α5) as compared to that in the proliferative IMC, indicating that similar Laminin α5 regulation may also be involved in the maintenance of IMC contractile state.

Maintenance of differentiated IMC required a synergic work of different regulators

We further investigated the gene ontology analysis of the pathway enrichment in the contractile IMC compared with the proliferative IMC. The most significant enrichment of upregulated genes was found in MAPK, BMP and canonical Wnt signaling pathways while downregulated genes were enriched in MAPK, ERK1/2 and ERBB pathways (**Fig 3.5A**). The profound transcriptional change in MAPK signaling indicated an extensive remodeling in the contractile IMC compared with the proliferative IMC. The enrichment of downregulated genes in ERK1/2 and ERBB pathways, again, highlighted the decreased activity of proliferation in the contractile IMC. Wnts and BMPs are often considered as the master regulator of the intestinal tissue development[118]. In the muscularis medium, exogenous noggin, the BMP antagonist, and R-spondin 1, the Wnt pathway agonist, were added to modulate the BMP-noggin balance and the Wnt signaling in IMC culture, respectively[88]. It is not surprising to see that transcriptional changes happened in those signaling pathways. We discovered that *Wnt10b*, *Wnt2b* and *Wnt7b* were the most differentially expressed Wnts, and *Fzd10*, *Fzd6*, *Fzd4*, *Fzd9* were the most differentially upregulated Wnt receptors in the contractile IMC compared with the proliferative IMC (**Fig 3.5B**). Meanwhile, the most highly upregulated BMPs in the contractile IMC were *Bmp3* and *Bmp7* (**Fig 3.5C**).

Apart from MAPK, Wnt and BMP signaling, many other regulators were also active. Notably, synapse function and organization highly depend on Ephrins-Eph signaling[119]. We observed a co-activation of the Eph receptor-encoding genes (*Ephb1*, *Ephb2*, *Ephb3*, adjusted p = 3.96E-33, 1.21E-11, 7.00E-27, respectively) in the contractile IMC, which was paralleled by the significant upregulation of the various markers of different neuronal synapses (**Fig 3.5D**). In addition, we found that in the muscularis medium, R-spondin 1

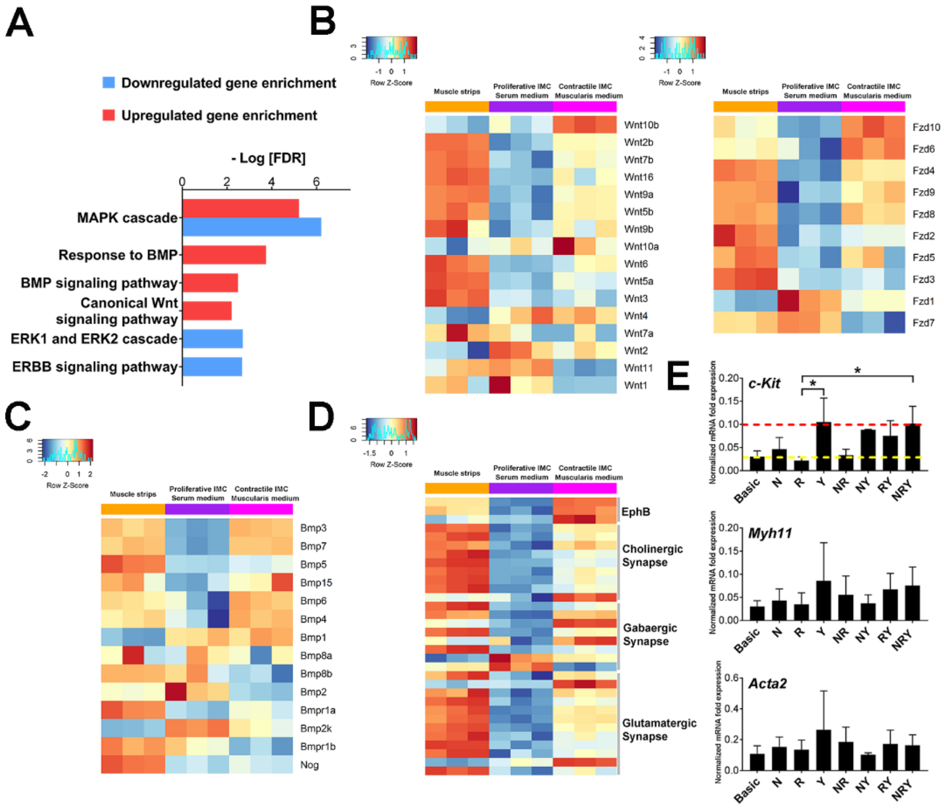

Fig. 3.5 The maintenance of IMC maturation and contractility was regulated by a collection of pathways. (**A**) Functional enrichment analysis of upregulated and downregulated genes in contractile IMC compared with proliferative IMC (n = 3 biological independent sample for each condition). Differentially expressed genes with adjusted *p*-value < 0.05 were used. FDR, FDR adjusted *p*-value. Expression levels of marker genes for (**B**) Wnt pathways, (**C**) BMP pathways, and (**D**) synapse organization across different conditions (n = 3 biologically independent samples). (**E**) Relative mRNA expression of indicated markers at d14 in the basic medium (Basic), basic medium plus noggin (N), basic medium plus R-spondin 1 (R), basic medium plus Y 27632 (Y), basic medium plus noggin and R-spondin 1 (NR), basic medium plus noggin and Y 27632 (NY), basic medium plus R-spondin 1 and Y 27632 (RY), and muscularis medium (NRY), real-time RT-PCR. Control: muscle strips; housekeeping gene: *Gapdh*. Error bars, S.D. (n = 3 biologically independent samples). Two-tailed Student's t-test, *$p < 0.05$.

and noggin together were not sufficient to support the pacemaker ICC, while the further addition of ROCK inhibitor Y27632 promoted a significant increase of the ICC marker *c-Kit* (**Fig 3.5E**). Previously, ROCK inhibitor Y27632 was never associated with ICC maintenance in the intestinal muscle. However, the ability of Y27632 to support c-Kit expression and c-Kit+ cells were seen in several studies[120,121]. Some experimental results showed that short-term addition of Y27632 inhibited the electrical- or chemical-induced smooth muscle contraction[122–124]. In our culture, the spontaneous contractions of IMC in the muscularis medium did not improve on the removal of Y27632. The existence of Y27632 did not cause any decline in the expression of muscle-related genes such as *Myh11* and *Acta2* either (**Fig. 3.5E**).

Proliferative IMC vs. contractile IMC: the ability to support intestinal mucosa was varied

Epithelium-mesenchyme crosstalk is vital for the normal developmental process of the intestine[118,125–129]. A collection of genes encoding crucial regulators of the intestinal epithelial homeostasis were significantly increased in the contractile IMC when compared with the proliferative IMC (**Fig 3.6**). Thus, the data indicated that IMC at different differentiation level could produce different signals to the intestinal mucosa.

3.4 Discussion

Decades of work dedicated to the intestinal muscle has unveiled many details in the muscle development and function. However, many questions remain unanswered. In this study, to understand the phenotype change of intestinal smooth muscle cells and the mechanism behind the maintenance of the intestinal muscle function, we investigated the transcriptional changes in the contractile IMC compared with the proliferative IMC utilizing

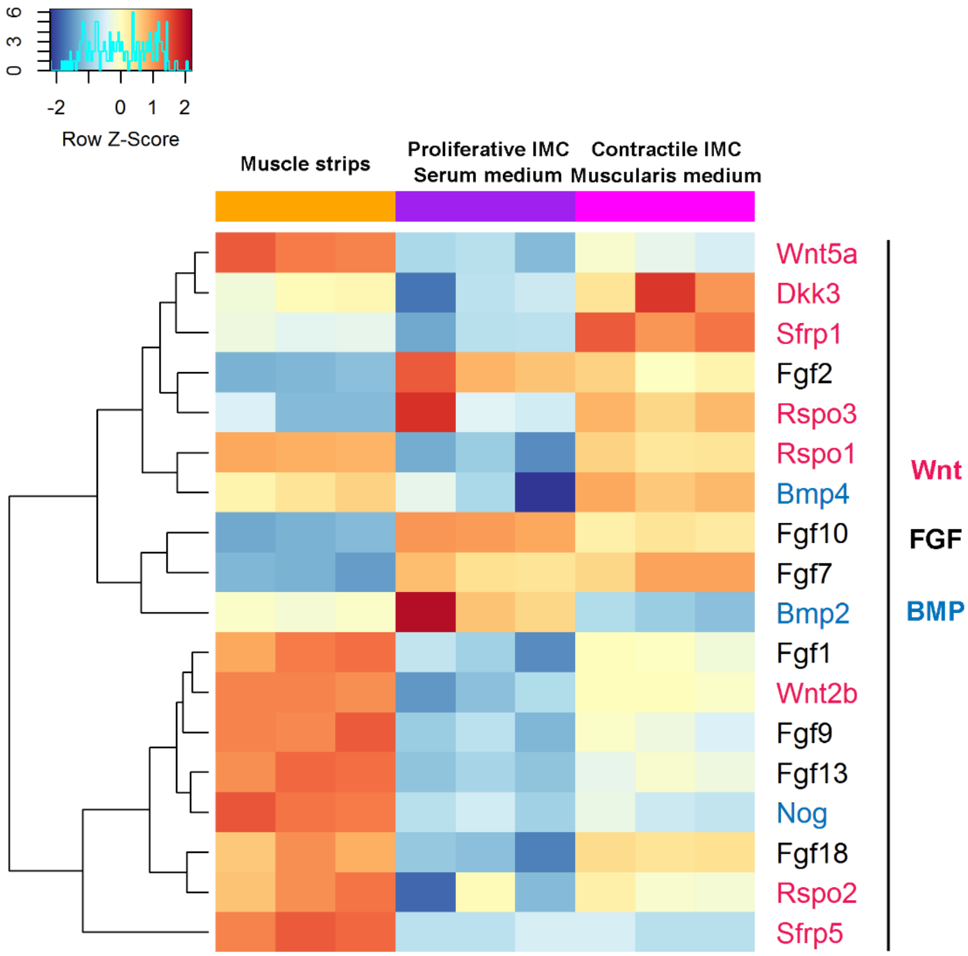

Fig. 3.6 IMC's ability to support intestinal mucosa varied at different states. Expression levels of potential affecters of intestinal epithelium across different conditions (n = 3 biologically independent samples). Hierarchical clustering is based on euclidean distance.

RNA-seq methodology. The maintenance of IMC contractility and maturation relies on the cooperated work of various factors, each having multiple and overlapping roles in this process. We identified several Wnt/BMP regulators, such as *Wnt2b*, *Wnt7b*, *Bmp3* and *BMP11*, which previously were not associated with intestinal muscle development but highly expressed in the contractile IMC as well as in the native muscle strips. ROCK inhibitor has never been considered as a potential promoter for ICC development. Here we demonstrated its powerful effect on ICC preservation. It is also interesting to see that proliferative smooth muscle cells correlated with the co-activation of a group of growth factor genes. In the muscularis medium, contractile IMC grew on the well-plate plastics. The organization of the cells was substantially different from that seen in native tissue. It is predictable to see that the expression pattern of ECM components varied between the native tissue and the contractile IMC in culture. However, despite the variation in other ECM components, IMC in the muscularis medium, which preserved high muscle contractility, produced a level of *Eln* similar to that seen in native tissue. Elastin deposition might be an essential need for IMC contraction. The results in this study indicate that IMC continually read and respond to the environment cues from ECM; selectively deposit, rearrange and remove specific materials; and, in this way, promote the structural integrity to support their own functionality.

The differentiation of the intestinal muscle does not start until after the neural crest cells enter the gut during embryonic development[130]. The ENS-SMC relation has long been discussed but without a clear elucidation. In the contractile IMC, neurons and glial cells were functionally active whereas, in the proliferative IMC, almost no detectable neural activity was observed. The preservation of the differentiation level of IMC might depend on the presence of neurons in the system. Studies on ENS-SMC relation should be a worthwhile extension of the present work.

3.5 Acknowledgements

The author thanks J.C.Y. Dunn for supervising the whole project; J. Wang and M.G. Martin for library preparation; Z. Liu and B.X. Ling for Data pre-processing.

The author also thanks all the staff at the High Throughput Sequencing Facility of the Broad Stem Cell Research Center at UCLA for performing the RNA-sequencing experiment.

CHAPTER FOUR

PERIODICALLY CONTRACTING MUSCLE SHEETS

4.1 Introduction

In the native tissue, intestinal muscle is arranged in two perpendicular oriented layers. The myenteric plexus lies in between those two muscle layers, consisting of enteric ganglia, thick neurite bundles and individual nervous fibers innervating the muscle. The enteric nervous system contains about 100 million neurons[93] in different subtypes. It is a complex network of sensory neurons, interneurons, inhibitory motor neurons and excitatory motor neurons[50]. In addition, studies also reveal the extensive heterogeneity of enteric glial cells[51,131] and the pacemaker ICC[132]. Previously we have observed different neuronal subtypes and ICC subtypes in IMC cultured in the muscularis medium. Enteric neurons and glia form ganglia-like aggregates in the muscularis medium with thick neurite bundle fanning out from the aggregates and the single innervating fibers. However, the neuronal fibers are not regularly organized as what have seen *in vivo*. Smooth muscle cells tend to form clusters instead of strip-like structure. IMC growing on the well-plate plastics do not preserve the tissue microarchitecture. Tissue morphology and structure are of great importance for the tissue function. The IMC culture in the muscularis medium can be combined with other technologies for applications in the intestinal regeneration. To guide IMC for more organized structure, we incorporated an aligned electrospun sheet into the culture system.

The electrospun scaffold has been considered as a good candidate to provide topological control of muscle cells[133–137]. Parameters like fiber orientation[136,138–141] and diameter[134,142–144] have been shown to have great influence on cell morphology, protein and gene expression. In this study, we used poly-caprolactone (PCL) and gelatin for the scaffold fabrication. To mimic the double-layered muscle structure *in vitro*, we fabricated the double-layered PCL scaffolds with orthogonally aligned fibers.

4.2 Materials and Methods

For materials and methods in "**Mice and human specimens**", "**IMC isolation** ", "**Cell culture for IMC**", "**Contractile assessment**", "**Immunofluorescence**", "**Quantitative real-time RT-PCR**", and "**Statistics**", please check **CHAPTER TWO, 2.2 Materials and Methods**.

Scaffold fabrication

11% (w/w) Poly-caprolactone (PCL, Durect Lactel, Cupertino, CA) or gelatin (Sigma, St. Louis, MO) in 1,1,1,3,3,3-hexafluoro-2-propanol (HFIP, Sigma) was prepared 1-day prior to electrospinning and well mixed. In some studies, 11% PCL in Chloroform (Sigma) was also prepared for electrospinning. A customized electrospinning set was built in the lab with a syringe pump, a high voltage supplier and a rotating mandrel as the collector. The mandrel was 3 mm in diameter. The rotating speed was 3000 rpm. For PCL scaffolds, the experiment was conducted at 13.5 kV and the target volume for each scaffold was 0.15

mL. For gelatin scaffolds, the experiment was conducted at 18.5 kV and the target volume for each scaffold was 0.5ml. For PCL scaffolds with two perpendicular layers, one layer of aligned fibers was first fabricated. Then the first layer of the fibers was removed from the mandrel, rotated to 90 degrees and then re-taped on the mandrel. The second layer of aligned fibers was collected on top of the first layer. The scaffolds were removed from the mandrel and cut into the size of a well of a 48-well plate. The gelatin scaffold was crosslinked by glutaraldehyde (Sigma) vapor for 7 days in the vacuum desiccator (Fisher). Then both PCL and gelatin scaffold were plasma etched. After plasma etching, gelatin scaffolds were soaked into 1M glycine (Sigma) water solution for 5 days to wash off excessive glutaraldehyde. Both PCL and gelatin scaffold were sterilized by 70% ethanol. PCL scaffolds were coated by the neutralized collagen (Advanced BioMatrix, Carlsbad, CA) prior to cell seeding. The seeding density on each scaffold was 0.6 to 1 million per scaffold.

Scanning electron microscopy (SEM)

The surface of PCL and gelatin scaffolds were examined using Nova NanoSEM 230 (FEI, Hillsboro, Oregon) or Hitachi S-3400N VP (Tokyo, Japan) SEM. For Nova NanoSEM 230, scaffolds were mounted on the conductive carbon tape (Ted Pella, Redding, California), and imaged at low vacuum mode. For Hitachi S-3400N VP-SEM, wet scaffolds were imaged at -15 ℃, low vacuum mode.

Alignment assessment

Fiber alignment was assessed based on the SEM image of the scaffold, using ImageJ and its plug-in called OrientationJ. The alignment coherency coefficient was calculated by the software, ranging from 0 to 1, with 1 representing a 100% alignment. At least three sample areas were selected for each sample for the alignment assessment.

4.3 Results

Controlling the alignment of PCL fibers

The common setting of electrospinning includes a syringe, a pump, a high voltage supply to create the electrical field, and a counter electrode (**Fig 4.1A**). To fabricate aligned fibers, the counter electrode is often a rotating mandrel. In the electrospinning process, a high electrical field is applied to the polymer solution droplet to cause its deformation and finally the ejection of the charged jet. The jet is drawn to the counter electrode where the fiber is collected. While the jet is traveling in air, the solvent of the polymer solution evaporates, leading to the formation of the dry polymer fiber. Almost all the parameters of electrospinning can affect the alignment of the polymer fibers, including the concentration of the polymer solution, the volatility and polarity of the solvent, the viscosity of the polymer solution, the feeding rate of the polymer solution, the applied voltage, the speed of the rotating mandrel and even the distance between the syringe and the collector.

It has been proposed[145] that the key relation that affects the fiber alignment is the relation between the fiber flow rate (V_1) and the linear speed (V_2) of the rotating collector surface (**Fig 4.1B**). The fiber flow rate is different from the feeding rate of the polymer. Polymer jets usually undergoes complex 3D whipping when traveling in air. The flow rate of the polymer jet represents how fast the fiber will deposit onto the mandrel. In order to achieve a fair alignment of the fibers, the fiber flow rate should match the linear speed at the surface of the rotating collector[145]. In this way, polymer fiber can be tightly taken up by the collector to lead to the aligned structure[145]. If the flow rate is too fast, loops of the fibers

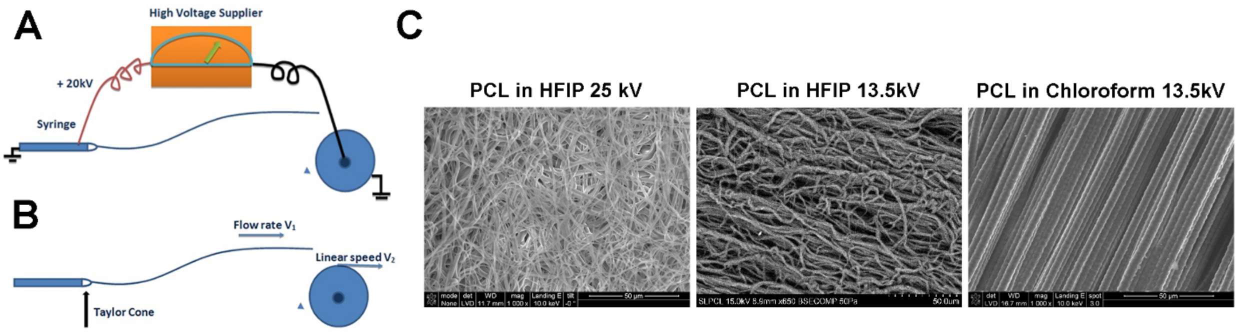

Fig. 4.1 Controlling the alignment of the electrospun fibers. (**A**) Schematic showing the basic setup of the electrospinning. (**B**) Schematic showing the key relation between the flow rate of the fiber and the linear speed of the rotating mandrel surface. (**C**) SEM images showing electrospun fibers fabricated at different conditions. Scale bars, 50 µm.

and randomly oriented fibers will be collected on the mandrel. The extreme phenomenon will be, instead of using the rotating mandrel, using a static metal plate to collect the fiber. In this condition, the “linear speed” of the collector (the static metal plate) surface is zero. Any flow rates will be considered “too fast” to match with the linear speed. That is why, for electrospinning using metal plates as a collector[146], only random fibers will be fabricated. On the other side, if the flow rate is too slow, fibers will break before reaching the collector[145].

The linear speed of the mandrel surface is determined by the radius of the mandrel and the angular rotating speed of the mandrel. The increase of the linear speed of the mandrel surface can be realized by increasing either the radius or the angular rotating speed. Here in this study, both of the radius and the angular rotating speed were fixed due to our experimental instrument setting. Our focus was put on the adjustment of the flow rate. Many factors can affect the flow rate, among which one of the most important is the applied voltage. The higher the voltage is, the faster the flow rate of the polymer jet will be. Initially, 25 kV was used to electrospin the PCL fiber. Although the angular rotating speed of the mandrel was already very high to reach 3000 RPM, the degree of the alignment is less than 10% (**Fig 4.1C**). We then lowered the voltage to 12.5 kV to 13.5 kV, the alignment of the PCL fibers was markedly increased (**Fig 4.1C**). However, the voltage cannot be reduced without limit. The voltage has to be high enough to initiate the polymer jet.

Another interesting discovery was that the property of the solvent could impact the alignment of the fiber. When everything else was fixed, PCL dissolved in chloroform turned to form more aligned fibers than that in HFIP (**Fig 4.1C**). The property of the solvent was often considered as an active regulator of the morphology and the diameter of the electrospun fibers. Here we provided the evidence to show that it also mediated the fiber alignment.

Although fibers generated from PCL in chloroform had a higher degree of alignment, the fiber diameters also increased (**Fig 4.1C**). The aligned fiber produced by PCL in HFIP at 12.5 kV to 13.5 kV had a more natural morphology and a smaller diameter (**Fig 4.1C**). IMC grew on the aligned fibers generated from PCL in HFIP demonstrated better contractility than that growing on the aligned fibers produced by PCL in chloroform. We, therefore, chose the aligned PCL-in-HFIP fibers for further assessment and investigation.

Electrospun PCL scaffolds to provide morphological control for IMC

In the muscularis medium, the PCL sheets seeded with IMC periodically moved due to spontaneous contractions of IMC (**Fig 4.2A**, **S4.1 Video**, n = 3 bio-independent samples), demonstrating a more coordinated movement than that seen in IMC cultured on plastics. MHC^{+} smooth muscle cells and β-tubulin III^{+} neuronal plexus lined up along with the PCL fiber structure, while the ICC formed a rudimentary network (**Fig 4.1B**-**C**). Interestingly, IMC seeded on the same scaffold but cultured in the traditional serum medium did not show any distinct movement.

To mimic the real tissue, we also fabricated the double-layered PCL scaffold with orthogonally aligned fibers (**Fig 4.3A**). IMC grew on the double-layered scaffold exhibited two perpendicular layers (**Fig 4.3B**).

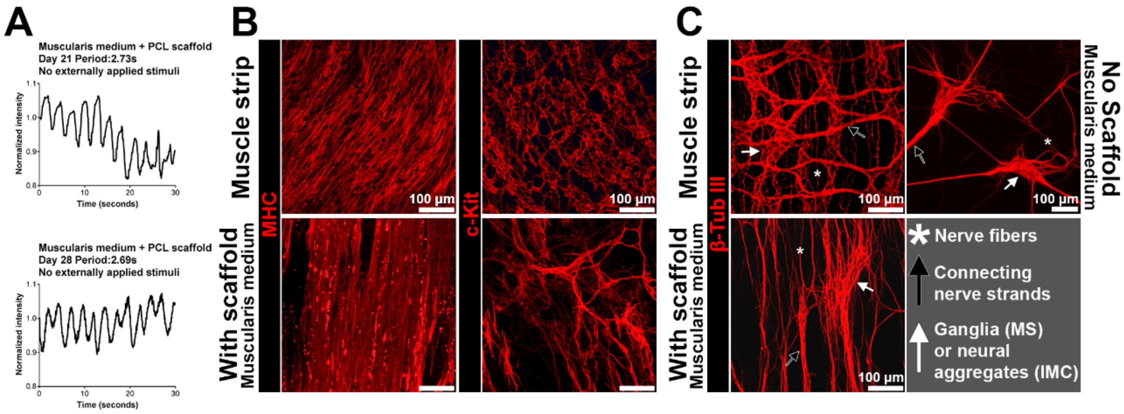

Fig. 4.2 Spontaneous periodic contractions of IMC sheets on aligned electrospun PCL scaffolds in the muscularis medium. (**A**) Typical recordings of spontaneous periodic contractions of IMC sheets on PCL scaffolds in the muscularis medium (n = 3 biologically independent samples, at room temperature, 22 to 25 °C, **S4.1 Video**). (**B**) Top views of mature smooth muscle cells (MHC) and ICC networks (c-Kit) in muscle strips and in IMC cultured on PCL scaffold in the muscularis medium at day 28, showing microarchitecture of muscle and ICC (confocal images, for MHC staining on muscle strips, mainly the circular muscle layer). (**C**) Top views of neurons (β-tubulin III) in muscle strips, IMC cultured on PCL scaffold and on culture plastic in the muscularis medium at day 28, showing aligned microarchitecture of neurons (confocal images for muscle strips and IMC on scaffolds). Key elements of myenteric plexus are pointed out: ganglia in muscle strips (MS) or ganglia-like neural aggregates in cultured IMC (white arrows), thick neurite bundles (black arrows) and neural fibers (white asterisks). Scale bars, 100 µm.

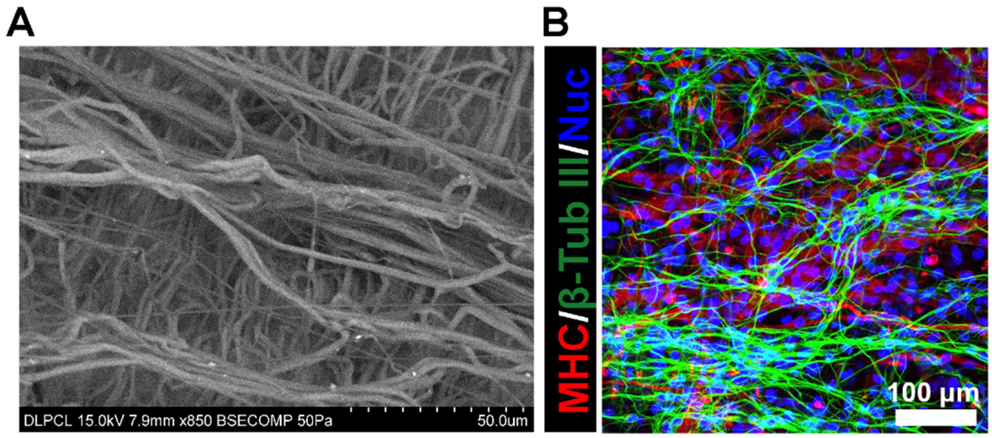

Fig. 4.3 IMC on double-layered PCL scaffolds. (**A**) Representative SEM image showing double-layered structure of the scaffold. (**B**) Top views of smooth muscle cells (MHC) and neurons (β-tubulin III) in IMC cultured on double-layered PCL scaffold in the muscularis medium at d28, showing microarchitecture of muscle and neurons (confocal images). Scale bars, 100 µm.

Electrospun gelatin scaffolds as a softer substrate to better accommodate IMC contractility

Compared with the smooth contractile motion of muscle strips, the movement of IMC on PCL scaffolds tended to be more rigid and confined, suggesting that a softer and more elastic material is preferred to promote the flexible movements of IMC. Gelatin which has a low elastic modulus was then employed to fabricate the electrospun scaffold. At the same concentration, the viscosity of the gelatin-HFIP solution was much lower than that of the PCL-HFIP solution. The applied voltage was adjusted up to 18.5 kV to prevent the break-up of the fluid jet. However, the increase of the voltage diminished the degree of the alignment of gelatin fibers (**Fig 4.4A**). The gelatin sheets of IMC demonstrated gigantic periodic movement (**Fig 4.4B**, **S4.2 Video**, n = 6 biological independent samples). IMC contraction caused the visible folding of the gelatin scaffold (**S4.2 Video**). However, IMC on the gelatin scaffold did not form oriented aligned structure (**Fig 4.4C**). RT-PCR results showed a collective upregulation of the marker genes such as *Myh11, c-Kit*, *Tubb3* and *Gfap* in IMC grew on the gelatin scaffolds than those on the PCL scaffolds (**Fig 4.4D**).

4.4 Discussion

The muscularis medium is ready to complement alternative techniques for applications in the intestinal regeneration. Particularly, polymer scaffolds with aligned structure is capable of providing sufficient topological cues for IMC culture. With aligned PCL scaffolds, IMC in the muscularis medium displayed enhanced architecture with more organized contractile movements. In contrast, IMC culturing on the same PCL scaffold in

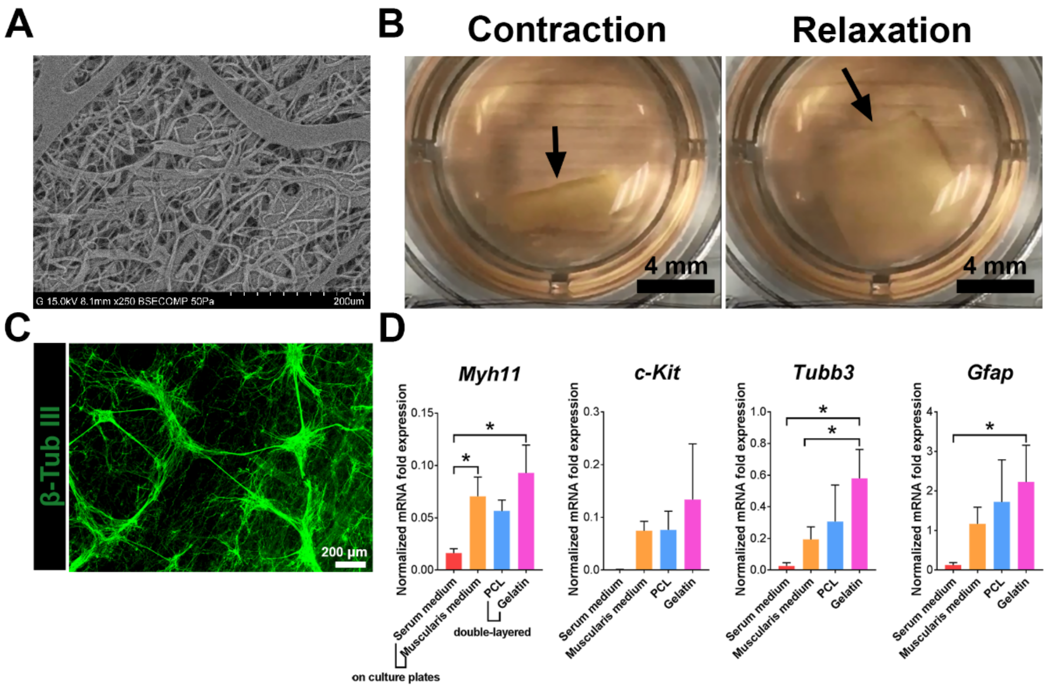

Fig. 4.4 IMC on gelatin scaffolds in the muscularis medium. (**A**) Representative SEM image showing the surface of gelatin scaffolds. (**B**) Shape changes (arrow) of the IMC on the gelatin scaffolds in the muscularis medium at d21, matching **S4.2 Video**. (**C**) Immunofluorescence of β-tubulin III in IMC growing on the gelatin scaffold in the muscularis medium at d28. Nuclei (DAPI, blue). Scale bars, 200 µm. (**D**) Relative mRNA expression of genes of IMC in the indicated conditions at d28, real-time RT-PCR. Control: muscle strips; housekeeping gene: *Gapdh*. Error bars, S.D. (n = 3 biologically independent samples for IMC on double-layered PCL; n = 4 biologically independent samples for all the other conditions). One way ANOVA with Tukey's post hoc test, *p < 0.05.

the traditional serum medium formed similar aligned morphology but demonstrated no distinct movement. These findings highlight the indispensable role of the muscularis medium for the functional regeneration of IMC sheets. IMC grew on the gelatin scaffold in the muscularis medium demonstrated much better contractility and less organized morphology than that seen on PCL scaffolds. Future design of the scaffold should focus on the optimization of the alignment of gelatin scaffolds. In addition, smooth muscle cells, neurons and ICC may have different requirements regarding the substrate stiffness and composition. Therefore a mixture of different materials may be desirable in order to fulfill various biological and mechanical needs. Moreover, special factors for vasculature may also be integrated into the scaffold. With such optimizations of the scaffolds, the functional IMC sheets may eventually become the replacement tissue for treatment of related intestinal diseases.

4.5 Acknowledgements

The author thanks J.C.Y. Dunn for supervising the whole project.

The author also thanks X. Guo, A. Liu and X. Bao for helpful suggestions and critical reading of the manuscript; K. Ding and Z. Wang for scientific discussions; all the staff of the Division of Laboratory Animal Medicine at UCLA.

This research was supported by US National Institutes of Health (NIH) grant R01 DK083119 to J.C.Y.D. and Q.W. was supported by a scholarship from China Scholarship Council (CSC). The funders had no role in study design, data collection and analysis, decision to publish, or preparation of the manuscript.

CHAPTER FIVE

INTESTINAL MUSCLE-EPITHELIUM INTERACTION

5.1 Introduction

In the small intestine, smooth muscle layers initiate peristalsis flow to help with food transit, while the epithelium layer facilitates the food digestion. The crosstalk between epithelium and smooth muscle is crucial for the development of both of them[147]. A recent study[81] reveals that epithelium morphogenesis closely links to the development of the intestinal muscle through a strain-dependent mechanism. Epithelium and intestinal muscle also communicate with each other using a signaling feedback loop which involves Hedgehog, bone morphogenetic protein (BMP) and Wnt pathways[118,148]. It would be beneficial to establish an effective culture condition for further study of the epithelium-smooth muscle interrelationship *in vitro*. Here we show that, when combined with the culture technology of epithelium[18,72–74], the muscularis medium can support not only cells from muscularis, but also cells from mucosa. While epithelium-muscularis co-cultures have been described in other systems[3,26,28,29,35], this is the first primary-cell based epithelium-muscularis co-culture that has spontaneous, periodic contractions.

5.2 Materials and Methods

For materials and methods in “**Mice and human specimens**”, “**IMC isolation** ”, “**Cell culture for IMC**”, “**Contractile assessment**”, “**Immunofluorescence**”, “**Quantitative real-time RT-PCR**”, and “**Statistics**”, please check **CHAPTER TWO, 2.2 Materials and Methods**. The antibodies, validated primers and probes used were listed in **S5.1 Table**.

Isolation of intestinal crypts

Murine intestinal crypts were isolated by a previously reported method[72]. Murine intestinal tissue was removed from the animal and cut open in cold PBS. With mucosa surface facing up, the excess mucoid material was scrapped by the tweezer tips. Next the specimen was washed several times until the solution remained clear. The specimen then was cut into approximately 1 cm^2 pieces, transferred into 30 ml of 2.5 mmol/L EDTA in PBS and incubated for 30 minutes at 4˚C. At the end of incubation, 15 ml supernatant was discarded with intestinal fragments settled at the bottom of the tube. 15 ml of cold PBS was added into the tissue and the total 30 ml solution with tissue was vortexed for 3 seconds x 10 times. After the fragments settled down at the bottom, the supernatant was collected and saved on ice (Crypt fraction 1). 15 ml of PBS was added into the tissue again and the process was repeated six times (Crypt fraction 1-6). Samples then were centrifuged at 100 rcf for 2 minutes. About 13 ml of the supernatant was discarded and the pellets were re-suspended in the rest of the solution with the addition of 10% FBS. The purity of crypt fractions was examined under microscope. Several fractions were pooled together based on the need of experiments. The pooled sample was purified by the combination of a 100-μm and a 70-μm filter (BD Biosciences, Bedford, MA). Next the crypts were spun at 100 rcf for 2 minutes and resuspended at a density of 300 crypts in 25 μl Matrigel (BD Biosciences). The crypts with Matrigel were placed onto the 48-well culture plates. Matrigel was allowed to polymerize at 37 ˚C for 15 minutes. Isolation of human crypts was conducted in a similar way except that instead of 2.5 mM EDTA, 16 mM EDTA with 1 mM Dithiothreitol was used in this procedure. Murine epithelium at Passage 0 to 1 and human epithelium from adult patients at Passage 11 to 12 were used for co-culture.

Intestinal epithelium-IMC co-culture

IMC were cultured in the muscularis medium for 21 days before adding epithelial cells. For passaged epithelial cells, epithelial cells/Matrigel with culture media were removed from the wells and collected into Eppendorf tubes. The cells/Matrigel were quickly spun for 3 seconds x 3 times. Upon removal of the supernatant, 500 µl TrypLE™ Select Enzyme was added to digest the Matrigel for 5 minutes at 37 ˚C. After the digestion, 500 µl DMEM with 10% FBS was added to each tube. The content in each tube was well mixed, and quickly spun for 3 seconds x 3 times. The supernatant was discarded. The pellet was resuspened into the muscularis medium (murine cells) or human muscularis medium (human cells) and directly placed onto the cultured IMC. For fresh crypts, crypts were resuspended into the muscularis medium (murine cells) and directly placed onto the cultured IMC after isolation. For each well on a 24-well plate, about 500 units of epithelial structures or crypts were seeded on IMC. For indirect epithelium-muscle co-culture, the pellet was resuspended in Matrigel and placed onto the 0.4-µm polyester transwell (Fisher) inserts. Matrigel was allowed to polymerize at 37 ˚C for 15 minutes. The inserts then were placed in the wells with IMC cultured at the bottom. Medium was added both in the wells and on top of the inserts. Co-culture was maintained in a 37˚C incubator with 5% carbon dioxide for 4 days.

5.3 Results

Muscularis medium supported both epithelium and IMC with contractions

When incorporated with the culture technology[18] of intestinal epithelium, the muscularis medium can also support the co-culture of both epithelium and functional IMC (**Fig 5.1A**, n = 6 bio-independent samples). In conventional EC medium, the growth of epithelium required exogenous EGF[18]. Without exogenous EGF and matrigel, almost no epithelial cells from the crypts could proliferate (**Fig 5.1B**, n = 3 bio-independent samples). Interestingly, when directly co-cultured with IMC, even without exogenous EGF and matrigel, epithelium in the muscluaris medium did proliferate (Ki67$^+$ cells, **Fig 5.1B**, n = 3 bio-independent samples), suggesting IMC could mediate the proliferation pattern of epithelium. In direct co-culture, the epithelium contained a variety of cell types including enterocytes (*Vil1*), goblet cells (*Muc2*), enteroendocrine cells (*ChgA*), Paneth cells (*Lyz1*) and the epithelial stem cells (*Lgr5*, **Fig 5.1C**, n = 3 bio-independent samples). Immunofluorescence (n = 3 bio-independent samples) showed the co-expression of chromogranin A (Chga), Mucin 2 (Muc 2), lysozyme (Lyz) and villin (Vil, **Fig 5.1D**). IMC in direct co-culture continued to contract and expressed various markers of normal muscularis (**Fig 5.1E**, n = 3 bio-independent samples). Immunofluorescence (n = 3 bio-independent samples) further confirmed the presence of mature smooth muscle cells and the network of ICC (**Fig 5.1F**). Neurons and glial cells in direct co-culture retained the histotypic organization of the enteric ganglia-like neural aggregates, with interconnecting strands and dense mesh of outgrowing processes (**Fig 5.1F**). In addition, serosal mesothelial cells also existed in co-culture (**Fig 5.2**).

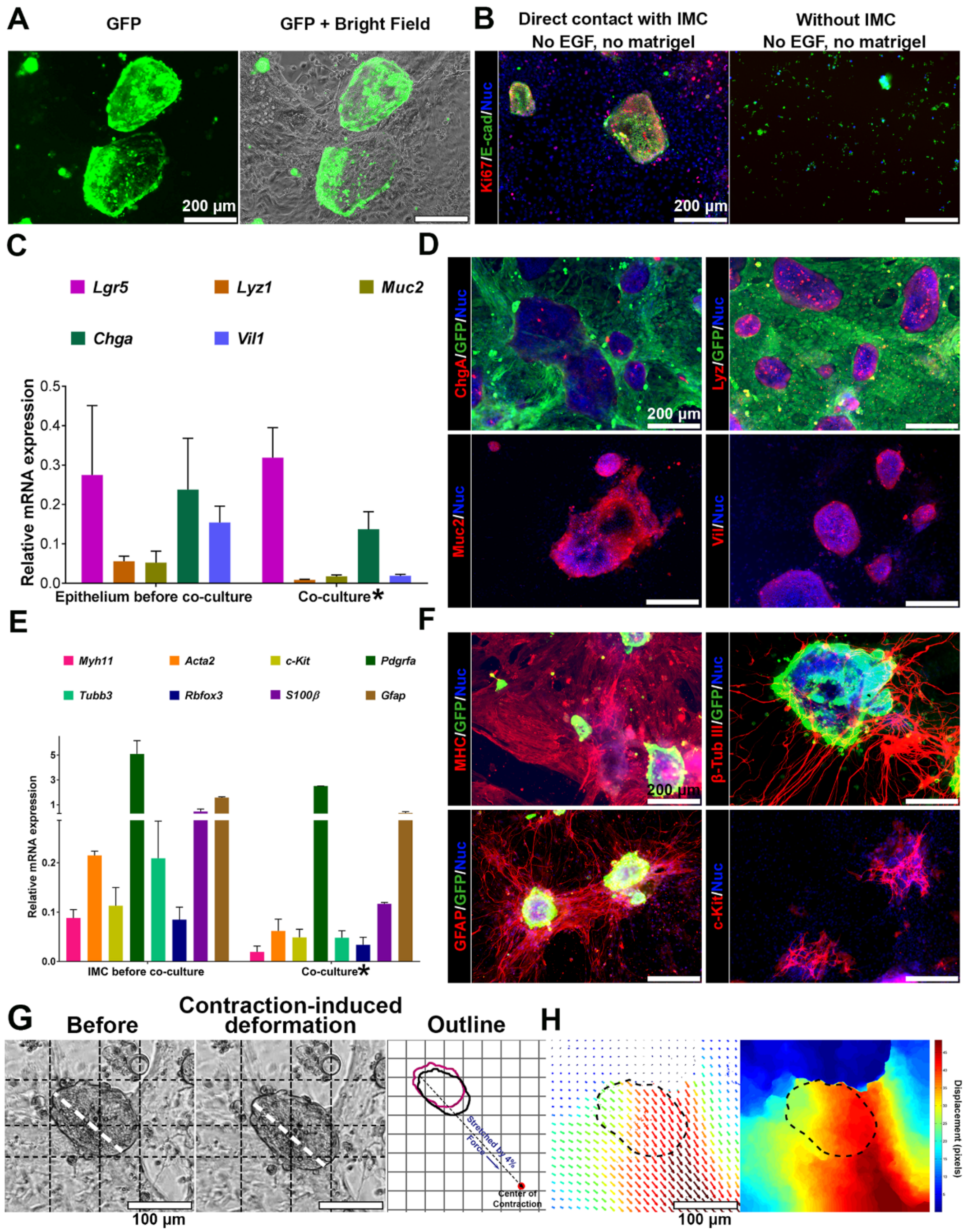

Fig. 5.1 Intestinal epithelium and functional IMC both survive in the muscularis medium. (**A**) GFP epithelium after 4-day co-culture with non-GFP IMC. (**B**) Proliferation (Ki67, red) of epithelium (E-cadherin, E-cad, green) when cultured alone or with IMC. (**C**) Relative mRNA expression of indicated epithelial markers of epithelium before co-culture and cells after 4-day co-culture*. (**D**) Immunofluorescence of ChgA, Lyz, Muc2, Vil and GFP for GFP IMC and non-GFP epithelium after 4-day co-culture. (**E**) Relative mRNA expression of indicated IMC markers of IMC before co-culture and cells after 4-day co-culture*. (**F**) Immunofluorescence of MHC, c-Kit, β-tubulin III, GFAP and GFP for GFP epithelium and non-GFP IMC after 4-day co-culture. (**G**) One representative epithelial cell cluster in co-culture (**S5.1 Video**) before (left) and after (middle) being stretched and the outlines (right image; before: magenta; after: black; grid, 50 μm; dashed line indicates the direction of IMC contraction; the number 4% was a reflection of the length change of the cluster before and after stretching along the direction of IMC contraction). (**H**) Optical-flow analysis of the same epithelial cell cluster in (**G**). The direction and length of arrows represent the direction and magnitude of the displacement at each location. The heat map is to visualize the magnitude of displacement of each pixel as the epithelial cell cluster being stretched. Dashed line outlines the area of the epithelial cell cluster before being stretched. RT-PCR in (**C**, **E**). Control: crypts (**C**), muscle strips (**E**); housekeeping gene: *Gapdh*. Error bars, S.D. (n = 3 biologically independent samples). Scale bars, 200 μm (**A**-**B**, **D**, **F**); 100 μm (**G**-**H**). DAPI (blue) for nuclei in (**B**, **D**, **F**). *The mRNA level in co-culture was normalized to *Gapdh* expressed by **all** cells (both epithelium and IMC) in co-culture. However, most of the epithelial or IMC markers (except *c-Kit*, *Chga* and *Pdgfra*) were mainly expressed by epithelial cells or IMC respectively. Therefore the mRNA level showed here for co-culture is artificially lower.

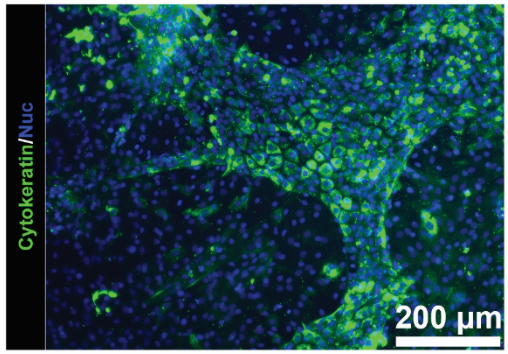

Fig. 5.2 Serosal mesothelial cells also existed in epithelium-muscularis co-culture. Immunofluorescence of cytokeratin after 4-day co-culture of epithelium and IMC.

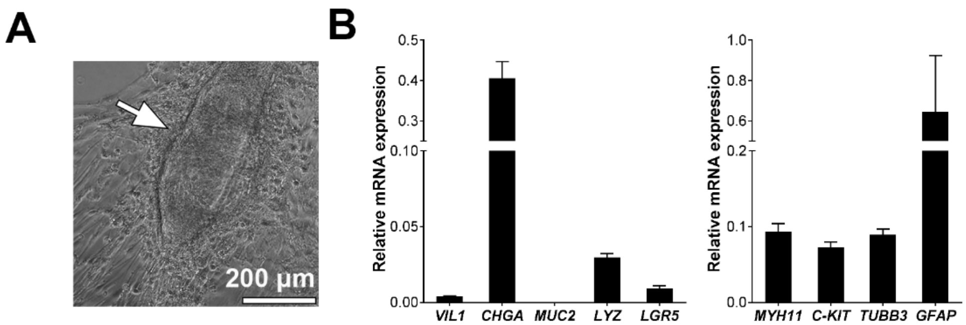

Fig. 5.3 Human IMC and epithelium co-culture in the human muscularis medium. (**A**) IMC and human epithelium (arrow) in co-culture. Scale bar, 200 µm. (**B**) Relative mRNA expression of indicated epithelial or IMC markers of cells after 4-day co-culture. Control: Human crypts or human muscle strips, housekeeping gene: *GAPDH* (see note* in **Fig 5.1**). Error bars, S.D. (n = 3 wells).

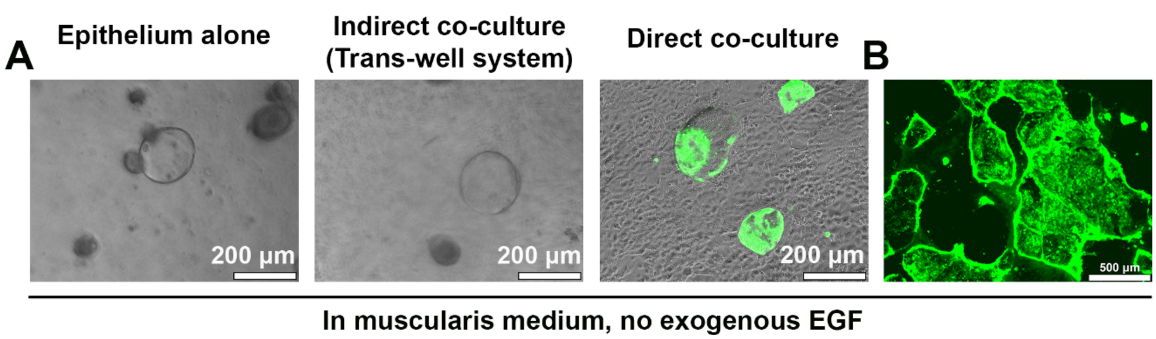

Fig. 5.4 Physical separation abolished the beneficial effects of IMC on intestinal epithelium. (**A**) Representative images of intestinal epithelium cultured for 4 days in monoculture, indirect co-culture with IMC in a trans-well configuration and direct co-culture with IMC (GFP+ epithelium and non-GFP IMC). Scale bars, 200 µm. (**B**) Representative GFP fluorescence image at lower magnification of GFP epithelium in direct co-culture with non-GFP IMC. Scale bar, 500 µm.

IMC contractions also persisted in direct co-culture (**S5.1 Video**, n = 6 bio-independent samples). Epithelial cells mechanically interacted with IMC. Driven by the stress gradient, epithelial cells in direct co-culture were periodically stretched by the contracting IMC (**Fig 5.1G**, **S5.1 Video**). The stress gradient was reflected by the non-uniform displacements within one epithelial cluster (**Fig 5.1H**). The degree of strain was affected by the size of the epithelial structures and their relative location to the contracting IMC.

Directly co-cultured human epithelium and IMC also survived in human muscularis medium (**Fig 5.3**, n = 3 wells). IMC exhibited rhythmic contractions with epithelium attached on top (**S5.2 Video**, n = 3 bio-independent samples).

Physical separation abolished the beneficial effects of IMC on intestinal epithelium

As indicated by Ki67 staining (**Fig 5.1B**), IMC efficiently enhanced the growth of epithelial cells in intimately apposed co-culture. However, when separating the two cell populations by a 0.8-mm distance in a trans-well-engaged indirect co-culture, the beneficial effects of IMC on intestinal epithelium was completely lost (**Fig 5.4**). In the absence of exogenous EGF, no noticeable difference was observed in the size of the epithelial cell clusters between mono-epithelial culture and epithelium-IMC co-culture in the trans-well configuration (**Fig 5.4**). The results suggested that IMC impacts epithelium in a proximity-dependent way.

5.4 Discussion

Intestinal tissue engineering[2,16,149] and strategies of intestinal replacement require regeneration of both functional epithelium and muscularis under defined serum-free conditions. With the addition of intestinal epithelium, the new media here can support not only cells from muscularis, but also up to 11 different cell types from mucosa, muscularis and serosa (**Figs 5.1-5.3**). Our culture system may serve as a platform for more complex and comprehensive studies of other cell types as well. In addition, peristalsis normally results in periodic waves of both muscularis and mucosa. The active mechanical factor is crucial to normal tissue physiology but always missing in traditional culture systems. Although the architecture of the co-culture requires further optimization, our co-culture system has recapitulated the cyclic mechanical strains by the natural contraction of IMC and re-established this coupled mechanical relation between epithelium and muscularis.

5.5 Acknowledgements

The author thanks J.C.Y. Dunn for supervising the whole project; K. Wang for performing the optical flow analysis for videos of co-culture and human samples; P. Lin for assisting the isolation of crypts and providing helpful advice on co-culture experiments; M.G. Martin and C.M. Walthers for editing the manuscript.

The author thanks S.Y. Lewis and J. Wang for providing human intestinal epithelial cells and the RNA of human crypts; all the staff of the Division of Laboratory Animal Medicine at UCLA; V. Ciobanu and his team at Department of Pathology and Laboratory Medicine, David Geffen School of Medicine at UCLA and staff at Ronald Reagan UCLA Medical Center for providing human tissue.

This research was supported by US National Institutes of Health (NIH) grant R01 DK083119 to J.C.Y.D. and Q.W. was supported by a scholarship from China Scholarship Council (CSC). The funders had no role in study design, data collection and analysis, decision to publish, or preparation of the manuscript.

CHAPTER SIX

CONCLUSIONS AND FUTURE DIRECTIONS

6.1 Further improvement of the media

The maintenance of the contractile IMC by the muscularis medium is a result of an intricate balance of different regulators. IMC contains various cell types. Different cells require different signals for their growth and differentiation. A task for near future would be to understand how each component in the muscularis medium would specifically influence each type of cells, and how other molecules could be potentially added into the culture to further improve the support of IMC. To achieve this, the first step would be to identify the molecular signature of SMC, neurons and ICC. Then, the molecular signature of each cell type can be used to screen for molecules that are potentially beneficial to SMC, neurons or ICC and also to track the changes of those cells in culture during the testing process. Once the potential molecule candidates for a specific type of cells are found after the screening, further studies are needed to identify their effects on the neighboring non-target cells in the culture. The concentration of the molecules should be optimized based on not only their beneficial effects of the targeted cell type but also their "side effects" on non-target cells. Finally, the combination of different molecule candidates should also be assessed to further examine the interactions between different compounds. The optimal combination of new molecules can be determined using methods such as factorial designs[150] and media blending[151].

6.2 Conclusions and future directions

This work provides an effective serum-free methodology to restore the contractile function of the intestinal muscularis cells *in vitro*. The most unique and important contribution of this work is that we developed the first serum-free culture media that successfully maintain smooth muscle cells, ICC, the enteric neurons, and the glial cells altogether with appropriate cell morphologies, protein and gene expression, and the continuous periodic contractile activities for an extended time *in vitro*, so far only possible in intact muscle tissue. The work built a more realistic model in therapeutic testing and future mechanistic studies of gut motility disorders. It also expands the toolkit for intestinal regeneration.

However, this is not the end of the story. Several important questions remain. It is still unclear how enteric neurons and muscle affect each other in the intestinal development and homeostasis. Such studies would be a necessary future step and can be investigated utilizing the culture condition established in this work. Another task for the near future would be to optimize the bio-scaffolds for intestinal muscle regeneration to accommodate muscle contractile function and the various needs from different cell populations in the intestinal muscle. Besides, more efforts are required to understand how bioengineered muscle tissue would integrate and react with the surrounding host tissue during implantation.

The future is optimistic. Through integration of multiple disciplines such as biology, material science, data science and medicine, tissue-engineered intestine might eventually become clinically available as a novel treatment for SBS.

APPENDICES

Appendices for Chapter 2

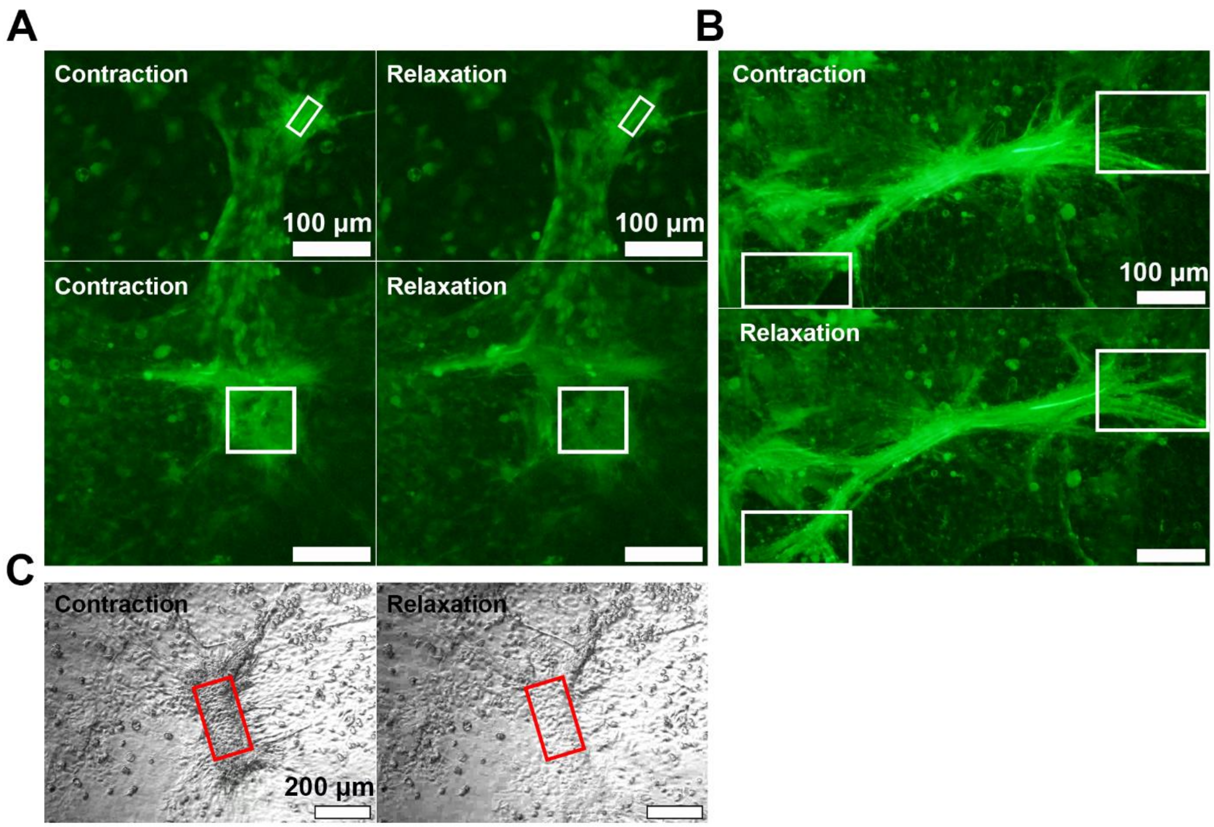

S2.1 Fig. Contractions of cell clusters were represented by the intensity change. (**A**) Averaged fluorescence intensity of regions within the white boxes increased when the cell clusters contracted and decreased when the cell clusters relaxed. (**B**) For non-GFP cells in phase contrast videos, the mean intensity decreased (darker) as the cell cluster turned into contraction state (red boxes). Scale bars, 200 µm. (**C**) The cell cluster contracted to reveal the background at the edge (white boxes). Scale bars in (**A**, **C**), 100 µm.

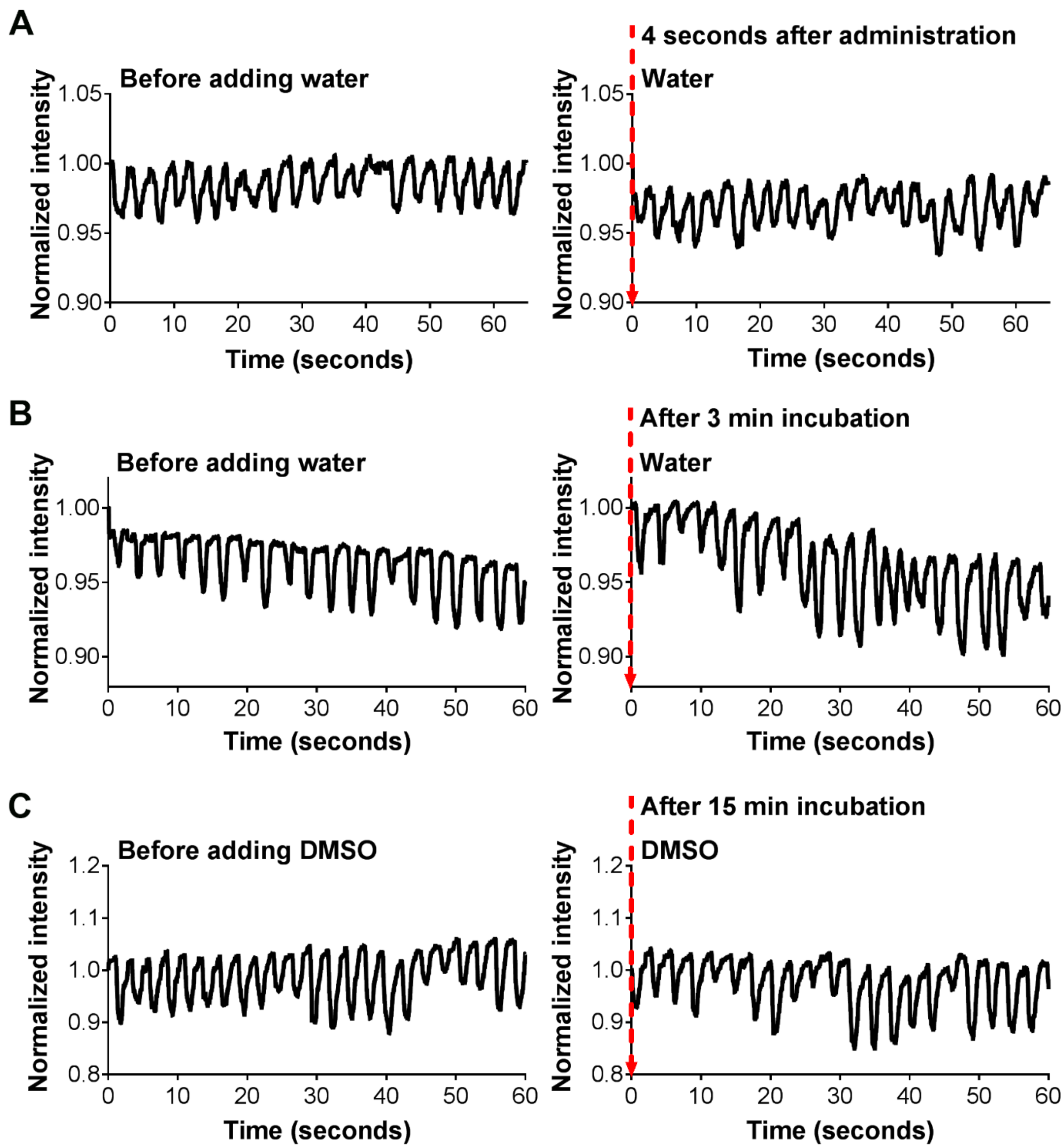

S2.2 Fig. Drug vehicles (distilled water and DMSO) had little effect on the contraction frequency of IMC in the muscularis medium. (**A**) Representative recordings of the immediate effect of distilled water on IMC in the muscularis medium at d28 (n = 3 biologically independent samples). (**B**) Representative recordings of the effect of distilled water on IMC in the muscularis medium at d28 after a 3-min incubation at 37°C (n = 3 biologically independent samples). (**C**) Representative recordings of the effect of DMSO on IMC in the muscularis medium at d28 after a 15-min incubation at 37°C (n = 3 biologically independent samples). Seven different drugs were used in this study, including carbachol, SNP, DMPP, hexamethonium, L-NAME, TTX and niflumic acid. All of the drugs were dissolved in distilled water, except niflumic acid in DMSO. The water solution of carbachol, DMPP and hexamethonium had an immediate effect on IMC, while SNP, L-NAME and TTX required a 3 to 5-min incubation at 37°C before showing a steady effect. We therefore tested the immediate effect of water (**A**) and its later effect after a 3-min incubation at 37°C (**B**). For niflumic acid dissolved in DMSO, IMC was incubated with the drug solution for 15 mins at 37°C prior to video recording. Here we tested the DMSO effect after the 15-min incubation at 37°C.

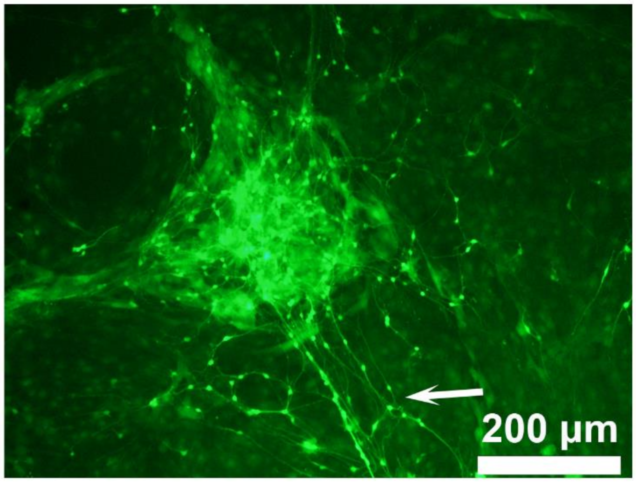

S2.3 Fig. IMC in the EC medium displayed neurites-like structure. Representative GFP fluorescence image of murine IMC in EC medium at day 7. The arrow indicates the neurites-like fibers in culture.

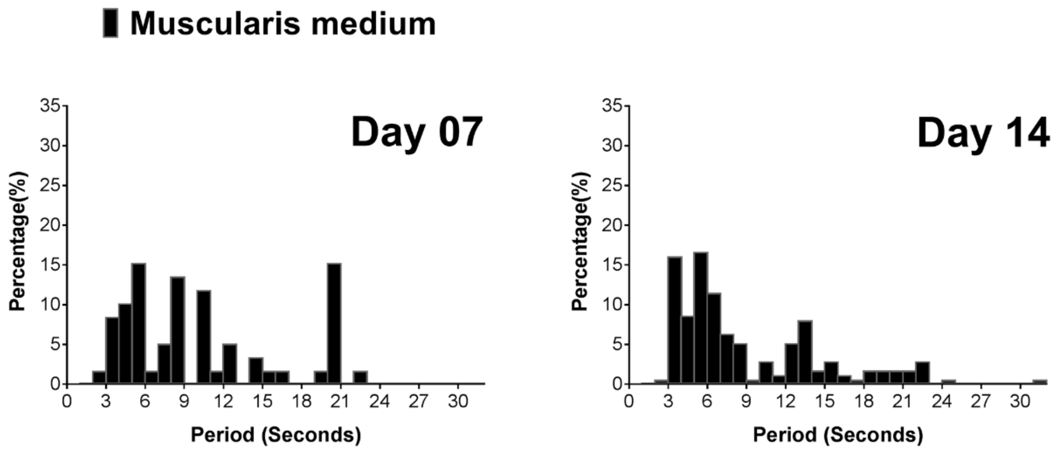

S2.4 Fig. Contractions of IMC at early time points in the muscularis medium. Distributions of contraction periods of IMC in the muscularis medium at day 7 (*59*, **6**; N = *59* cell clusters from n = **6** biologically independent samples) and 14 (*174*, **7**).

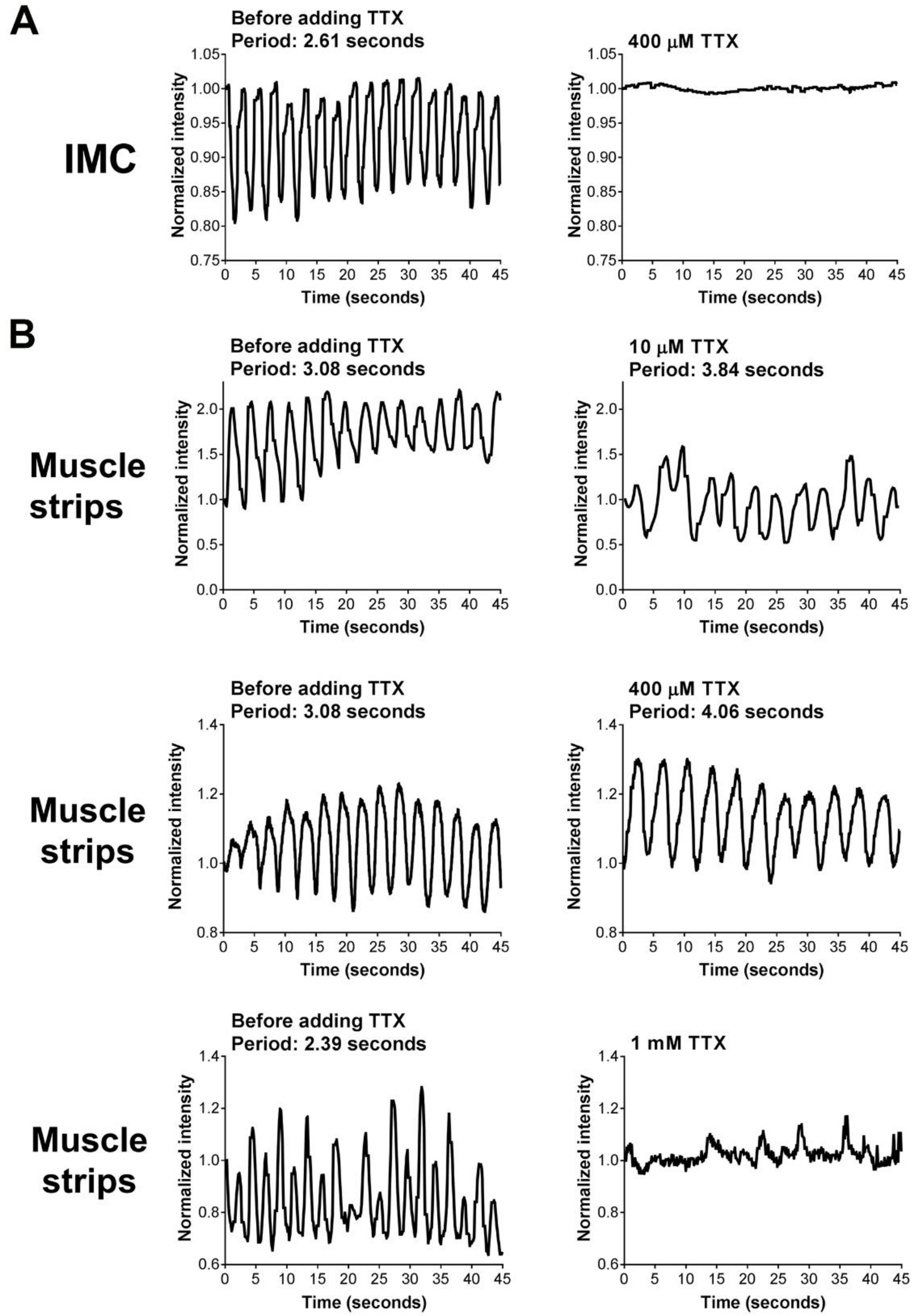

S2.5 Fig. Effects of TTX on fresh muscle strips and IMC in the muscularis medium. (**A**) Representative recordings of the effect of TTX at 400 µM on IMC in the muscularis medium at d28, matching **S2.14 Video**. (**B**) Representative recordings of the effects of TTX at 10 µM, 400 µM and 1 mM on fresh muscle strips, matching **S2.15 Video**.

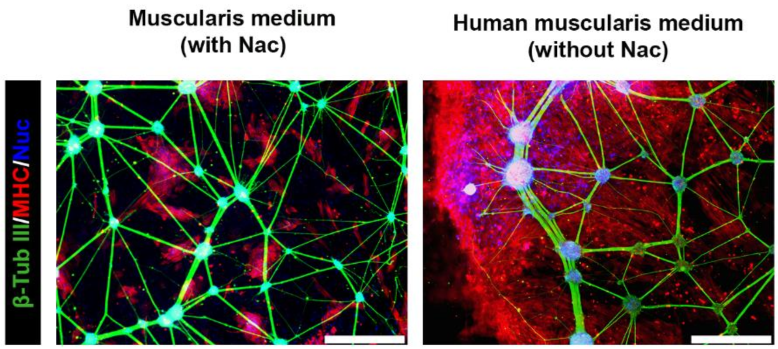

S2.6 Fig. The presence of Nac substantially limited the survival of mature human smooth muscle cells. MHC (smooth muscle cells) and β-Tub III (neurons) staining of human fetal IMC in muscularis medium (with Nac) and human muscularis medium (without Nac) after 21-day culture. DAPI (blue) stained the nuclei.

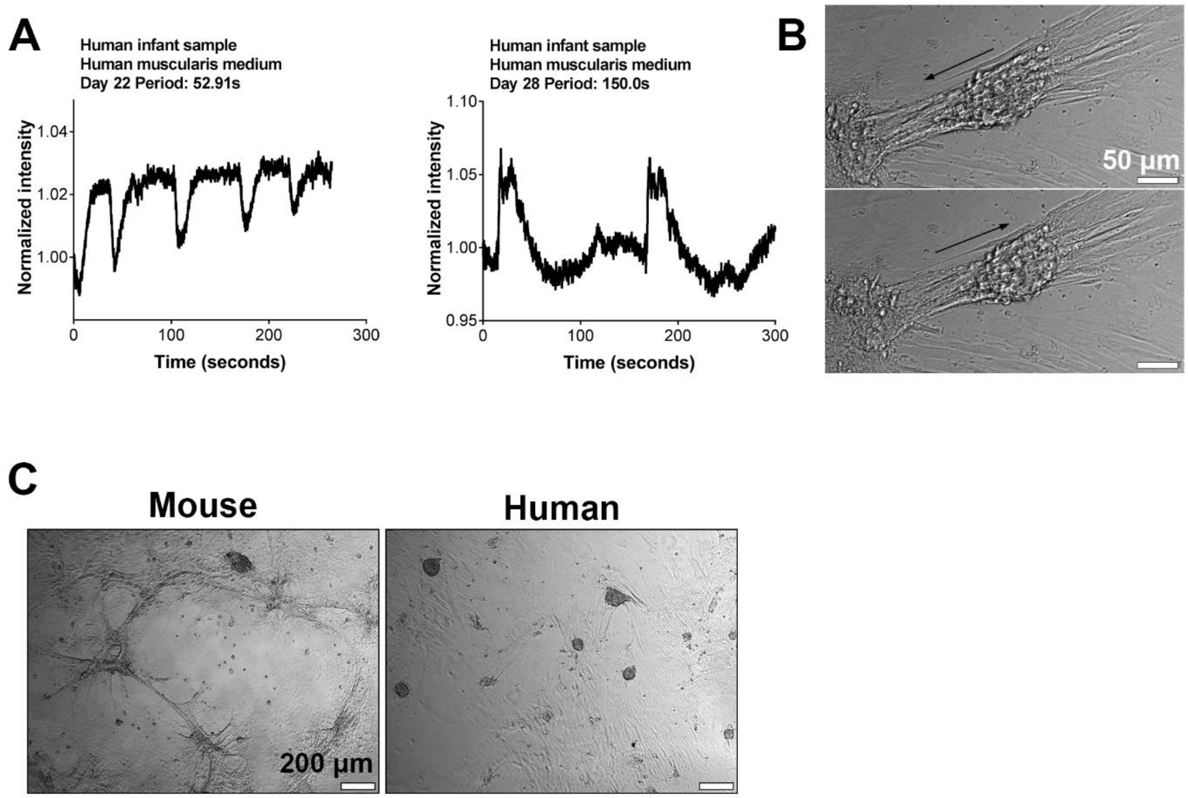

S2.7 Fig. Periodic contractions of human postnatal IMC in the human muscularis medium. (**A**) Recordings of periodic contractions of one human infant IMC cluster in the human muscularis medium at day 22 (**S2.17 Video**). (**B**) Recordings of periodic contractions of one human postnatal IMC cluster in the human muscularis medium at day 28 (left) and its phase contrast images at contraction and relaxation states (right), corresponding to **S2.17 Video**. Black arrows indicate the direction of movement. Scale bars, 50 µm. (**C**) Morphological difference between murine and human infant IMC at day 28 in the muscularis and human muscularis media, respectively. Similar to the contractions of murine IMC, contractions of human infant IMC were also initiated at the location of the cell clusters. In general, the human intestinal muscularis complexes were denser and smaller than the murine intestinal muscularis complexes. Scale bars, 200 µm.

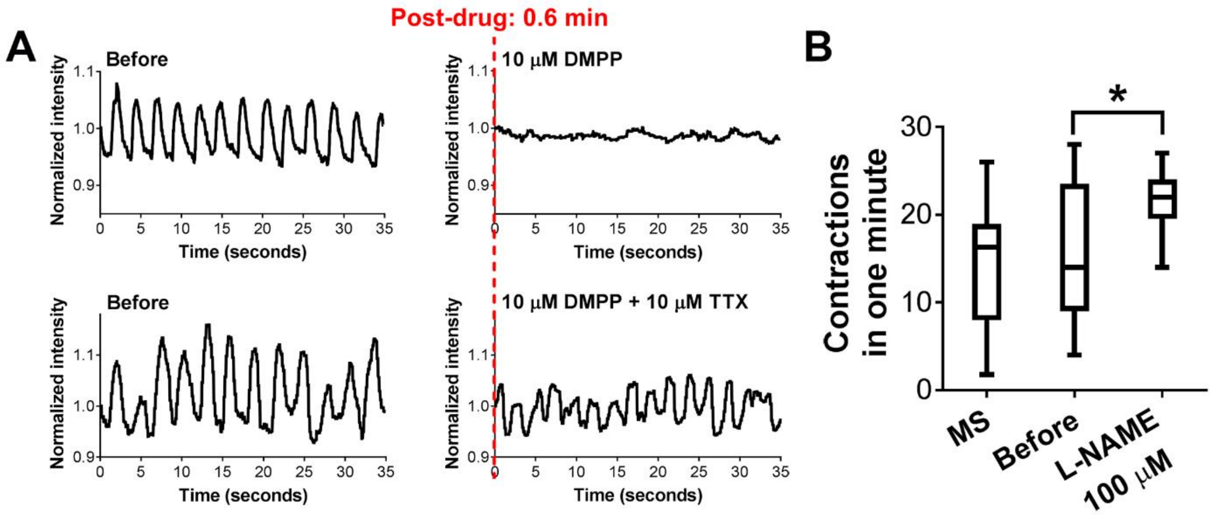

S2.8 Fig. Supplemental information of DMPP, TTX and L-NAME effects. (**A**) Representative recordings of the effects of 10 μM DMPP or DMPP with 10 μM TTX (5 min pretreatment) on IMC cultured in the muscularis medium at d28. (**B**) Numbers of contractions in one minute of muscle strips (MS, N = 62 spots from n = 21 animals) and IMC in the muscularis medium at d28 before and after adding 100 μM L-NAME (N = 25 cell clusters from n = 3 biologically independent samples; two-tailed paired Student's t-test, **p* < 0.05). Standard Tukey box-plots. All the contractile assessments were conducted at room temperature (22 to 25 °C).

S2.1 Table Antibodies, primers and probes used in the study (Chapter 2)

Primary antibodies for immunostaining			
Target	Vendor	Catalog #	Dilution
Smooth muscle myosin heavy chain 11	Abcam (Cambridge, MA)	ab53219	1: 100
Neuron specific beta III Tubulin	Abcam	ab78078	1: 200
GFAP	Abcam	ab7260	1: 200
Wide spectrum cytokeratin	Abcam	ab9377	1: 200
CD117 (c-Kit)	eBioscience (San Diego, CA)	16-1172-82	1: 200
Secondary antibodies for immunostaining			
Product name	Vendor	Catalog #	Dilution
Alexa Fluor® 594 goat anti-mouse IgG	Life Technologies	A-11032	1: 200
Alexa Fluor® 594 goat anti-rabbit IgG	Life Technologies	A-11037	1: 200*
Alexa Fluor® 488 goat anti-mouse IgG	Life Technologies	A-11029	1: 200
Alexa Fluor® 488 goat anti-rabbit IgG	Life Technologies	A-11034	1: 200*
Alexa Fluor® 594 goat anti-rat IgG	Life Technologies	A-11007	1: 200

Note: * For staining of myosin heavy chain, the dilution of the secondary antibody is 1:100.

Primers and probes for real time RT-PCR			
TaqMan® Gene Expression Assays			
Gene symbol	Taqman Assay ID	Gene symbol	Taqman Assay ID
Gapdh	Mm99999915_g1	*Chat*	Mm01221880_m1
Myh11	Mm00443013_m1	*Calb1*	Mm00486647_m1
Acta2	MM01546133_m1	*Vip*	Mm00660234_m1
Pdgfra	Mm00440701_m1	*Th*	Mm00447557_m1

Tubb3	Mm00727586_s1	*Nos1*	Mm01208059_m1
Rbfox3	Mm01248771_m1	*Syp*	Mm00436850_m1
S100β	Mm00485897_m1	*Dlg4*	Mm00492193_m1
Gfap	Mm01253033_m1		
Customized primers and probes for real time RT-PCR			
Gene symbol	Sequences		
c-Kit	forward primer CCGTGAACTCCATGTGGCTAAAGA, reverse primer GGTGCCAGCTATTGTGCTTTACCT, probe [6-FAM]-TGAACCCTCAGCCTCAGCACATAGC[Tamra-Q]		
MYH11	forward primer AAGCTCTGGAAGAGGGGAAG, reverse primer GCTGAAGCCTGTTCTTGGTC		
C-KIT	forward primer TGACTTACGACAGGCTCGTG, reverse primer CCACTGGCAGTACAGAAGCA		
TUBB3	forward primer AACGAGGCCTCTTCTCACAA, reverse primer GGCCTGAAGAGATGTCCAAA		
GFAP	forward primer ACATCGAGATCGCCACCTAC, reverse primer ATCTCCACGGTCTTCACCAC		
GAPDH	forward primer CAGCCTCAAGATCATCAGCA, reverse primer TGTGGTCATGAGTCCTTCCA		

S2.2 Table Components in the EC medium and their possible functions in IMC culture

Component	*In vitro* effects on IMC culture	For IMC contractility
Advanced DMEM/F12	Nutrient provider	Required
B27	Role in neural differentiation and growth	Required
N2	Role in neural differentiation and growth	Required
HEPES (*10 mM*)	pH adjuster	Required
GlutaMAX (*2 mM*)	Maintenance of cell culture	Required
Antibiotic-antimycotic	Antibiotics	Not necessary
N-Acetylcysteine (Nac, *1 mM*)	Prevention of neuronal apoptosis; induction of apoptosis in smooth muscle cells	Having controversial effects; concentration need to be carefully decided
Y27632 (*10 μM*)	Pathway signal (ROCK inhibitor)	Together required, synergistic effect, potentially targeting ICC and smooth muscle cells
R-Spondin1 (*1 μg/ml*)	Pathway signal (Wnt pathway enhancer)	
Noggin (*100 ng/ml*)	Pathway signal (BMP pathway inhibitor)	
EGF (*50 ng/ml*)	Cell proliferation	"Inhibiting" IMC contraction

EC medium

Muscularis medium

Nutritious basal

Signaling controller

S2.3 Table Selected results of medium component assessment for IMC culture

A

From EC medium, subtracting:	IMC contraction
B27	–
N2	–
HEPES	–
GlutaMAX	–
N-Acetylcysteine (Nac)	–
Y27632	–
R-Spondin1	–
Noggin	–
EGF	+++

B

From EC medium, subtracting:	IMC contraction
B27, EGF	++
N2, EGF	++
HEPES, EGF	++
GlutaMAX, EGF	++
Nac, EGF	++
Y27632, EGF	++
R-Spondin1, EGF	++
Noggin & EGF	++

C

From EC medium, subtracting:	IMC contraction
Y27632, R-Spondin1, EGF	++
Y27632, Noggin, EGF	++
R-Spondin1, Noggin, EGF	++
Y27632, R-Spondin1, Noggin, EGF	++

D

From DMEM, adding:	IMC contraction
B27	–
N2	–
HEPES	–
GlutaMAX	–
N-Acetylcysteine (Nac)	–
Y27632	–
R-Spondin1	–
Noggin	–

E

From DMEM, adding:	IMC contraction
B27,N2	–
B27,Nac	–
N2, Nac	–
B27,N2,Nac	–
B27, HEPES	+

Note: **(A-C)** Components in EC medium were subtracted either alone or in combination at a time. **(D-E)** Components were added in basal DMEM either alone or in combination at a time. Prior to the evaluation of contractility, IMC were cultured for 14 days in each condition. "–", no contraction after culture for 14 days; "+", visible, spontaneous contraction; "++", visible, spontaneous, periodic contraction; "+++", visible, spontaneous, periodic contractions with a higher contraction frequency.

S2.1 Note The development of the muscularis medium for IMC culture

The EC medium contained 10 different supplements (**S2.2 Table**). We conducted a thorough literature review and summarized potential effects of each supplement on IMC culture (**S2.2 Table**)[27,84,85,152–154]. Based on previous studies and our initial results, we hypothesized that, one or more components in EC medium inhibited IMC contraction. In addition, we assumed that antibiotic-antimycotic (ABAM, the antibiotics) in EC medium had little effect on IMC contractility and did not perform any test related to this component. To identify critical components for IMC contraction, we subtracted each component at a time from EC medium and assessed the contractility of murine IMC in resultant media after 14-day culture (**S2.3A Table**). We observed that, upon withdrawal of EGF from EC medium, murine IMC in this new medium (the muscularis medium) started to generate consistent periodic contractions similar to those from native tissue, implying that EGF in EC medium prevented IMC contraction. Also studies have shown that EGF can induce the dedifferentiation of smooth muscle cells[23].The "inhibitory" effect of EGF on IMC contraction was further confirmed by the fact that the established contractions of IMC in muscularis medium could be abolished by the addition of EGF at the same concentration.

We separated components in the muscularis medium into two groups: the nutritious basal group, in which components provided the basic nutrients for cell differentiation and growth; and the signaling controller group containing the signal molecules that regulates different pathways (**S2.2 Table**). We then subtracted components in the muscularis medium one at a time to test whether the remaining components were all required for IMC contraction. We found that removing any component from the muscularis medium attenuated but not completely abolished IMC contractions (**S2.3B Table**). In addition, each component alone is not sufficient to initiate contractions (**S2.3D Table**). These results, when combined, indicated that it is the synergistic effect of all the components in the muscularis medium that promoted the spontaneous and periodic contractions with a frequency matching that of native tissue (at day 28).

To identify the minimum components required for the initiation of IMC contraction, we first investigated the effects of signal molecules and subtracted them either alone or in combination from the muscularis medium (**S2.3B**, **C Table**). Our results revealed that removal of all the three signal molecules together did not abolish the contraction but reduced the contraction speed (**S2.3C Table**). We then analyzed the components in the nutritious basal group with emphasis on B27, N2 and Nac (**S2.3E Table**). These molecules are known to have positive effects on the growth and differentiation of ENS[27,155], which might be crucial for IMC contractility. We also noted that when HEPES, the pH adjustor, was added in system, more neurons were preserved. As summarized in **S2.3E Table**, B27, N2, and Nac, either alone or in combination, could not provide sufficient support for IMC to generate contraction within 14 days. However, in the presence of HEPES, B27 and HEPES could promote the contraction of IMC. In summary, the minimum essential factor cocktail to initiate IMC contraction was B27 plus HEPES, but cells in this medium contracted in an irregular manner. The inclusion of Noggin, R-spondin and Y27632 (NRY) in the muscularis medium improved the contractility of IMC to better match that of muscle strips, however, after removing NRY from the muscularis medium, it was still sufficient to maintain the periodic contractions of IMC for over 56 days except with a broader distribution of periods that peaked around 5 seconds (i.e. cells contract in a slower manner).

S2.1 Code Contraction frequency test for GFP cells

```
function multiROI()

[filename,filepath,~] = uigetfile('*.*',  'All Files (*.*)');

video_handle = VideoReader(fullfile(filepath, filename));

reference_frame = read(video_handle, 1);

frame_num = video_handle.NumberOfFrames;

% compute an average intensity change map

average_intensity_change = zeros(video_handle.Height, video_handle.Width);

for frame_idx = 1 : frame_num

    curr_frame = read(video_handle, frame_idx);

    average_intensity_change = average_intensity_change + im2double(curr_frame(:, :,
2));

end

average_intensity_change = average_intensity_change ./ frame_num;

%figure(1), subplot(121); imshow(reference_frame);

figure(1), imagesc(average_intensity_change); axis image;

roi_num =input('Input the number of ROIs you want to select in this video:');

roi_masks = cell(roi_num, 1);

roi_images = cell(roi_num, 1);

for roi_idx = 1 : roi_num
```

```
    message = sprintf('%d out of %d ROI. Left click and hold to begin drawing.\nSimply
lift the mouse button to finish',...
        roi_idx, roi_num);
    uiwait(msgbox(message));
    hFH = imfreehand();
    roi_masks{roi_idx} = hFH.createMask();
    pos = hFH.getPosition();
    % define bounding box
    x1 =  max(1, min(round(min(pos(:,2))), video_handle.Height));
    y1 =  max(1, min(round(min(pos(:,1))), video_handle.Width));
    x2 =  max(1, min(round(max(pos(:,2))), video_handle.Height));
    y2 =  max(1, min(round(max(pos(:,1))), video_handle.Width));
    roi_image_r = reference_frame(:, :, 1) .* uint8(roi_masks{roi_idx});
    roi_image_g = reference_frame(:, :, 2) .* uint8(roi_masks{roi_idx});
    roi_image_b = reference_frame(:, :, 3) .* uint8(roi_masks{roi_idx});
    roi_images{roi_idx} = cat(3, ...
        roi_image_r(x1:x2, y1:y2), ...
        roi_image_g(x1:x2, y1:y2), ...
        roi_image_b(x1:x2, y1:y2));
end
```

```
fprintf('Start processing.\n');

average_intensity = zeros(frame_num, roi_num);

average_interval = 1.0 / video_handle.FrameRate;

for i = 1 : frame_num

    raw_frame = read(video_handle, i);

    green_channel = double(raw_frame(:, :, 2));

    % abandon red and blue channel, because mostly no data is available

    for roi_idx = 1 : roi_num

        average_intensity(i, roi_idx) = mean(green_channel(roi_masks{roi_idx}));

    end

end

% filter out the first dark period

thres = mean(average_intensity) - 3 * std(average_intensity);

valid_frame_indices = zeros(roi_num, 1);

for roi_idx = 1 : roi_num

    indices = sort(find(average_intensity(:, roi_idx) >= thres(roi_idx)), 'ascend');

    valid_frame_indices(roi_idx) = indices(1);

end

for roi_idx = 1 : roi_num
```

```
figure; hold on;
title(sprintf('ROI %d', roi_idx));
subplot(231); imagesc(roi_images{roi_idx}(:, :, 2)); axis image; title(sprintf('Image ROI %d', roi_idx));
axis off;
truncated_average_intensity = average_intensity(valid_frame_indices(roi_idx):end, roi_idx);
truncated_timestamps = [valid_frame_indices(roi_idx) : frame_num] .* average_interval;
Y = fft(truncated_average_intensity);
n=length(Y);
Y=Y(1:ceil(n/2));
n=length(Y);
mY=abs(Y);
subplot(233); hold on;
FREQ=(0:n-1)*(video_handle.FrameRate /(2*n));
semilogy(FREQ, mY);
xlabel('Frequency (Hz)');
title('Periodogram of Depolarization');
subplot(232); hold on;
```

```
xlabel('Time (seconds)');

ylabel('Intensity (percent)');

title('Mean Intensity Over Time');

plot(truncated_timestamps, truncated_average_intensity);

Z=fftshift(mY);

f0 = (-n/2:n/2-1)*.5*(video_handle.FrameRate/(length(Y)));  % 0-centered frequency
range

subplot(235); hold on;

plot(f0,Z);

xlabel('Frequency (Hz)');

title('Zero-shift Periodogram of Depolarization');

[pks,locs] = findpeaks(Z);

[pkvals,idx] = sort(pks,'descend'); %sort to vector

pkvals(2); %second largest value - the first is always 0 and doesn't mean anything

index=find(Z==pkvals(2));

mainFrequencyStr=num2str(f0(index));

plot(f0(index),Z(index),'r.', 'MarkerSize',25);

text(f0(index),Z(index),['Frequency = ',mainFrequencyStr, ' Hz']);

Frequency = f0(index);

axis([0 ceil(10*f0(index)) 0 ceil(2*pkvals(2))]);
```

```
    fprintf('ROI %d: Frequency %f Hz\n', roi_idx, f0(index));

    % I do the same thing for the inverse of the frequency, aka the period.

    period=1./FREQ;

    subplot(236); hold on;

    plot(period,mY);

    [pks2,locs2] = findpeaks(mY);

    [pkvals2,idx2] = sort(pks2,'descend'); %sort to vector

    pkvals2(1); % largest value

    index2=find(mY==pkvals2(1));

    mainPeriodStr=num2str(period(index2));

    plot(period(index2),mY(index2),'r.', 'MarkerSize',25);

    text(period(index2),mY(index2),['Period = ',mainPeriodStr, ' Seconds']);

    xlabel('Period (seconds)');

    axis([0 ceil(2*period(index2)) 0 ceil(2*pkvals2(1))]);

    fprintf('ROI %d: Period %f seconds.\n', roi_idx, period(index2));

end

end
```

S2.2 Code Contraction frequency test for GFP cells (strong background noise)

Also used for testing the frequency of the oscillations of fluorescently labeled Ca^{2+}

```
function multiROI_heq()

[filename,filepath,~] = uigetfile('*.*',  'All Files (*.*)');

video_handle = VideoReader(fullfile(filepath, filename));

frame_num = video_handle.NumberOfFrames;

% compute an average intensity change map

average_intensity_change = zeros(video_handle.Height, video_handle.Width);

average_frame_intensity = zeros(frame_num, 1);

for frame_idx = 1 : frame_num

    curr_frame = im2double(read(video_handle, frame_idx));

    average_intensity_change = average_intensity_change + curr_frame(:, :, 2);

    average_frame_intensity(frame_idx) = mean(mean(curr_frame(:, :, 2)));

end

average_intensity_change = average_intensity_change ./ frame_num;

[sorted_intensity, sorted_idx] = sort(average_frame_intensity);

reference_index = find(sorted_intensity >= median(average_frame_intensity));

reference_index = sorted_idx(reference_index(1));

reference_frame = read(video_handle, reference_index);

reference_hist = imhist(reference_frame(:, :, 2));

%figure(1), subplot(121); imshow(reference_frame);
```

```
figure(1), imagesc(average_intensity_change); axis image;


roi_num =input('Input the number of ROIs you want to select in this video:');

roi_masks = cell(roi_num, 1);

roi_images = cell(roi_num, 1);

for roi_idx = 1 : roi_num

    message = sprintf('%d out of %d ROI. Left click and hold to begin drawing.\nSimply
lift the mouse button to finish',...

        roi_idx, roi_num);

    uiwait(msgbox(message));

    hFH = imfreehand();

    roi_masks{roi_idx} = hFH.createMask();

    pos = hFH.getPosition();

    % define bounding box

    x1 =  max(1, min(round(min(pos(:,2))), video_handle.Height));

    y1 =  max(1, min(round(min(pos(:,1))), video_handle.Width));

    x2 =  max(1, min(round(max(pos(:,2))), video_handle.Height));

    y2 =  max(1, min(round(max(pos(:,1))), video_handle.Width));

    roi_image_r = reference_frame(:, :, 1) .* uint8(roi_masks{roi_idx});

    roi_image_g = reference_frame(:, :, 2) .* uint8(roi_masks{roi_idx});
```

```
    roi_image_b = reference_frame(:, :, 3) .* uint8(roi_masks{roi_idx});
    roi_images{roi_idx} = cat(3, ...
        roi_image_r(x1:x2, y1:y2), ...
        roi_image_g(x1:x2, y1:y2), ...
        roi_image_b(x1:x2, y1:y2));
end
fprintf('Start processing.\n');
average_intensity = zeros(frame_num, roi_num);
raw_intensity = zeros(frame_num, roi_num);
average_interval = 1.0 / video_handle.FrameRate;
for i = 1 : frame_num
    raw_frame = read(video_handle, i);
    raw_channel = double(raw_frame(:, :, 2));
    green_channel = double(histeq(raw_frame(:, :, 2), reference_hist));
    % abandon red and blue channel, because mostly no data is available
    for roi_idx = 1 : roi_num
        average_intensity(i, roi_idx) = mean(green_channel(roi_masks{roi_idx}));
        raw_intensity(i, roi_idx) = mean(raw_channel(roi_masks{roi_idx}));
    end
```

```
end

for roi_idx = 1 : roi_num

    figure; title(sprintf('ROI %d', roi_idx));

    % show original roi image patch

    subplot(121);

    imagesc(roi_images{roi_idx}(:, :, 2)); axis image; axis off;

    title(sprintf('Image ROI %d', roi_idx));

    truncated_average_intensity = average_intensity(:, roi_idx);

    truncated_timestamps = (1 : frame_num) .* average_interval;

    % show average intensity over time

    subplot(122); hold on;

    plot(truncated_timestamps, truncated_average_intensity); hold on;

    filtered_average_intensity = medfilt1(truncated_average_intensity, 30);

    [pks, locs] = findpeaks(filtered_average_intensity);

    locs = truncated_timestamps(locs);

    scatter(locs, pks, 'v');

    xlabel('Time (seconds)');

    ylabel('Average Intensity');

    title('Mean Intensity Over Time');
```

```
    Y = fft(truncated_average_intensity);
    n=length(Y);
    Y=Y(1:ceil(n/2));
    n=length(Y);
    mY=abs(Y);
    Z=fftshift(mY);
    f0 = (-n/2:n/2-1)*.5*(video_handle.FrameRate/(length(Y)));  % 0-centered frequency range
    [pks,locs] = findpeaks(Z);
    [pkvals,~] = sort(pks,'descend'); %sort to vector
    index=find(Z==pkvals(2));
    fprintf('ROI %d: FFT based frequency %f(Hz).\n', ...
        roi_idx, f0(index));
    fprintf('ROI %d: FFT based period %f(seconds)\n', ...
        roi_idx, 1 ./ f0(index));
end
end
```

S2.3 Code Contraction frequency test for non-GFP cells

```
function multiROI_heq()
[filename,filepath,~] = uigetfile('*.*',  'All Files (*.*)');
```

```
video_handle = VideoReader(fullfile(filepath, filename));

frame_num = video_handle.NumberOfFrames;

% compute an average intensity change map

average_intensity_change = zeros(video_handle.Height, video_handle.Width);

average_frame_intensity = zeros(frame_num, 1);

for frame_idx = 1 : frame_num

    curr_frame = rgb2gray(im2double(read(video_handle, frame_idx)));

    average_intensity_change = average_intensity_change + curr_frame;%(:, :, 2);

    average_frame_intensity(frame_idx) = mean(mean(curr_frame));

end

average_intensity_change = average_intensity_change ./ frame_num;

[sorted_intensity, sorted_idx] = sort(average_frame_intensity);

reference_index = find(sorted_intensity >= median(average_frame_intensity));

reference_index = sorted_idx(reference_index(1));

reference_frame = rgb2gray(read(video_handle, reference_index));

reference_hist = imhist(reference_frame);

%figure(1), subplot(121); imshow(reference_frame);

figure(1), imagesc(histeq(average_intensity_change)); axis image;

roi_num =input('Input the number of ROIs you want to select in this video:');
```

```
roi_masks = cell(roi_num, 1);

roi_images = cell(roi_num, 1);

for roi_idx = 1 : roi_num

    message = sprintf('%d out of %d ROI. Left click and hold to begin drawing.\nSimply
lift the mouse button to finish',...

        roi_idx, roi_num);

    uiwait(msgbox(message));

    hFH = imfreehand();

    roi_masks{roi_idx} = hFH.createMask();

    pos = hFH.getPosition();

    % define bounding box

    x1 =  max(1, min(round(min(pos(:,2))), video_handle.Height));

    y1 =  max(1, min(round(min(pos(:,1))), video_handle.Width));

    x2 =  max(1, min(round(max(pos(:,2))), video_handle.Height));

    y2 =  max(1, min(round(max(pos(:,1))), video_handle.Width));

    roi_image = reference_frame .* uint8(roi_masks{roi_idx});

    roi_images{roi_idx} = roi_image;

end

fprintf('Start processing.\n');

average_intensity = zeros(frame_num, roi_num);
```

```
raw_intensity = zeros(frame_num, roi_num);

average_interval = 1.0 / video_handle.FrameRate;

for i = 1 : frame_num

    raw_frame = rgb2gray(read(video_handle, i));

    raw_channel = double(raw_frame);

   green_channel = double(histeq(raw_frame, reference_hist));

    for roi_idx = 1 : roi_num

        average_intensity(i, roi_idx) = mean(green_channel(roi_masks{roi_idx}));

        raw_intensity(i, roi_idx) = mean(raw_channel(roi_masks{roi_idx}));

    end

end

for roi_idx = 1 : roi_num

    figure; title(sprintf('ROI %d', roi_idx));

    % show original roi image patch

    subplot(121);

    imagesc(roi_images{roi_idx}); axis image; axis off;

    title(sprintf('Image ROI %d', roi_idx));

    truncated_average_intensity = average_intensity(:, roi_idx);

    truncated_timestamps = (1 : frame_num) .* average_interval;
```

```
% show average intensity over time

subplot(122); hold on;

plot(truncated_timestamps, truncated_average_intensity); hold on;

filtered_average_intensity = medfilt1(truncated_average_intensity, 30);

[pks, locs] = findpeaks(filtered_average_intensity);

locs = truncated_timestamps(locs);

scatter(locs, pks, 'v');

xlabel('Time (seconds)');

ylabel('Average Intensity');

title('Mean Intensity Over Time');

Y = fft(truncated_average_intensity);

n=length(Y);

Y=Y(1:ceil(n/2));

n=length(Y);

mY=abs(Y);

Z=fftshift(mY);

f0 = (-n/2:n/2-1)*.5*(video_handle.FrameRate/(length(Y)));  % 0-centered frequency
range

[pks,locs] = findpeaks(Z);

[pkvals,~] = sort(pks,'descend'); %sort to vector
```

```
    index=find(Z==pkvals(2));
   fprintf('ROI %d: FFT based frequency %f(Hz).\n', ...
       roi_idx, f0(index));
    fprintf('ROI %d: FFT based period %f(seconds)\n', ...
       roi_idx, 1 ./ f0(index));
end
end
```

Appendices for Chapter 3

S3.1 Table Gene enrichment analysis of PC1 highest loading genes (Top 10 GO terms)

Positive loading		
ID	Name	*p*-value
GO:0002376	immune system process	1.93E-98
GO:0006955	immune response	2.97E-87
GO:0006952	defense response	1.82E-75
GO:0002682	regulation of immune system process	8.72E-62
GO:0002684	positive regulation of immune system process	3.19E-61
GO:0009605	response to external stimulus	7.35E-59
GO:0006954	inflammatory response	4.77E-56
GO:0050896	response to stimulus	6.75E-53
GO:0006950	response to stress	1.66E-52
GO:0001775	cell activation	9.04E-52
Negative loading		
ID	Name	*p*-value
GO:0043269	regulation of ion transport	2.30E-23
GO:0032501	multicellular organismal process	1.45E-22
GO:0030182	neuron differentiation	3.71E-22
GO:0048699	generation of neurons	5.11E-22
GO:0006812	cation transport	8.96E-22

GO:0065008	regulation of biological quality	1.10E-21
GO:0051049	regulation of transport	4.31E-21
GO:0003008	system process	6.14E-21
GO:0022008	neurogenesis	6.90E-21
GO:0006936	muscle contraction	1.25E-20

Appendices for Chapter 5

S5.1 Table Antibodies, primers and probes used in the study (Chapter 5)

Primary antibodies for immunostaining			
Target	Vendor	Catalog #	Dilution
Smooth muscle myosin heavy chain 11	Abcam (Cambridge, MA)	ab53219	1: 100
Neuron specific beta III Tubulin	Abcam	ab78078	1: 200
GFAP	Abcam	ab7260	1: 200
Wide spectrum cytokeratin	Abcam	ab9377	1: 200
GFP	Abcam	ab13970	1: 200
CD117 (c-Kit)	eBioscience (San Diego, CA)	16-1172-82	1: 200
Villin	Santa Cruz (San Cruz, CA)	sc-28283	1: 200
Lysozyme	Santa Cruz	sc-292850	1: 200
Mucin 2	Santa Cruz	sc-7314	1: 200
Chromogranin A	Santa Cruz	sc-393941	1: 200
Ki67	Abcam	ab16667	1: 200
E-Cadherin	BD biosciences (San Jose, CA)	610182	1: 200
Secondary antibodies for immunostaining			
Product name	Vendor	Catalog #	Dilution
Alexa Fluor® 594 goat anti-mouse IgG	Life Technologies	A-11032	1: 200
Alexa Fluor® 594 goat anti-rabbit IgG	Life Technologies	A-11037	1: 200*
Alexa Fluor® 488 goat anti-mouse IgG	Life Technologies	A-11029	1: 200
Alexa Fluor® 488 goat anti-rabbit IgG	Life Technologies	A-11034	1: 200*

Alexa Fluor® 488 goat anti-chicken IgY	Abcam	ab150169	1: 200
Alexa Fluor® 594 goat anti-rat IgG	Life Technologies	A-11007	1: 200

Note: * For staining of myosin heavy chain, the dilution of the secondary antibody is 1:100.

Primers and probes for real time RT-PCR

TaqMan® Gene Expression Assays

Gene symbol	Taqman Assay ID	Gene symbol	Taqman Assay ID
Gapdh	Mm99999915_g1	*Chat*	Mm01221880_m1
Myh11	Mm00443013_m1	*Calb1*	Mm00486647_m1
Acta2	MM01546133_m1	*Vip*	Mm00660234_m1
Pdgfra	Mm00440701_m1	*Th*	Mm00447557_m1
Tubb3	Mm00727586_s1	*Nos1*	Mm01208059_m1
Rbfox3	Mm01248771_m1	*Syp*	Mm00436850_m1
S100β	Mm00485897_m1	*Dlg4*	Mm00492193_m1
Gfap	Mm01253033_m1	*GAPDH*	Hs02758991_g1
Lyz1	Mm00657323_m1	*MUC2*	Hs03005103_g1
Muc2	Mm01276696_m1	*LYZ*	Hs00426232_m1
Chga	Mm00514341_m1	*CHGA*	Hs00900375_m1
Vil1	Mm00494146_m1	*VIL1*	Hs01031724_m1
Lgr5	Mm00438890_m1	*LGR5*	Hs00969422_m1

Customized primers and probes for real time RT-PCR

Gene symbol	Sequences
c-Kit	forward primer CCGTGAACTCCATGTGGCTAAAGA, reverse primer GGTGCCAGCTATTGTGCTTTACCT, probe [6-FAM]-TGAACCCTCAGCCTCAGCACATAGC[Tamra-Q]

MYH11	forward primer AAGCTCTGGAAGAGGGGAAG, reverse primer GCTGAAGCCTGTTCTTGGTC
C-KIT	forward primer TGACTTACGACAGGCTCGTG, reverse primer CCACTGGCAGTACAGAAGCA
TUBB3	forward primer AACGAGGCCTCTTCTCACAA, reverse primer GGCCTGAAGAGATGTCCAAA
GFAP	forward primer ACATCGAGATCGCCACCTAC, reverse primer ATCTCCACGGTCTTCACCAC
GAPDH	forward primer CAGCCTCAAGATCATCAGCA, reverse primer TGTGGTCATGAGTCCTTCCA

REFERENCES

1. Shekherdimian, S., Scott, A., Chan, A. & Dunn, J. C. Y. Intestinal lengthening in rats after massive small intestinal resection. *Surgery* **146,** 291–5 (2009).

2. Dunn, J. C. Y. Is the tissue-engineered intestine clinically viable? *Nat. Clin. Pract. Gastroenterol. Hepatol.* **5,** 366–7 (2008).

3. Grikscheit, T. C. *et al.* Tissue-engineered small intestine improves recovery after massive small bowel resection. *Ann. Surg.* **240,** 748–754 (2004).

4. Norsa, L. *et al.* Long term outcomes of intestinal rehabilitation in children with neonatal very short bowel syndrome: Parenteral nutrition or intestinal transplantation. *Clin. Nutr.* **xxx,** 1–8 (2018).

5. Sullins, V. F. *et al.* Intestinal lengthening in an innovative rodent surgical model. *J. Pediatr. Surg.* **49,** 1791–1794 (2014).

6. Squires, R. H. *et al.* Natural history of pediatric intestinal failure: initial report from the Pediatric Intestinal Failure Consortium. *J. Pediatr.* **161,** 723–8.e2 (2012).

7. Wales, P. W. & Christison-Lagay, E. R. Short bowel syndrome: epidemiology and etiology. *Semin. Pediatr. Surg.* **19,** 3–9 (2010).

8. Bharadwaj, S. *et al.* Update on the management of intestinal failure. *Cleve. Clin. J. Med.* **83,** 841–848 (2016).

9. Seidner, D. L. *et al.* Reduction of Parenteral Nutrition and Hydration Support and Safety With Long-Term Teduglutide Treatment in Patients With Short Bowel Syndrome−Associated Intestinal Failure: STEPS-3 Study. *Nutr. Clin. Pract.* **33,**

520–527 (2018).

10. Rouch, J. D. & Dunn, J. C. Y. New insights and interventions for short bowel syndrome. *Curr Pediatr Rep.* **5,** 1–5 (2017).

11. Sullins, V. F. *et al.* Function of mechanically lengthened jejunum after restoration into continuity. *J. Pediatr. Surg.* **49,** 971–975 (2014).

12. Scott, A. *et al.* Mechanical lengthening in multiple intestinal segments in-series. *J. Pediatr. Surg.* **51,** 957–959 (2016).

13. Park, J., Puapong, D. P., Wu, B. M., Atkinson, J. B. & Dunn, J. C. Y. Enterogenesis by mechanical lengthening: Morphology and function of the lengthened small intestine. *J. Pediatr. Surg.* **39,** 1823–1827 (2004).

14. Huynh, N. *et al.* Three-dimensionally printed surface features to anchor endoluminal spring for distraction enterogenesis. *PLoS One* **13,** e0200529 (2018).

15. Dubrovsky, G. & Dunn, J. C. Y. Mechanisms for intestinal regeneration. *Curr. Opin. Pediatr.* **30,** 424–429 (2018).

16. Shieh, S. J. & Vacanti, J. P. State-of-the-art tissue engineering: From tissue engineering to organ building. *Surgery* **137,** 1–7 (2005).

17. Sato, T. & Clevers, H. Growing self-organizing mini-guts from a single intestinal stem cell: mechanism and applications. *Science (80-.).* **340,** 1190–4 (2013).

18. Sato, T. *et al.* Single Lgr5 stem cells build crypt-villus structures in vitro without a mesenchymal niche. *Nature* **459,** 262–5 (2009).

19. Yin, X. *et al.* Niche-independent high-purity cultures of Lgr5+ intestinal stem cells

and their progeny. *Nat. Methods* **11,** 106–12 (2014).

20. Rich, A. *et al.* Local presentation of Steel factor increases expression of c-kit immunoreactive interstitial cells of Cajal in culture. *Am. J. Physiol. Gastrointest. Liver Physiol.* **284,** G313–G320 (2003).

21. Jessen, K. R., Saffrey, M. J. & Burnstock, G. The enteric nervous system in tissue culture. I. Cell types and their interactions in explants of the myenteric and submucous plexuses from guinea pig, rabbit and rat. *Brain Res.* **262,** 17–35 (1983).

22. Nakayama, S. & Torihashi, S. Spontaneous rhythmicity in cultured cell clusters isolated from mouse small intestine. *Jpn. J. Physiol.* **52,** 217–27 (2002).

23. Sobue, K., Hayashi, K. & Nishida, W. Expressional regulation of smooth muscle cell-specific genes in association with phenotypic modulation. *Mol. Cell. Biochem.* **190,** 105–18 (1999).

24. Wang, Y., Ahmad, A. a, Sims, C. E., Magness, S. T. & Allbritton, N. L. In vitro generation of colonic epithelium from primary cells guided by microstructures. *Lab Chip* **14,** 1622–31 (2014).

25. Wells, J. M. & Spence, J. R. How to make an intestine. *Development* **141,** 752–60 (2014).

26. Workman, M. J. *et al.* Engineered human pluripotent-stem-cell-derived intestinal tissues with a functional enteric nervous system. *Nat. Med.* **23,** 49–61 (2016).

27. Fattahi, F. *et al.* Deriving human ENS lineages for cell therapy and drug discovery in Hirschsprung disease. *Nature* **531,** 105–109 (2016).

28. Kuwahara, M. *et al.* In vitro organogenesis of gut-like structures from mouse

embryonic stem cells. *Neurogastroenterol Motil* **16,** 14–18 (2004).

29. Yoshida, A., Chitcholtan, K., Evans, J. J., Nock, V. & Beasley, S. W. In vitro tissue engineering of smooth muscle sheets with peristalsis using a murine induced pluripotent stem cell line. *J. Pediatr. Surg.* **47,** 329–35 (2012).

30. Múnera, J. O. *et al.* Differentiation of Human Pluripotent Stem Cells into Colonic Organoids via Transient Activation of BMP Signaling. *Cell Stem Cell* **21,** 51–64.e6 (2017).

31. Raghavan, S. & Bitar, K. N. The influence of extracellular matrix composition on the differentiation of neuronal subtypes in tissue engineered innervated intestinal smooth muscle sheets. *Biomaterials* **35,** 7429–40 (2014).

32. Zakhem, E., Raghavan, S., Gilmont, R. R. & Bitar, K. N. Chitosan-based scaffolds for the support of smooth muscle constructs in intestinal tissue engineering. *Biomaterials* **33,** 4810–4817 (2012).

33. Rego, S. L., Zakhem, E., Orlando, G. & Bitar, K. N. Bioengineering functional human sphincteric and non-sphincteric gastrointestinal smooth muscle constructs. *Methods* (2015). doi:10.1016/j.ymeth.2015.08.014

34. Grikscheit, T. C. *et al.* Tissue-engineered large intestine resembles native colon with appropriate in vitro physiology and architecture. *Ann. Surg.* **238,** 35–41 (2003).

35. Levin, D. E. *et al.* Human tissue-engineered small intestine forms from postnatal progenitor cells. *J. Pediatr. Surg.* **48,** 129–37 (2013).

36. Gjorevski, N. *et al.* Designer matrices for intestinal stem cell and organoid culture. *Nature* **539,** 560–564 (2016).

37. Cortez, A. R. *et al.* Transplantation of human intestinal organoids into the mouse mesentery: A more physiologic and anatomic engraftment site. *Surg. (United States)* **0,** 1–8 (2018).

38. Zakhem, E., Elbahrawy, M., Orlando, G. & Bitar, K. N. Successful implantation of an engineered tubular neuromuscular tissue composed of human cells and chitosan scaffold. *Surgery* **158,** 1598–1608 (2015).

39. Stankus, J. J., Guan, J., Fujimoto, K. & Wagner, W. R. Microintegrating smooth muscle cells into a biodegradable, elastomeric fiber matrix. *Biomaterials* **27,** 735–44 (2006).

40. Olsson, C. & Holmgren, S. The control of gut motility. *Comp. Biochem. Physiol. Part A Mol. Integr. Physiol.* **128,** 479–501 (2001).

41. Campbell, I. Gut motility and its control. *Anaesth. Intensive Care Med.* **13,** 59–61 (2012).

42. Sanders, K. M., Koh, S. D., Ro, S. & Ward, S. M. Regulation of gastrointestinal motility--insights from smooth muscle biology. *Nat. Rev. Gastroenterol. Hepatol.* **9,** 633–45 (2012).

43. Program, E. N. & Rochester, M. C. Kit / stem cell factor receptor-induced phosphatidylinositol 3 ¢ -kinase signalling is not required for normal development and function of interstitial cells of Cajal in mouse gastrointestinal tract. *Neurogastroenterol Motil* **15,** 643–653 (2003).

44. Walthers, C. M., Lee, M., Wu, B. M. & Dunn, J. C. Y. Smooth Muscle Strips for Intestinal Tissue Engineering. *PLoS One* **9,** e114850 (2014).

45. Zakhem, E., Raghavan, S. & Bitar, K. N. Neo-innervation of a bioengineered intestinal smooth muscle construct around chitosan scaffold. *Biomaterials* **35,** 1882–9 (2014).

46. Collins, J., Borojevic, R., Verdu, E. F., Huizinga, J. D. & Ratcliffe, E. M. Intestinal microbiota influence the early postnatal development of the enteric nervous system. *Neurogastroenterol. Motil.* **26,** 98–107 (2014).

47. Ueno, T., Duenes, J. A., Zarroug, A. E. & Sarr, M. G. Nitrergic mechanisms mediating inhibitory control of longitudinal smooth muscle contraction in mouse small intestine. *J. Gastrointest. Surg.* **8,** 831–841 (2004).

48. Chamley-Campbell, J., Campbell, G. R. & Ross, R. The smooth muscle cell in culture. *Physiol. Rev.* **59,** 1–61 (1979).

49. Nakayama, S., Kajioka, S., Goto, K., Takaki, M. & Liu, H. N. Calcium-associated mechanisms in gut pacemaker activity. *J. Cell. Mol. Med.* **11,** 958–968 (2007).

50. Furness, J. B. The enteric nervous system and neurogastroenterology. *Nat. Rev. Gastroenterol. Hepatol.* **9,** 286–294 (2012).

51. Boesmans, W., Lasrado, R., Vanden Berghe, P. & Pachnis, V. Heterogeneity and phenotypic plasticity of glial cells in the mammalian enteric nervous system. *Glia* **63,** 229–241 (2015).

52. Blair, P. J., Rhee, P. L., Sanders, K. M. & Ward, S. M. The significance of interstitial cells in neurogastroenterology. *J. Neurogastroenterol. Motil.* **20,** 294–317 (2014).

53. Wieck, M. M. *et al.* Human and murine tissue-engineered colon exhibit diverse neuronal subtypes and can be populated by enteric nervous system progenitor cells

when donor colon is aganglionic. *Tissue Eng. Part A* **22,** 53–64 (2016).

54. Orlando, G. *et al.* Cell and organ bioengineering technology as applied to gastrointestinal diseases. *Gut* **62,** 774–86 (2013).

55. Moore-Olufemi, S. D., Olsen, A. B., Hook-Dufresne, D. M., Bandla, V. & Cox, C. S. Transforming Growth Factor-Beta 3 Alters Intestinal Smooth Muscle Function: Implications for Gastroschisis-Related Intestinal Dysfunction. *Dig. Dis. Sci.* **60,** 1206–1214 (2014).

56. Bitar, K. N., Raghavan, S. & Zakhem, E. Tissue engineering in the gut: Developments in neuromusculature. *Gastroenterology* **146,** 1614–1624 (2014).

57. Scirocco, A. *et al.* Cellular and Molecular Mechanisms of Phenotypic Switch in Gastrointestinal Smooth Muscle. *J. Cell. Physiol.* **231,** 295–302 (2016).

58. Rodríguez, L. V *et al.* Clonogenic multipotent stem cells in human adipose tissue differentiate into functional smooth muscle cells. *Proc. Natl. Acad. Sci. U. S. A.* **103,** 12167–12172 (2006).

59. Brittingham, J., Phiel, C., Trzyna, W. C., Gabbeta, V. & McHugh, K. M. Identification of distinct molecular phenotypes in cultured gastrointestinal smooth muscle cells. *Gastroenterology* **115,** 605–617 (1998).

60. Revaud, J., Weinzaepfel, P., Harchaoui, Z. & Schmid, C. EpicFlow : Edge-Preserving Interpolation of Correspondences for Optical Flow. in *CVPR - IEEE Conference on Computer Vision & Pattern Recognition* (2015). doi:10.1063/1.4905777

61. Gulbransen, B. D. & Sharkey, K. A. Purinergic Neuron-to-Glia Signaling in the

Enteric Nervous System. *Gastroenterology* **136,** 1349–1358 (2009).

62. McGrath, J. C., Monaghan, S., Templeton, A. G. B. & Wilson, V. G. Effects of basal and acetylcholine-induced release of endothelium-derived relaxing factor on contraction to alpha-adrenoceptor agonists in a rabbit artery and corresponding veins. *Br. J. Pharmacol.* **99,** 77–86 (1990).

63. Hwang, S. J. *et al.* Expression of anoctamin 1/TMEM16A by interstitial cells of Cajal is fundamental for slow wave activity in gastrointestinal muscles. *J Physiol* **587,** 4887–904 (2009).

64. Benabdallah, H., Messaoudi, D. & Gharzouli, K. The spontaneous mechanical activity of the circular smooth muscle of the rabbit colon in vitro. *Pharmacol. Res.* **57,** 132–141 (2008).

65. Frei, E. *et al.* Calcium-dependent and calcium-independent inhibition of contraction by cGMP/cGKI in intestinal smooth muscle. *Am. J. Physiol. Gastrointest. Liver Physiol.* **297,** G834-9 (2009).

66. Yanagida, H., Yanase, H., Sanders, K. M. & Ward, S. M. Intestinal surgical resection disrupts electrical rhythmicity, neural responses, and interstitial cell networks. *Gastroenterology* **127,** 1748–1759 (2004).

67. Tsvilovskyy, V. V. *et al.* Deletion of TRPC4 and TRPC6 in Mice Impairs Smooth Muscle Contraction and Intestinal Motility In Vivo. *Gastroenterology* **137,** 1415–1424 (2009).

68. Hara, Y., Kubota, M. & Szurszewski, J. H. Electrophysiology of smooth muscle of the small intestine of some mammals. *J. Physiol.* **372,** 501–20 (1986).

69. Cordero-Erausquin, M., Marubio, L. M., Klink, R. & Changeux, J. P. Nicotinic receptor function: New perspectives from knockout mice. *Trends Pharmacol. Sci.* **21,** 211–217 (2000).

70. BerčíK, P., Bouley, L., Dutoit, P., Blum, A. L. & Kucera, K. Quantitative analysis of intestinal motor patterns: Spatiotemporal organization of nonneural pacemaker sites in the rat ileum. *Gastroenterology* **119,** 386–394 (2000).

71. Hibberd, T. J. *et al.* Synaptic Activation of Putative Sensory Neurons By Hexamethonium-Sensitive Nerve Pathways in Mouse Colon. *Am. J. Physiol. - Gastrointest. Liver Physiol.* **314,** G53–G64 (2018).

72. Lei, N. Y. *et al.* Intestinal subepithelial myofibroblasts support the growth of intestinal epithelial stem cells. *PLoS One* **9,** e84651 (2014).

73. Lahar, N. *et al.* Intestinal subepithelial myofibroblasts support in vitro and in vivo growth of human small intestinal epithelium. *PLoS One* **6,** e26898 (2011).

74. Chen, Y. *et al.* Application of three-dimensional imaging to the intestinal crypt organoids and biopsied intestinal tissues. *Sci. World J.* **2013,** 624342 (2013).

75. Komuro, T. *Atlas of Interstitial Cells of Cajal in the Gastrointestinal Tract*. (Springer Dordrecht Heigelberg London, 2012). doi:10.1017/CBO9781107415324.004

76. Hao, M. M. & Young, H. M. Development of enteric neuron diversity. *J. Cell. Mol. Med.* **13,** 1193–1210 (2009).

77. Jessen, K. R. & Mirsky, R. Glial cells in the enteric nervous system contain glial fibrillary acidic protein. *Nature* **286,** 736–737 (1980).

78. Zhang, Q. *et al.* Expression of neurexin and neuroligin in the enteric nervous system

and their down-regulated expression levels in Hirschsprung disease. *Mol. Biol. Rep.* **40,** 2969–2975 (2013).

79. Azuma, Y. T., Samezawa, N., Nishiyama, K., Nakajima, H. & Takeuchi, T. Differences in time to peak carbachol-induced contractions between circular and longitudinal smooth muscles of mouse ileum. *Naunyn. Schmiedebergs. Arch. Pharmacol.* **389,** 63–72 (2016).

80. Bolton, B. T. B. The depolarizing action of acetylcholine or carbachol in intestinal smooth muscle. *J. Physiol.* 647–671 (1972).

81. Shyer, A. E. *et al.* Villification: how the gut gets its villi. *Science* **342,** 212–8 (2013).

82. Berridge, M. J. Smooth muscle cell calcium activation mechanisms. *J. Physiol.* **586,** 5047–61 (2008).

83. Sanders, K. . & Ward, S. . Nitric oxide as a mediator of nonadrenergic noncholinergic neurotransmission. *Am. J. Physiol.* **262,** G379–G392 (1992).

84. Chen, S. *et al.* N-acetyl-L-cysteine protects against cadmium-induced neuronal apoptosis by inhibiting ROS-dependent activation of Akt/mTOR pathway in mouse brain Sujuan. *Neuropathol Appl Neurobiol.* **40,** 759–777 (2014).

85. Tsai, J. C. *et al.* Induction of apoptosis by pyrrolidinedithiocarbamate and N-acetylcysteine in vascular smooth muscle cells. *J. Biol. Chem.* **271,** 3667–70 (1996).

86. Huber, A. & Badylak, S. F. Phenotypic changes in cultured smooth muscle cells: limitation or opportunity for tissue engineering of hollow organs? *J. Tissue Eng. Regen. Med.* **6,** 505–11 (2012).

87. Kim, H. J., Huh, D., Hamilton, G. & Ingber, D. E. Human gut-on-a-chip inhabited by

microbial flora that experiences intestinal peristalsis-like motions and flow. *Lab Chip* **12,** 2165–74 (2012).

88. Wang, Q. *et al.* Bioengineered intestinal muscularis complexes with long-term spontaneous and periodic contractions. *PLoS One* **13,** e0195315 (2018).

89. Dobin, A. *et al.* STAR: Ultrafast universal RNA-seq aligner. *Bioinformatics* **29,** 15–21 (2013).

90. Anders, S., Pyl, P. T. & Huber, W. HTSeq-A Python framework to work with high-throughput sequencing data. *Bioinformatics* **31,** 166–169 (2015).

91. Love, M. I., Huber, W. & Anders, S. Moderated estimation of fold change and dispersion for RNA-seq data with DESeq2. *Genome Biol.* **15,** 1–21 (2014).

92. Huang, D. W., Sherman, B. T. & Lempicki, R. A. Systematic and integrative analysis of large gene lists using DAVID bioinformatics resources. *Nat. Protoc.* **4,** 44–57 (2009).

93. Goldstein, A., Hofstra, R. & Burns, A. Building a brain in the gut: development of the enteric nervous system. *Clin. Genet.* **83,** 307–316 (2013).

94. Wang, Z., Wang, D.-Z., Pipes, G. C. T. & Olson, E. N. Myocardin is a master regulator of smooth muscle gene expression. *Proc. Natl. Acad. Sci. U. S. A.* **100,** 7129–34 (2003).

95. Zacharias, W. J. *et al.* Hedgehog signaling controls homeostasis of adult intestinal smooth muscle. *Dev. Biol.* **355,** 152–162 (2011).

96. Halim, D. *et al.* Loss-of-Function Variants in MYLK Cause Recessive Megacystis Microcolon Intestinal Hypoperistalsis Syndrome. *Am. J. Hum. Genet.* **101,** 123–129

(2017).

97. Abouhamed, M., Reichenberg, S., Robenek, H. & Plenz, G. Tropomyosin 4 expression is enhanced in dedifferentiating smooth muscle cells in vitro and during atherogenesis. *Eur. J. Cell Biol.* **82,** 473–482 (2003).

98. Moussallem, M. D., Olenych, S. G., Scott, S. L., Keller, T. C. S. & Schlenoff, J. B. Smooth muscle cell phenotype modulation and contraction on native and cross-linked polyelectrolyte multilayers. *Biomacromolecules* **10,** 3062–3068 (2009).

99. Reynolds, C. M., Eguchi, S., Frank, G. D. & Motley, E. D. Signaling mechanisms of heparin-binding epidermal growth factor-like growth factor in vascular smooth muscle cells. *Hypertension* **39,** 525–9 (2002).

100. Evangelista, L. S. *et al.* Sildenafil promotes smooth muscle preservation and ameliorates fibrosis through modulation of extracellular matrix and tissue growth factor gene expression after bilateral cavernosal nerve resection in the rat. *J Sex Med* **8,** 1048–1060 (2011).

101. Muñoz-Cánoves, P., Scheele, C., Pedersen, B. K. & Serrano, A. L. Interleukin-6 myokine signaling in skeletal muscle: A double-edged sword? *FEBS J.* **280,** 4131–4148 (2013).

102. Chen, S.-E., Jin, B. & Li, Y.-P. TNF-α regulates myogenesis and muscle regeneration by activating p38 MAPK. *Am j Physiol Cell Physiol.* **292,** C1660–C1671 (2007).

103. Hannon, K., Kudla, A. J., McAvoy, M. J., Clase, K. L. & Olwin, B. B. Differentially expressed fibroblast growth factors regulate skeletal muscle development through

autocrine and paracrine mechanisms. *J Cell Biol* **132,** 1151–1159 (1996).

104. Dahiya, S. *et al.* Elevated levels of active matrix metalloproteinase-9 cause hypertrophy in skeletal muscle of normal and dystrophin-deficient mdx mice. *Hum. Mol. Genet.* **20,** 4345–4359 (2011).

105. Zheng, B., Han, M. & Wen, J. K. Role of Krüppel-like factor 4 in phenotypic switching and proliferation of vascular smooth muscle cells. *IUBMB Life* **62,** 132–139 (2010).

106. Aksoy, I. *et al.* Klf4 and Klf5 differentially inhibit mesoderm and endoderm differentiation in embryonic stem cells. *Nat. Commun.* **5,** (2014).

107. Zhu, Y. *et al.* Restenosis Inhibition and Re-differentiation of TGFβ/Smad3-activated Smooth Muscle Cells by Resveratrol. *Sci. Rep.* **7,** 1–17 (2017).

108. Vanuytsel, T., Senger, S., Fasano, A. & Shea-Donohue, T. Major signaling pathways in intestinal stem cells. *Biochim. Biophys. Acta* **1830,** 2410–26 (2013).

109. Li, X. *et al.* Deconvoluting the intestine: molecular evidence for a major role of the mesenchyme in the modulation of signaling cross talk. *Physiol. Genomics* **29,** 290–301 (2007).

110. Hao, M. M. *et al.* Enteric nervous system assembly: Functional integration within the developing gut. *Dev. Biol.* **417,** 168–181 (2016).

111. Johannes, J. & Thuneberg, L. Interstitial Cells of Cajal in Human Small Intestine. *Gastroenterology* **100,** 1417–1431 (1991).

112. Pai, A., Leaf, E. M., El-Abbadi, M. & Giachelli, C. M. Elastin degradation and vascular smooth muscle cell phenotype change precede cell loss and arterial

medial calcification in a uremic mouse model of chronic kidney disease. *Am. J. Pathol.* **178,** 764–773 (2011).

113. Li, D. Y. *et al.* Elastin is an essential determinant of arterial morphogenesis. *Nature* **393,** 276–280 (1998).

114. Golder, M. *et al.* Longitudinal muscle shows abnormal relaxation responses to nitric oxide and contains altered levels of NOS1 and elastin in uncomplicated diverticular disease. *Color. Dis.* **9,** 218–228 (2007).

115. Karnik, S. K. *et al.* A critical role for elastin signaling in vascular morphogenesis and disease. *Development* **130,** 411–423 (2003).

116. Kanehisa, M., Furumichi, M., Tanabe, M., Sato, Y. & Morishima, K. KEGG: New perspectives on genomes, pathways, diseases and drugs. *Nucleic Acids Res.* **45,** D353–D361 (2017).

117. Bolcato-Bellemin, A. L. *et al.* Laminin α5 chain is required for intestinal smooth muscle development. *Dev. Biol.* **260,** 376–390 (2003).

118. McLin, V. a, Henning, S. J. & Jamrich, M. The role of the visceral mesoderm in the development of the gastrointestinal tract. *Gastroenterology* **136,** 2074–91 (2009).

119. Hruska, M. & Dalva, M. B. Ephrin regulation of synapse formation, function and plasticity. *Mol Cell Neurosci.* **50,** 35–44 (2012).

120. Kan, L. *et al.* Rho-Associated Kinase Inhibitor (Y-27632) Attenuates Doxorubicin-Induced Apoptosis of Human Cardiac Stem Cells. *PLoS One* **10,** 1–21 (2015).

121. Lee, J., Park, S. & Roh, S. Y-27632, a ROCK inhibitor, delays senescence of putative murine salivary gland stem cells in culture. *Arch. Oral Biol.* **60,** 875–882

(2015).

122. Park, J. K. *et al.* Role of rho-kinase activity in angiotensin II-induced contraction of rabbit clitoral cavernosum smooth muscle. *Int. J. Impot. Res.* **14,** 472–477 (2002).

123. Rees, R. W. *et al.* Y-27632, A Rho-kinase inhibitor, inhibits proliferation and adrenergic contraction of prostatic smooth muscle cells. *J. Urol.* **170,** 2517–2522 (2003).

124. Hisaoka, T. *et al.* Enhancement of Rho/Rho-kinase system in regulation of vascular smooth muscle contraction in tachycardia-induced heart failure. *Cardiovasc. Res.* **49,** 319–329 (2001).

125. Danopoulos, S., Schlieve, C. R., Grikscheit, T. C. & Al Alam, D. Fibroblast Growth Factors in the Gastrointestinal Tract: Twists and Turns. *Dev. Dyn.* **246,** 344–352 (2017).

126. Greicius, G. *et al.* *PDGFRα* $^{+}$ pericryptal stromal cells are the critical source of Wnts and RSPO3 for murine intestinal stem cells in vivo. *Proc. Natl. Acad. Sci.* 201713510 (2018). doi:10.1073/pnas.1713510115

127. Valenta, T. *et al.* Wnt Ligands Secreted by Subepithelial Mesenchymal Cells Are Essential for the Survival of Intestinal Stem Cells and Gut Homeostasis. *Cell Rep.* **15,** 911–918 (2016).

128. Shaker, A. & Rubin, D. C. Intestinal stem cells and epithelial-mesenchymal interactions in the crypt and stem cell niche. *Transl. Res.* **156,** 180–187 (2010).

129. Crosnier, C., Stamataki, D. & Lewis, J. Organizing cell renewal in the intestine: stem cells, signals and combinatorial control. *Nat. Rev. Genet.* **7,** 349–59 (2006).

130. Wallace, A. S. & Burns, A. J. Development of the enteric nervous system, smooth muscle and interstitial cells of Cajal in the human gastrointestinal tract. *Cell Tissue Res.* **319,** 367–382 (2005).

131. Gulbransen, B. D. & Sharkey, K. A. Novel functional roles for enteric glia in the gastrointestinal tract. *Nat. Rev. Gastroenterol. Hepatol.* **9,** 625–632 (2012).

132. Mostafa, R. M., Moustafa, Y. M. & Hamdy, H. Interstitial cells of Cajal, the Maestro in health and disease. *World J. Gastroenterol.* **16,** 3239–3248 (2010).

133. Choi, J. S., Lee, S. J., Christ, G. J., Atala, A. & Yoo, J. J. The influence of electrospun aligned poly(epsilon-caprolactone)/collagen nanofiber meshes on the formation of self-aligned skeletal muscle myotubes. *Biomaterials* **29,** 2899–906 (2008).

134. Braghirolli, D. I., Steffens, D. & Pranke, P. Electrospinning for regenerative medicine: a review of the main topics. *Drug Discov. Today* **19,** 743–53 (2014).

135. Ostrovidov, S. *et al.* Myotube formation on gelatin nanofibers - multi-walled carbon nanotubes hybrid scaffolds. *Biomaterials* **35,** 6268–77 (2014).

136. Xu, C. Aligned biodegradable nanofibrous structure: a potential scaffold for blood vessel engineering. *Biomaterials* **25,** 877–886 (2004).

137. Zhang, J. *et al.* Wet-spun poly(ε-caprolactone) microfiber scaffolds for oriented growth and infiltration of smooth muscle cells. *Mater. Lett.* **132,** 59–62 (2014).

138. Mo, X. ., Xu, C. ., Kotaki, M. & Ramakrishna, S. Electrospun P(LLA-CL) nanofiber: a biomimetic extracellular matrix for smooth muscle cell and endothelial cell proliferation. *Biomaterials* **25,** 1883–1890 (2004).

139. Wang, Y. *et al.* Electrospun Tubular Scaffold with Circumferentially Aligned Nano fibers for Regulating Smooth Muscle Cell Growth. **6,** 2958–2962 (2014).

140. Rayatpisheh, S. *et al.* Combining cell sheet technology and electrospun scaffolding for engineered tubular, aligned, and contractile blood vessels. *Biomaterials* **35,** 2713–9 (2014).

141. Vatankhah, E. *et al.* Phenotypic Modulation of Smooth Muscle Cells by Chemical and Mechanical Cues of Electrospun Tecophilic/Gelatin Nano fi bers. (2014).

142. Whited, B. M. & Rylander, M. N. The influence of electrospun scaffold topography on endothelial cell morphology, alignment, and adhesion in response to fluid flow. *Biotechnol. Bioeng.* **111,** 184–95 (2014).

143. Christopherson, G. T., Song, H. & Mao, H.-Q. The influence of fiber diameter of electrospun substrates on neural stem cell differentiation and proliferation. *Biomaterials* **30,** 556–64 (2009).

144. Wang, H. B., Mullins, M. E., Cregg, J. M., McCarthy, C. W. & Gilbert, R. J. Varying the diameter of aligned electrospun fibers alters neurite outgrowth and Schwann cell migration. *Acta Biomater.* **6,** 2970–8 (2010).

145. Huang, Z.-M., Zhang, Y.-Z., Kotaki, M. & Ramakrishna, S. A review on polymer nanofibers by electrospinning and their applications in nanocomposites. *Compos. Sci. Technol.* **63,** 2223–2253 (2003).

146. Cirillo, V., Guarino, V., Alvarez-Perez, M. A., Marrese, M. & Ambrosio, L. Optimization of fully aligned bioactive electrospun fibers for 'in vitro' nerve guidance. *J. Mater. Sci. Mater. Med.* (2014). doi:10.1007/s10856-014-5214-4

147. McHugh, K. M. Molecular analysis of gastrointestinal smooth muscle development. *J. Pediatr. Gastroenterol. Nutr.* **23,** 379–94 (1996).

148. Crosnier, C., Stamataki, D. & Lewis, J. Organizing cell renewal in the intestine : stem cells , signals and combinatorial control. **7,** 349–359 (2006).

149. Khademhosseini, A. & Langer, R. A decade of progress in tissue engineering. *Nat. Protoc.* **11,** 1775–1781 (2016).

150. Wejse, P. L., Ingvorsen, K. & Mortensen, K. K. Xylanase production by a novel halophilic bacterium increased 20-fold by response surface methodology. *Enzyme Microb. Technol.* **32,** 721–727 (2003).

151. Jordan, M. *et al.* Cell culture medium improvement by rigorous shuffling of components using media blending. *Cytotechnology* **65,** 31–40 (2013).

152. Pfitzer, G. Regulation of myosin phosphorylation in smooth muscle. *J Appl Physiol* **91,** 497–503 (2001).

153. Barker, N. Adult intestinal stem cells: critical drivers of epithelial homeostasis and regeneration. *Nat. Rev. Mol. Cell Biol.* **15,** 19–33 (2014).

154. Noah, T. K., Donahue, B. & Shroyer, N. F. Intestinal development and differentiation. *Exp. Cell Res.* **317,** 2702–10 (2011).

155. Hansen, M. B. Neurohumoral control of gastrointestinal motility. *Physiol. Res.* **52,** 1–30 (2003).